RELIABILITY ANALYSIS METHODS FOR POWER SYSTEMS WITH SUBSTANTIAL PENETRATION OF RENEWABLE GENERATING RESOURCES

A Dissertation
Presented to
The Academic Faculty

by

Abdullah Alamri

In Partial Fulfillment
of the Requirements for the Degree
Doctor of Philosophy in the
School of Electrical and Computer Engineering

Georgia Institute of Technology
May 2019

RELIABILITY ANALYSIS METHODS FOR POWER SYSTEMS WITH SUBSTANTIAL PENETRATION OF RENEWABLE GENERATING RESOURCES

Approved by:

Dr. Meliopoulos, A.P. Sakis, Advisor

School of Electrical and Computer Engineering

Georgia Institute of Technology

Dr. Grijalva, Santiago

School of Electrical and Computer Engineering

Georgia Institute of Technology

Dr. Saeedifard, Maryam

School of Electrical and Computer Engineering

Georgia Institute of Technology

Dr. Molzahn, Daniel

School of Electrical and Computer Engineering

Georgia Institute of Technology

Dr. Gebraeel, Nagi Z

School of Industrial and Systems Engineering

Georgia Institute of Technology

Date Approved: March 12, 2020

I dedicate this thesis to:

My parents, Mr. Saad Alamri and Mrs. Mahasen Alhazmi,

I am who I am because of your support, care, love, kindness and motivation.

My lovely wife, Somaya Almaghamsy, and my two beautiful angels, Esraa and Anas,

I would not have made it this far with you. Thanks for your constant love and sacrifice.

ACKNOWLEDGEMENTS

I have been incredibly fortunate to pursue a Ph.D. degree in electrical engineering at this prestigious school, the Georgia Institute of Technology. I deeply appreciate the love and support I have received during this beautiful journey. For the beloved ones who live thousands of miles away: my parents and siblings. I have no words to thank you for your continuous support, love and motivation. Also, I am eternally grateful to my dear wife Somaya for her overwhelming love, constant support, caring and believing in me. I would not have been able to achieve all of this without you.

Especially, I would like to express my sincere gratitude to my advisor, mentor and role model Prof. Meliopoulos, A.P. Sakis. I am very thankful for his guidance, clear directions, patience and immense knowledge in every aspect of my research. As I will pursue career in academia, Prof. Meliopoulos has set a role model I look up to. It has been a great honor working with Prof. Meliopoulos and I could not have gone this far without his support and guidance.

My sincere thanks also go to Prof. Saeedifard, Maryam, Prof. Gebraeel, Nagi, Prof. Grijalva, Santiago, and Prof. Molzahn, Daniel for serving in my Ph.D. defense committee. I appreciate their time, encouragement, suggestions and invaluable comments that helped to improve further my work.

During my study, I have met many great students. Their friendship and support are appreciated. Especially, I would like to thank the current and former students of Power Systems Control and Automation Laboratory: Dr. Hussain Albinali, Maad AlOwaifeer, Stella Kampezidou, Dr. Seyyedmohammadsadegh Vejdan, Gad Monga, Xie Boqi, Chiyang

Zhong, Orestis Vasios, Juan Lazarte and Emeka Obikwelu. Also, I would like to express my appreciation to the Saudi students group for their great help, friendship and all the good times we spent together.

I would like also to thank the Islamic University in Madinah represented in the United States by the Saudi Arabian Cultural Mission (SACM) for their support during the entire Ph.D. program.

TABLE OF CONTENTS

ACKNOWLEDGEMENTS **iv**

LIST OF TABLES **ix**

LIST OF FIGURES **xi**

LIST OF SYMBOLS AND ABBREVIATIONS **xviii**

SUMMARY **xx**

CHAPTER 1. INTRODUCTION **1**
1.1 Introduction **1**
1.2 Problem Statement and Proposed Research **3**
1.3 Thesis Outline **3**

CHAPTER 2. LITERATURE REVIEW **5**
2.1 Introduction **5**
2.2 Variable Generation Impact on Power System Reliability **6**
2.3 Energy Storage Systems Impact on Power System Reliability **9**

CHAPTER 3. Reliability Assessment Method **12**
3.1 The Probabilistic Production Costing **12**
3.1.1 Introduction 12
3.1.2 Mathematical formulation 14

CHAPTER 4. PROBABILITY CHARACTERIZATION OF WIND FARM POWER OUTPUT AND IMPACT ON SYSTEM RELIABILITY **19**
4.1 Problem Statement and Basic Calculations **19**
4.2 Mathematical Formulation of WF Power Output PDF computation **21**
4.2.1 Analytical Probabilistic Method 21
4.2.2 Non-Sequential Monte Carlo Simulation 26
4.2.3 Sequential Monte Carlo Simulation 27
4.3 Reliability Assessment Based on WF Generated Power PDF **29**
4.4 Case Study **30**
4.4.1 Analytical Probabilistic Method Results 32
4.4.2 Non-Sequential Monte Carlo Simulation Results 33
4.4.3 Sequential Monte Carlo Simulation Results 33
4.4.4 Reliability Assessment Results 35
4.5 Conclusions **36**

CHAPTER 5. PROBABILITY CHARACTERIZATION OF SOLAR FARM POWER OUTPUT AND IMPACT ON SYSTEM RELIABILITY **38**
5.1 Problem Statement and Basic Calculations **39**
5.2 Probabilistic Evaluation of SF Generated Power PDF **40**

5.2.1 Analytical Probabilistic Method 40
5.2.2 Non-Sequential Monte Carlo Simulation 44
5.2.3 Sequential Monte Carlo Simulation 46
5.2.4 Reliability Assessment Based on SF Power Output PDF 47
5.3 Case Study 48
5.3.1 Analytical Probabilistic Method Results 50
5.3.2 Non-Sequential Monte Carlo Simulation Results 51
5.3.3 Sequential Monte Carlo Simulation Results 51
5.3.4 Reliability Assessment Results 54
5.4 Conclusions 54

CHAPTER 6. UNIT COMMITMENT AND PROBABILISTIC RELIABILITY ASSESSMENT OF POWER SYSTEMS WITH VARIABLE GENERATION 56
6.1 Problem Statement 56
6.2 Unit Commitment Economic Dispatch Incorporating Solar Generation 57
6.3 Reliability Assessment Using the Probabilistic Production Costing 64
6.3.1 Conventional Generation Units 64
6.3.2 Equivalent Load/SF Representation 64
6.3.3 Reliability Assessment 64
6.4 Case Study 65
6.4.1 UCED Results 67
6.4.2 Reliability Assessment and Capacity Credit 68
6.5 Conclusions 70

CHAPTER 7. ENERGY STORAGE SIZING AND RELIABILITY ASSESSMENT FOR POWER SYSTEMS WITH VARIABLE GENERATION 71
7.1 Problem Statement 71
7.2 Energy Storage Sizing Optimization Formulation 73
7.3 Reliability Assessment Using the Probabilistic Production Costing 79
7.3.1 Equivalent Load Representation 79
7.4 Case Study 80
7.4.1 ESS Sizing Results 81
7.4.2 Reliability Assessment 83
7.5 Conclusions 84

CHAPTER 8. ANALYTICAL METHOD FOR ENERGY STORAGE SIZING AND RELIABILITY ASSESSMENT FOR POWER SYSTEMS WITH VARIABLE GENERATION 85
8.1 Problem Statement 85
8.2 Computation of SFs/WFs Generated Power Probability Distribution Function 87
8.2.1 SF Power Probability Distribution Function 87
8.2.2 WF Power Probability Distribution Function 87
8.3 Energy Storage Sizing Optimization Formulation 87
8.4 Reliability Assessment Using the Probabilistic Production Costing 92
8.5 Case Study 92
8.5.1 SFs/WFs Power Output PDF/CDF Results 93

8.5.2 ESS Sizing Results 101
8.5.3 Reliability Assessment Results 103
8.6 Conclusions 103

CHAPTER 9. ENERGY STORAGE SIZING AND PROBABILISTIC RELIABILITY ASSESSMENT FOR POWER SYSTEMS BASED ON COMPOSITE DEMAND 104
9.1 Problem Statement 105
9.2 Computation of SFs/WFs Expected Power Output 106
9.2.1 SF Expected Power Outputs 106
9.2.2 WF Expected Power Output 106
9.3 Correlation Coefficient and Composite Demand PDF Computation 107
9.3.1 Correlation Coefficient Computation 107
9.3.2 Composite Demand PDF and CDF Computation Computation 109
9.4 Energy Storage Sizing Optimization Formulation 110
9.5 Reliability Assessment Using the Probabilistic Production Costing 115
9.6 Case Study 115
9.6.1 Expected WF/SF Power Outputs Results 116
9.6.2 Correlation Coefficients and Composite Demand PDF 120
9.6.3 ESS Sizing Results 125
9.6.4 Reliability Assessment Results 128
9.7 Conclusions 128

CHAPTER 10. SUMMARY, CONTRIBUTIONS AND FUTURE RESEARCH DIRECTIONS 130
10.1 Summary 130
10.2 Contributions of This Research 131
10.3 Publications 133
10.4 Future Research Directions 134

APPENDIX A. THE IEEE RELIABILITY TEST SYSTEM - 1996 LOAD DESCRIPTION 136

APPENDIX B. CHAPTER 8 CASE STUDY FIGURES FOR THE 20% PENETRATION LEVEL 139

APPENDIX C. CHAPTER 9 CASE STUDY FIGURES FOR THE 20% PENETRATION LEVEL 148

REFERENCES 153

LIST OF TABLES

Table 4-1	$\rho_{WFG}(p_{WF})$ values at 0 ~10 $p_{WTS.reated}$.	35
Table 4-2	PPC results of all cases.	36
Table 5-1	ρ_{SFG} (p_{SF}) values in the range 0 ~10 $p_{SCG.reated}$.	53
Table 5-2	PPC results of all cases.	54
Table 6-1	SCG specifications.	66
Table 6-2	The 10 CGs specifications.	66
Table 6-3	The 10 CGs cost coefficients.	66
Table 6-4	The 10 CGs FORs.	67
Table 6-5	P_{SF} Utilization Example.	67
Table 6-6	Reliability assessment results.	69
Table 7-1	SCG specifications.	81
Table 7-2	WTS specifications.	81
Table 7-3	ESS specifications.	81
Table 7-4	Optimal sizing and cost of ESS.	82
Table 7-5	Reliability assessment results.	84

Table 8-1	ESS sizing results.	101
Table 8-2	Reliability assessment results.	103
Table 9-1	SCG specifications.	116
Table 9-2	ESS specifications.	116
Table 9-3	Correlation coefficient values.	120
Table 9-4	ESS sizing and cost results.	125
Table 9-5	Reliability assessment results.	128
Table A- 1	Daily load in percent of weekly peak.	136
Table A- 2	Weekly peak load in percent of annual peak.	137
Table A- 3	Hourly peak load in percent of daily peak.	138

LIST OF FIGURES

Figure 1-1	The three hieratical levels of reliability assessment.	1
Figure 2-1	The chronological load curve example.	5
Figure 2-2	The load duration curve.	6
Figure 3-1	The CG two-state availability model.	15
Figure 3-2	The load duration curve.	16
Figure 3-3	Convolution example between the ELDC and two CG units.	17
Figure 3-4	The values of LOLP and EUE.	18
Figure 4-1	Reliability assessment procedure in presence of wind generation.	20
Figure 4-2	The WTS two-state availability model.	22
Figure 4-3	WTS power curve and wind speed PDF relationship.	23
Figure 4-4	Probability tree for single WTS possible outcomes.	23
Figure 4-5	The WF availability PMF ($\rho_{WFA}(c_{WF})$).	25
Figure 4-6	The wind speed PDF.	31
Figure 4-7	The wind speed CDF.	31
Figure 4-8	The reliability test system.	31

Figure 4-9	ρ_{WFG} (p_{WF}) using the analytical method.	32
Figure 4-10	ρ_{WFG} (p_{WF}) using the NSMCS.	33
Figure 4-11	$\rho_{WFG}(p_{WF})$ using the SMCS.	34
Figure 4-12	F_{WFG} (p_{WF}) for all three methods.	35
Figure 5-1	Reliability assessment procedure in presence of solar generation.	39
Figure 5-2	The SCG two-state availability model.	41
Figure 5-3	SCG power and solar irradiance PDF relationship [16].	42
Figure 5-4	Probability tree for SCG possible outcomes.	42
Figure 5-5	The SF availability PMF ($\rho_{SFA}(c_{SF})$).	43
Figure 5-6	Solar radiation PDF.	49
Figure 5-7	Solar radiation CDF.	49
Figure 5-8	The example test system.	50
Figure 5-9	ρ_{SFG} (p_{SF}) using the analytical method.	51
Figure 5-10	$\rho_{SFG}(p_{SF})$ using NSMCS.	52
Figure 5-11	$\rho_{SFG}(p_{SF})$ using SMCS.	52
Figure 5-12	$F_{SFG}(p_{SF})$ for all three methods.	53
Figure 6-1	The piecewise production cost [41].	62

Figure 6-2	Staircase start-up cost function [42].	63
Figure 6-3	The ELCC of all penetration levels.	68
Figure 6-4	The ELCC and CC of all penetration levels.	70
Figure 7-1	Proposed computational procedure.	72
Figure 7-2	Reliability assessment procedure in presence of VG and ESS.	73
Figure 7-3	Unutilized VG comparison at 30% penetration.	82
Figure 7-4	ESS power and energy profiles at 30% penetration.	83
Figure 8-1	Winter season PDF and CDF of SF1 at 30% penetration level.	93
Figure 8-2	Spring season PDF and CDF of SF1 at 30% penetration level.	94
Figure 8-3	Summer season PDF and CDF of SF1 at 30% penetration level.	94
Figure 8-4	Fall season PDF and CDF of SF1 at 30% penetration level.	95
Figure 8-5	Winter season PDF and CDF of SF2 at 30% penetration level.	95
Figure 8-6	Spring season PDF and CDF of SF2 at 30% penetration level.	96
Figure 8-7	Summer season PDF and CDF of SF2 at 30% penetration level.	96
Figure 8-8	Fall season PDF and CDF of SF2 at 30% penetration level.	97
Figure 8-9	Winter season PDF and CDF of WF1 at 30% penetration level.	97
Figure 8-10	Spring season PDF and CDF of WF1 at 30% penetration level.	98

Figure 8-11	Summer season PDF and CDF of WF1 at 30% penetration level.	98
Figure 8-12	Fall season PDF and CDF of WF1 at 30% penetration level.	99
Figure 8-13	Winter season PDF and CDF of WF2 at 30% penetration level.	99
Figure 8-14	Spring season PDF and CDF of WF2 at 30% penetration level.	100
Figure 8-15	Summer season PDF and CDF of WF2 at 30% penetration level.	100
Figure 8-16	Fall season PDF and CDF of WF2 at 30% penetration level.	101
Figure 8-17	ESS power and energy profiles at 30% penetration.	102
Figure 8-18	Unutilized VG at 30% penetration (with/without ESS).	102
Figure 9-1	Historical demand data.	117
Figure 9-2	Historical wind speed data.	118
Figure 9-3	Historical solar radiation data.	118
Figure 9-4	Expected WF power output (p_{WF}) at 30% penetration level.	119
Figure 9-5	Expected SF power output (p_{SF}) at 30% penetration level.	119
Figure 9-6	Composite demand PDFs ($\rho_{CD}(cd)$) at 30% penetration level (Case 2).	122
Figure 9-7	Composite demand CDFs ($F_{CD}(cd)$) at 30% penetration level (Case 2).	122

Figure 9-8	$D-SF$ PDFs ($\rho_{D-SF}(d)$) at 30% penetration level (Case 3).	123
Figure 9-9	$D-SF$ CDFs ($\rho_{D-SF}(d)$) at 30% penetration level (Case 3).	123
Figure 9-10	WF power output ($\rho_{WFG}(p_{WF})$) PDFs at 30% penetration (Case 3).	124
Figure 9-11	WF power output ($F_{WFG}(p_{WF})$) PDFs at 30% penetration (Case 3).	124
Figure 9-12	ESS SOC for case 2 and 3 at 30% penetration level.	126
Figure 9-13	ESS SOC for case 2 and 3 at 30% penetration level.	126
Figure 9-14	ESS and CG reserve comparison between Case 2 and Case 3 at 30% penetration level.	127
Figure 9-15	ESS and CG reserve comparison between Case 2 and Case 3 at 20% penetration level.	127
Figure B- 1	Winter season PDF and CDF of SF1 at 20% penetration level.	139
Figure B- 2	Spring season PDF and CDF of SF1 at 20% penetration level.	140
Figure B- 3	Summer season PDF and CDF of SF1 at 20% penetration level.	140
Figure B- 4	Fall season PDF and CDF of SF1 at 20% penetration level.	141
Figure B- 5	Winter season PDF and CDF of SF2 at 20% penetration level.	141
Figure B- 6	Spring season PDF and CDF of SF2 at 20% penetration level.	142
Figure B- 7	Summer season PDF and CDF of SF2 at 20% penetration level.	142

Figure B- 8	Fall season PDF and CDF of SF2 at 20% penetration level.	143
Figure B- 9	Winter season PDF and CDF of WF1 at 20% penetration level.	143
Figure B- 10	Spring season PDF and CDF of WF1 at 20% penetration level.	144
Figure B- 11	Summer season PDF and CDF of WF1 at 20% penetration level.	144
Figure B- 12	Fall season PDF and CDF of WF1 at 20% penetration level.	145
Figure B- 13	Winter season PDF and CDF of WF2 at 20% penetration level.	145
Figure B- 14	Spring season PDF and CDF of WF2 at 20% penetration level.	146
Figure B- 15	Summer season PDF and CDF of WF2 at 20% penetration level.	146
Figure B- 16	Fall season PDF and CDF of WF2 at 20% penetration level.	147
Figure C- 1	Expected WF power output (p_{WF}) at 20% penetration level.	148
Figure C- 2	Expected SF power output (p_{SF}) at 20% penetration level.	149
Figure C- 3	Composite demand PDFs ($\rho_{CD}(cd)$) at 20% penetration level (Case 2).	149
Figure C- 4	Composite demand CDFs ($F_{CD}(cd)$) at 30% penetration level (Case 2).	150
Figure C- 5	$D-SF$ PDFs ($\rho_{D-SF}(d)$) at 20% penetration level (Case 3).	150
Figure C- 6	$D-SF$ PDFs ($F_{D-SF}(d)$) at 20% penetration level (Case 3).	151

Figure C- 7 WF power output (ρ_{WFG} (p_{WF})) PDFs at 20% penetration level. 151

Figure C- 8 WF power output (F_{WFG} (p_{WF})) PDFs at 20% penetration level. 152

Figure C- 9 ESS SOC for case 2 and 3 at 20% penetration level. 152

LIST OF SYMBOLS AND ABBREVIATIONS

CC	Capacity Credit
CG	Conventional Generation
ELCC	Effective Load Carrying Capacity
ESS	Energy Storage System
EUE	Expected Unserved Energy
FOR	Forced Outage Rate
ITM	Inverse Transform Method
LOLE	Loss of Load Expectation
LOLP	Loss of Load Probability
MCS	Monte Carlo Simulation
MILP	Mixed Integer Linear Programming
MIP	Mixed Integer Programming
PPC	Probabilistic Production Costing

RTS	Reliability Test System
SAM	System Advisory Model
SCG	Solar Cell Generator
SF	Solar Farm
UC	Unit Commitment
UCED	Unit Commitment Economic Dispatch
VG	Variable Generation
WF	Wind Farm
WTS	Wind Turbine System

SUMMARY

Today's typical power systems have a mix of conventional generation (CG) and variable generation (VG). Examples of VG are wind turbine systems (WTSs) and solar cell generators (SCGs). VG is characterized by intermittency and its integration into power systems affects power systems operation, reliability and planning practices. The focus of this research is generation adequacy when adding VG.

The objective of this thesis is to develop reliability assessment models of power systems with wind farms (WF) and/or solar farms (SF); each WF may have a number of WTSs and each SF may have a number of SCGs. These models involve finding WF/SF power output probability. Three different methods for computing the generated power probability distribution function (PDF) of a WF or a SF are proposed: (1) analytical method, (2) non-sequential Monte Carlo simulation, and (3) sequential Monte Carlo simulation. Historical wind speed/solar radiation data are utilized to perform the study. Further, force outage rates (FORs) of components are incorporated in the process of computing the WF/SF generated power PDF. All methods yield comparable results. The usefulness of the computed PDF is demonstrated by integrating them into a probabilistic production costing (PPC) model for assessing the reliability of a system comprising one or more WFs/SFs. A further development of these models includes a unit commitment economic dispatch model (UCED) to simulate real operation of power systems, specifically CG constraints in presence of VG at different penetration levels. Also, the UCED will be used to solve for optimal energy storage system (ESS) sizing and its expected charging and discharging power profile. This profile determines the expected ESS effect on reliability.

The optimal ESS sizing problem is modeled as a mixed integer linear program (MILP) that takes into account: (a) VG units FORs, (b) reserve and demand requirements, and (c) CG operational constraints. (d) seasonal wind speed, solar radiation, and demand correlation.

CHAPTER 1. INTRODUCTION

1.1 Introduction

The reliability of power systems is defined as the probability that electric power components continuously deliver electricity to customers with an acceptable quality of service. It should be noted that the reliability is defined for a given period and under certain operating conditions [1]-[4]. Reliability analysis methods are classified into three hierarchical levels: generation, transmission and distribution [3]. The generation level which is concerned with total system generation adequacy over a period of time and assumes 100% reliable and adequate transmission and distribution networks. In other words, it assesses power system generation adequacy to meet its demand assuming that transmission/distribution networks are capable of transmitting the power from generation to the customer without constraint. A higher level is created by adding transmission reliability analysis which accounts for transmission network failures capacity limitations. Lastly, adding the distribution network constraints to the reliability assessment yields to the highest hierarchical level which is more complex. This is shown in Figure 1-1.

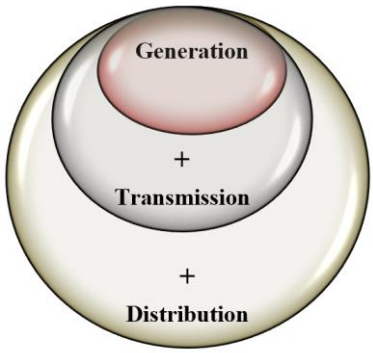

Figure 1-1. The three hieratical levels of reliability assessment.

The research of this thesis focuses on the first hierarchical level: generation level. Today's typical power system has a mix of conventional and renewable generation. Renewable energy, e.g., wind and solar, has increased due to the need to decrease greenhouse emissions and to address energy security concerns [5]. For instance, the International Energy Outlook 2019 shows that non-hydroelectric renewable energy share in the electricity sector is projected to increase 5.7% annually between the years 2018 and 2050. Moreover, the solar generation is globally forecasted to increase steadily and reach 6.7 trillion kWh by 2050 while the wind generation is forecasted to reach 8.3 trillion kWh by 2050 [6]. However, wind and solar power generations are characterized by intermittency and referred to as variable generation (VG) or not dispatchable. This characteristic affects system reliability and operating costs. Hence, assessing the reliability of power systems under different penetrations of VG is important. A holistic reliability assessment should take into consideration all generators possible outages and VGs' intermittent output.

Finally, the energy storage systems (ESSs) utilization and their effects on power systems reliability. The Energy Storage Association reports that the global ESSs market is currently growing exponentially and it is forecasted to have annual installation rate of 40 GW by 2022 [7]. ESSs come in various forms, depending on the technology used, and in different scales. The technologies that have been used to store energy include electrical, thermal, hydro, mechanical, and electrochemical [8]. These technologies make the characteristics and the applications of various ESS different. The applications of ESS include (a) supporting increased renewable generation penetration, (b) load peak shaving and (c) enhancing reliability of power systems [8]-[9]. These applications offer flexibility, improvement of power quality and increased reliability of power systems. An important

problem in power systems planning and reliability studies is ESS sizing in the presence of VG, and the overall impact of VG and ESS addition on power system reliability.

1.2 Problem Statement and Proposed Research

This research proposes probabilistic reliability assessment models for power systems under different penetration levels of VG. The VG comes from either solar cell generators (SCGs), wind turbine systems (WTS), or both. The models take into account weather prediction based on historical data of a certain location in addition to load forecast and forced outage rates (FORs) of VG and conventional generation (CG) units. Also, a model, based on the previous models, is developed to find the optimal ESS sizing, in presence of VG, and its effect on reliability. This model takes into account VG units forced outages, weather seasonal forecast error, demand and reserve requirements, and demand and VG correlation.

1.3 Thesis Outline

The dissertation consists of nine chapters. CHAPTER 2 is a review of the past and state-of-the-art research regarding quantification of VG and ESS effects on power systems. CHAPTER 3 presents in detail a and the reliability assessment method, namely the probabilistic production costing (PPC), and the importance of modeling load with the load duration curve (LDC); this method is used throughout the thesis. CHAPTER 4 and CHAPTER 5 present detailed derivation of probabilistic models of power output of a wind farm (WF) and a solar farm (SF), respectively. In addition, the two chapters show how these models are incorporated into the PPC method. CHAPTER 6 presents an additional development of the reliability assessment models in presence of VG by introducing the

UCED model. CHAPTER 7 integrates the optimal ESS sizing into the UCED model and explains how to quantify reliability when adding ESS in presence of VG. CHAPTER 8 presents the addition of seasonal variations to the model of CHAPTER 7. CHAPTER 9 presents an advanced model that integrates into the ESS sizing model the seasonal correlation between the demand and the VG. Finally, CHAPTER 10 presents conclusions and future research directions.

CHAPTER 2. LITERATURE REVIEW

2.1 Introduction

In traditional power system operation, demand is exogenous variable and there is uncertainty associated with its forecast. Thus, the historical chorological demand data is of importance to understand and study a specific power system. However, in planning and reliability studies, it is crucial to know the probability of having a certain level of the load. The load probabilistic model is the LDC [4]. The probability here is defined as percentage of time. To construct the LDC, the load is arranged in descending order of magnitude. As an illustrative example, a typical chronological load curve, shown in Figure 2-1, can be converted to a LDC with the time axes normalized as depicted in Figure 2-2. As discussed later, finding the LDC is important step in assessing the reliability when adding VG. The LDC in presence of VG and/or ESS is referred to as effective load duration curve (ELDC). The ELDC is an integral part in reliability assessment method used in this work, as discussed in detailed in the following chapter.

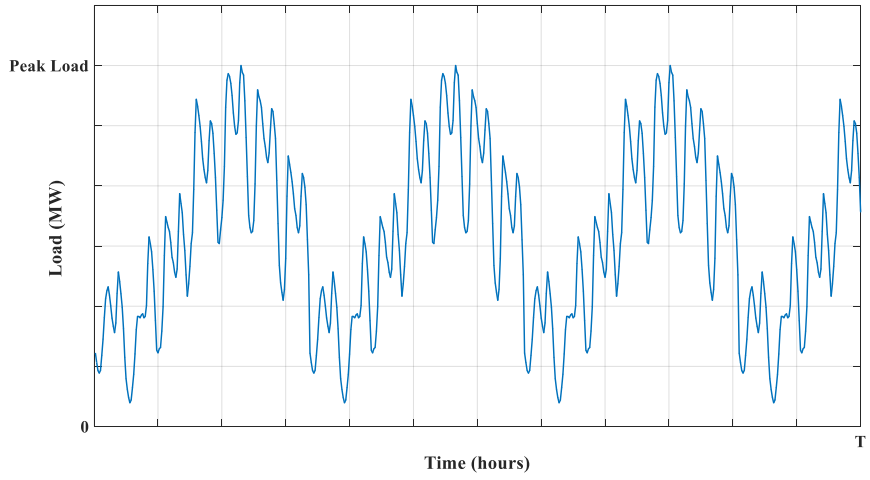

Figure 2-1. The chronological load curve example.

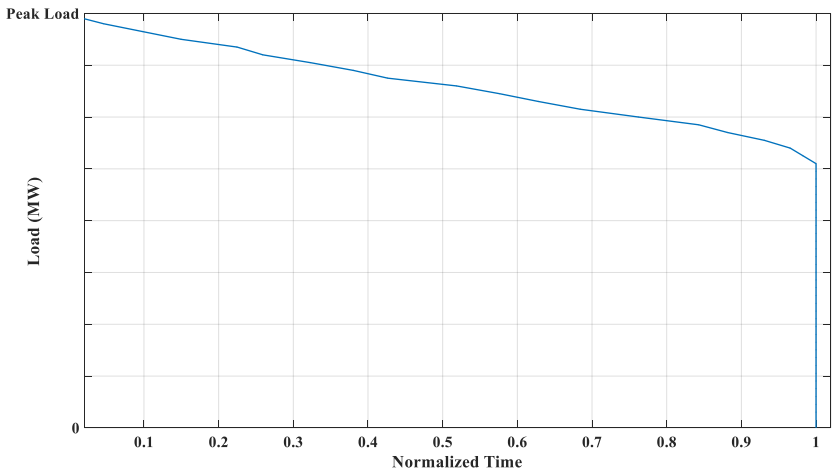

Figure 2-2. The load duration curve.

2.2 Variable Generation Impact on Power System Reliability

VG impact on power systems has been intensively studied. Taking wind generation as an example, there has been a plethora of studies on modeling its impact on power systems reliability. These studies use probabilistic modeling that falls into two categories: either analytical or Monte Carlo simulation (MCS). The latter one is either sequential (SMCS) or non-sequential (random) (NSMCS). The analytical method uses mathematical derivations to enumerate all possible outcomes and their probabilities. For example, reference [10] presented an analytical probabilistic reliability model for a number of WTSs taking into consideration WTS FOR. Reference [11] showed that a WTS generation model could be simplified to a 6-step analytical model that could be used to assess generation reliability with acceptable accuracy. On the other hand, MCS has been used to simulate the randomness of the wind power and the WTSs failures instead of directly enumerating all cases. For instance, both NSMCS and SMCS have been used to assess generation adequacy

and composite reliability assessment [12]-[14]. However, [11] and [13] used approximated models and ignored FOR of the WTSs.

On the other hand, there have been studies on modeling SCG impact on power systems reliability. Similarly, these studies used probabilistic modeling and are categorized as either analytical, NSMCS or SMCS. For example, reference [15] found the probability density function (PDF) of SCG as discrete function i.e., impulses that are equally spaced. The impulses were calculated based on the average daily output of the SCG. Reference [16] combined the solar radiation PDF and the SCG power output curve to model the SCG power output as multi-state model and computes the probability of being in each state (up-derated-down). For computational efficiency, it suggested using linear rounding to decrease the number of states in modeling the SCG power output. On the other hand, instead of analytically enumerating all possible events, MCS has been used to count for the randomness of solar radiation intensity and components failures of SCGs. For instance, SMCS was used to assess the reliability assessment of a power system containing a SCG and a WTS [17]. The method used in [17] is a modified method of modeling CG. Reference [18] used a solar radiation prediction method along with a PV three-state model to evaluate adding PVs to an isolated system. The reliability assessment in [18] was based on MCS. However, there is a need to develop models that compute WF/SF, which consists of number of WTSs/SCGs, power output pdf using the analytical and MCS methods that yield to comparable results. Hence, any method of the three, analytical, SMCS or NSMCS, can be used to probabilistically represents WF/SF output depending on its compatibility with the reliability assessment method. This becomes clear later when comparing these three methods, and when adding storage to the test system. All three methods take into

consideration outages of the WTSs/SCGs and weather predictions of a certain location. Notably, no method among the analytical and MCS is superior over the other. Instead, each has its own advantages and disadvantages as will be discussed later.

As the penetration level of VG increases, planning and operation should account for economic dispatch, reserve requirements and reliability requirements. All aforementioned could be accounted for in the formulation of the unit commitment economic dispatch (UCED). This problem can determine the expected impact of VGs under different penetration levels. The unit commitment (UC) determines the optimal commitment (OFF/ON decisions) schedule by simulating the operation of the system over a period of time. The UC problem in general has the following constraints:

1) CG minimum and maximum production limits.
2) CG minimum Up/Down times.
3) CG ramp Up/Down limits.
4) Demand and reserve requirements.

Many models have been developed to solve the UC problem. These methods include dynamic programing, Lagrangian relaxation, genetic algorithm, fuzzy logic algorithm, and mixed integer programming (MIP) [19]-[21]. The focus of this work is on solving the UC using MIP. There have been numerous works on solving the UC problem for power systems without the presence of VGs using MIP. Starting with UC of CGs, reference [20] introduced a tighter description of the generation polytope by introducing a new class of inequalities that led to faster computation time. In [21], a state-transition variables model that captures the generator transition instead of their ON/OFF statuses. In the presence of

VGs, the traditional UC model could be modified to account for VGs. For instance, reference [22] used a mixed integer quadratic programing (MIQP) to solve a UC problem of an insular power system that incorporates VG. In [22], VGs were modeled as CGs but with constraints that took into account the climate prediction that governed VGs' production. In [23], a day-ahead UCED model was proposed with finer time scale (5 mins). The model in [23] reported providing responsive ramping following abrupt VG output change. It also claimed difficulty in applying long look-head horizons especially for large systems due to its computational requirement.

2.3 Energy Storage Systems Impact on Power System Reliability

Finally, incorporating energy storage systems (ESSs), in addition to VGs, to a power system and assessing reliability improvement. A plethora of literature exists on ESSs impact on power system reliability. Most of these studies assume an ESS size (power and energy ratings) and subsequently assess system reliability. A number of studies address the issue of optimal ESS sizing and then assessed reliability for the optimal ESS. Starting with the studies that assess reliability without ESS sizing, reference [24] used the Weibull distribution to model wind speeds and subsequently used SMCS to simulate a wind farm WF and CGs outputs. Then, it set criteria to calculate the portion of WF power to serve the demand directly and the portion to be stored. Finally, it assessed reliability contribution from adding ESSs. Reference [25] used MCS to assess the reliability of CGs, WTSs, ESSs, and hydro power plants, by chronologically coordinating WTSs and hydro plants. The wind speed was modeled as a time series auto-regressive moving average (ARMA) model while the ESS was modeled as the IEEE four-state model (reserve shutdown, in service, forced out but not needed, and forced out when needed). It showed that strategic coordination

between these resources could improve generation adequacy. Reference [26] introduced an analytical method to study ESSs impact in presence of WTSs generation. It analyzed the impact of ESSs initial stored energy and rated capacity analytically. The study found that initial stored energy has insignificant impact while rated capacity of ESSs had the most impact on reliability improvement. On the other hand, the study in [27] evaluated the reliability of hybrid SCG-ESS system using discrete time Markov chain (DTMC). The DTMC aimed to capture uncertainty in the SCG and ESS outputs. However, all aforementioned studies, did not address the issue of optimizing ESS size and [24], [25] and [27] did not include individual VG units (WTS or SCG) FORs but rather used aggregate models of WFs and SFs. However, the cost of ESS has been considerably high. Hence, the other set of studies on reliability assessment considered ESS optimal sizing. For instance, reference [28] introduced a probabilistic model for ESS sizing with peak shaving policy in presence of wind generation. The model was based on cyclic nonhomogeneous Markov chain and dealt with generation-load mismatch. It claimed that the model was fast and accurate, and with little sacrifice on profit, it could represent the WTSs-ESSs as reliable committed generation. For example, reference [29] considered the VG forecast error when sizing ESS using a two-stage stochastic model predictive control. Also, it considered wind forecast error as a chance constraint. With emphasis on reliability applications, reference [30], used pattern search-based optimization and SMCS to find the optimal size of hybrid SCG/WTS/ESS system components while maintaining certain reliability requirements. Reference [31] used a two-stage probabilistic model to solve for ESS-reserve sizing problem considering reliability by integrating loss of load index into ESS sizing. However, the literature lacks a holistic ESS sizing model that takes into account all aspects: WF/SF

outages, weather forecast error, meeting reserve requirements and load and VG correlation. The proposed ESS sizing model will account for all aforementioned aspects.

CHAPTER 3. RELIABILITY ASSESSMENT METHOD

The chapter presents the reliability assessment method that is going to be used for all cases discussed in later chapters. This method is called the probabilistic production costing method (PPC).

3.1 The Probabilistic Production Costing

3.1.1 Introduction

The probabilistic production costing is a probabilistic simulation method based on the Baleriaux, et al method that was introduced first in 1967 [32]. Production costing refers to any methodology that computes operating cost of an economic activity [33]. The problem that this method addresses is the simulation or the projection of power system operation cost over a period, given the load forecast, available generating units and their FORs [4]. As explained in [32] and [34], the method is based on using the probabilistic model of the electric load in addition to the probabilistic model of CGs expressed in terms of their FORs to assess the system reliability and compare future expansion plans. The solution is given through a series of convolutions between each CGs and the LDC; the mathematical formulation will be discussed in detail later. The method calculates the following indices:

1) Loss of load probability (LOLP): which is the probability that generation is insufficient; i.e., Probability (generation < load). Note that LOLP does not give indication of the severity of the loss.

2) Expected unserved energy (EUE): the expected energy not supplied to customers due to generation failure.
3) Expected energy generated by each CG unit.
4) Expected total generation cost.
5) Amount of environmental pollution by generation unit.

An important step when performing the PPC method is the merit of loading CG units. As described in [35], the most effective unit should be loaded first. In other words, the units of lowest average cost should be loaded first to meet the load starting from 0 MW to the unit rated capacity. Then, loading the second lowest average cost unit, and so on. One of the improvements to this loading procedure suggested in [34] was to divide the capacity of each CG unit into two blocks and these blocks are placed nonadjacent in the loading procedure. Every block has a different average production cost. This improvement increased accuracy and as the number of blocks increased, the accuracy improved. Reference [35] suggested a phased approach based on incremental loading procedure by dividing generation units into subsets based on their marginal cost, the minimum subset is loaded first. Taking into consideration the FORs of the components and maintenance, the projected cost could be calculated in phased manner by adding up the cost of generating electricity from each subset. The aforementioned works are examples of the early work on this method. There have been many published papers. For examples, reference [36] introduced a modification that takes into account energy limitation of generation facilities. Specifically focused on hydraulic units which were categorized as no energy storage or with energy storage (either large or restricted). The improved method alters the loading procedure to account for using energy storage relative to its type.

3.1.2 Mathematical formulation

A description of the PPC and the ELDC is as follows:

3.1.2.1 Conventional Generation Units

The CG unit is modeled as a 2-state Markov model: available or unavailable. In other words, either the unit is available with capacity equal to p_g^{max} or unavailable with capacity equal to zero, as shown in (3.1) and Figure 3-1.

$$Capacity_g = \begin{cases} P_g^{\max} & , \text{ if unit is operational} \\ 0 & , \text{ otherwise} \end{cases} \tag{3.1}$$

where p_g^{max} is the rated capacity of the g^{th} CG. The probability that the unit is unavailable is denoted by q. q is referred to as FOR and calculated as explained in [3]:

$$q_g = \frac{MTTR_g}{MTTR_g + MTTF_g} \tag{3.2}$$

$$1 - q_g = \frac{MTTR_g}{MTTR_g + MTTF_g} \tag{3.3}$$

where $MTTR_g$ is the unit mean time to repair and $MTTF_g$ is the mean time to failure. Both $MTTR_g$ and $MTTF_g$, and the repair and failure processes are exponentially distributed.

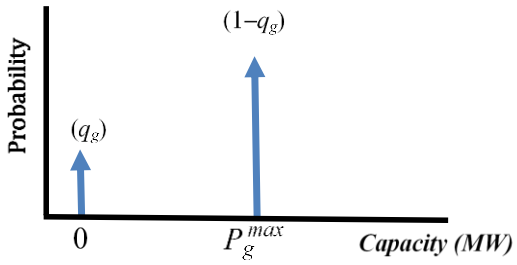

Figure 3-1. The CG two-state availability model.

3.1.2.2 Load/VG Representation

The net load is computed as follows:

$$\text{Net load}_t = \sum_{l=1}^{N_{load}} \text{Load}_{l,t} - \sum_{vg=1}^{N_{VG}} \text{VG}_{vg,t} - ESS\ Power_t \qquad \forall t \in T \tag{3.4}$$

Note that CHAPTER 4 and CHAPTER 5 assess the reliability when adding only VG; hence, the ESS power term in equation (3.4) is omitted. Figure 3-2 shown how the Net (or apparent) load is calculated generally in presence of VGs and ESS. Subsequently, the chronological net load curve is converted to an inverted probability distribution function (IPDF) as explained in [4]. The vertical axis of the IPDF is normalized time and horizontal axis is power.

3.1.2.3 Reliability Assessment and Production Cost

LOLP and EUE can be calculated using series of convolutions as explained in [4], [34] and [35]. Once the IPDF curve is constructed and FORs of all *G* units are known, the LOLP can be calculated as follows: the loading of a unit changes the apparent load on the remaining units as in (3.5):

$$L_g(l) = (1 - q_g)\, L_{g-1}(l + p_g^{max}) + q_g\, L_{g-1}(l) \qquad (3.5)$$

Figure 3-3 shows an example of convolving two CG units with the ELDC, and similarly it can be extended to *G* number of CG units. The curve L_0 is the ELDC and once the first CG is loaded, the resultant curve is L_1. Similrly, loading the second CG will give the curve L_2. This procedure is repeated till the *G*th CG is loaded.

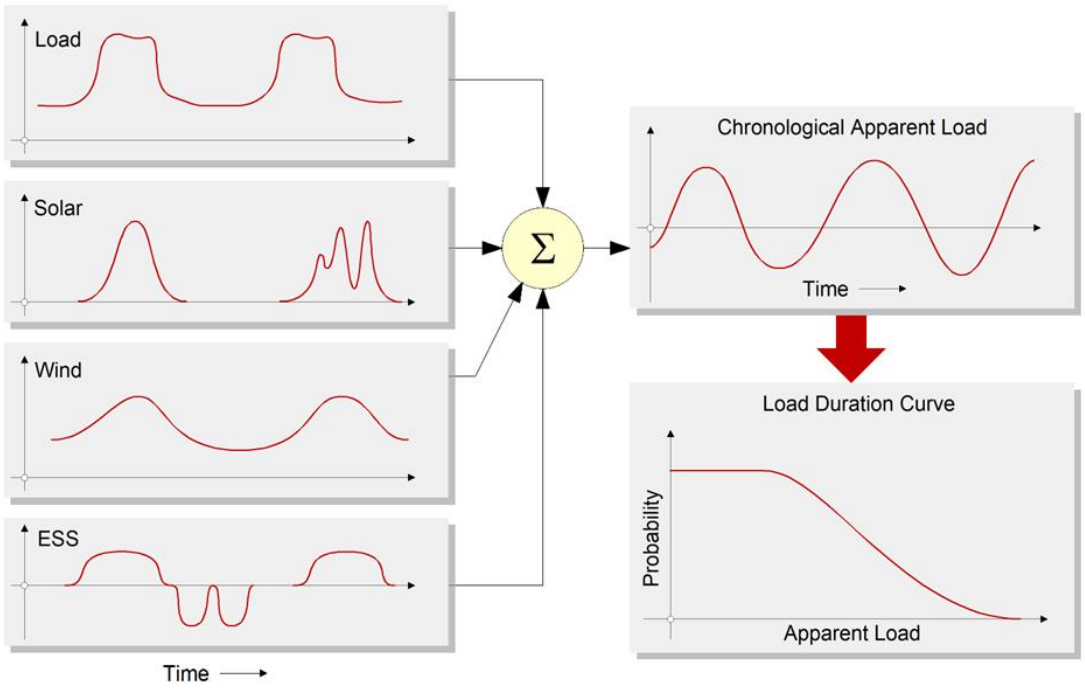

Figure 3-2. The load duration curve.

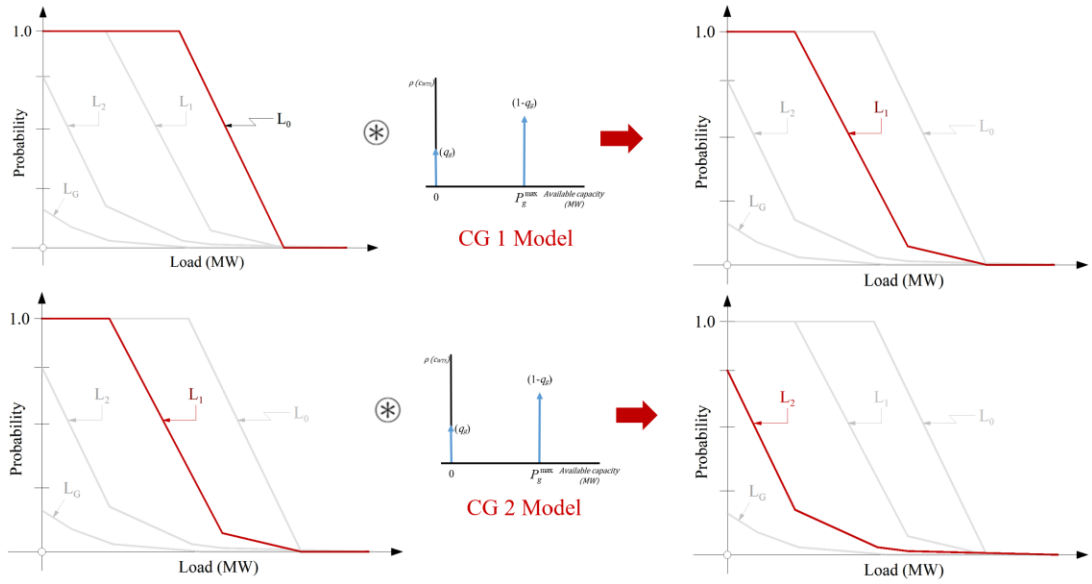

Figure 3-3. Convolution example between the ELDC and two CG units.

After all units are loaded, LOLP is simply:

$$LOLP = L_G(0) \tag{3.6}$$

EUE is computed after all units are loaded, i.e., L_G curve is constructed, as follows:

$$EUE = T \int_0^{Peak\ Load} L_G(l)\, dl \tag{3.7}$$

where *PeakLoad* is the system peak load and T is the simulation time.

EUE is the area under L_G multiplied by the total simulation time. The values of LOLP and EUE are shown Figure 3-4.

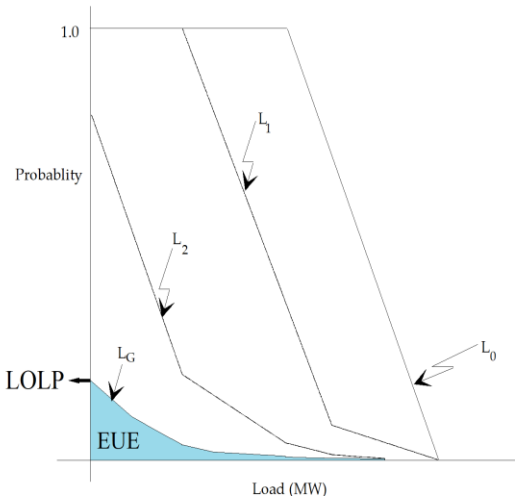

Figure 3-4. The values of LOLP and EUE.

The expected production cost for each CG, E_g, is computed as follows:

$$E_g = T(1-q_g)\int_0^{P_G^{max}} \frac{\partial f_g(l))}{dl} L_{g-1}(l)\, dl \qquad (3.8)$$

where $\frac{df_g(l)}{dl}$ is incremental cost of g^{th} CG unit.

Note that other costs, e.g., maintenance cost, are neglected. The VG production cost is zero. Hence, the total production cost is the summation of the CG production costs.

CHAPTER 4. PROBABILITY CHARACTERIZATION OF WIND FARM POWER OUTPUT AND IMPACT ON SYSTEM RELIABILITY

The chapter presents a computational procedure for the generated power probability distribution function ($\rho_{WFG}(p_{WF})$) of a WF consisting of N_{WTS} WTSs. The PDF is computed using three alternate methods: (1) analytical method, (2) NSMCS, and (3) SMCS. Once $\rho_{WFG}(p_{WF})$ has been computed, using any of the three probabilistic methods mentioned, a subsequent step is to assess the overall system reliability using the PPC Method. Specifically, the WF power output probabilistic model and the electric load probabilistic model are combined to create an equivalent load duration model. The CG system must supply the equivalent load. The PPC simulates the operation of the CG system and the main operational constraints (mainly economic dispatch) to determine the expected production from the conventional units, the LOLP, the EUE, etc. For comparison purposes, the system is also simulated assuming that the operation of WF is deterministic, i.e. forced outages of the WTSs are ignored. An overview of reliability assessment procedure in precedence of wind generation is shown in Figure 4-1.

4.1 Problem Statement and Basic Calculations

Given a number of WTSs i = 1,…, N_{WTS}. Each WTS has FOR equals to q_{WTSi} and capacity $p_{WTS.rated}$. The wind speed over period of time t =1,..,T is assumed given. The WTS power as a function of the wind speed is also given. It is desirable to compute the PDF of the WTS generation. Subsequently, the PDF of the power output of N_{WTS} number of WTSs

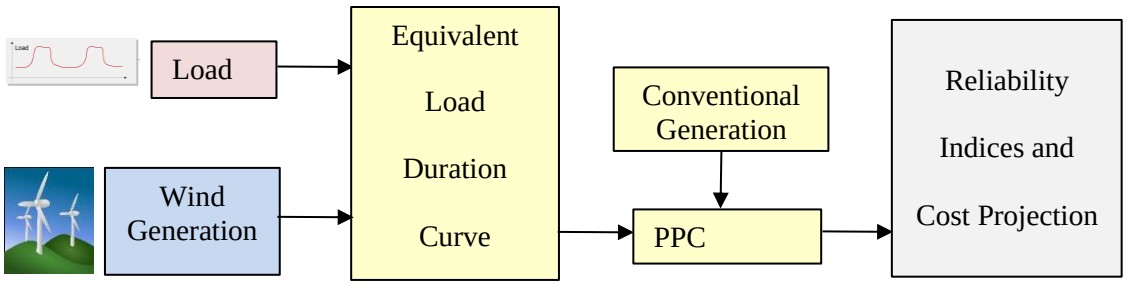

Figure 4-1. Reliability assessment procedure in presence of wind generation.

is computed. Moreover, it is also desirable to perform reliability assessment of a system, which incorporates a WF or multiple WFs, that probabilistically accounts for the WTSs unavailability and wind speed variation.

A first step is to use wind speed historical data to find the PDF of wind speed $\rho_V(v)$. One method to find $\rho_V(v)$ is to construct a histogram with a large number of bins. Subsequently, the histogram is converted to a PDF of wind speed. The fact that $\int_{-\infty}^{\infty}\rho_V(v)dv = 1$ is used to normalize the count of occurrences on the horizontal axes by dividing it over the histogram total area. Mathematically, this is expressed as follows:

$$f\left(bin_w\right) = \frac{\text{no. of occurrences of bin}_w}{\sum_1^W \text{bin width x no. of occurrences of bin}_w} \qquad (4.1)$$

Once $\rho_V(v)$ is known, the wind turbine power curve can be utilized to find the PDF of the WTS power ($\rho_{TG}(p_{WTS})$) as discussed in the next sections. p_{WTS} can be mathematically expressed as follows [37]:

$$p_{WTS} = \begin{cases} p_{WTS.rated}\left(\dfrac{V_t^{\,s} - v_{ci}^{\,s}}{v_{rated}^{\,s} - v_{ci}^{\,s}}\right) & \forall V_t \in \left(v_{ci}, v_{rated}\right) \\ p_{WTS.rated} & \forall V_t \in \left[v_{rated}, v_{co}\right) \\ 0 & \text{otherwise} \end{cases} \quad (4.2)$$

Where v_{ci} /v_{co} /v_{rated} are the WTS cut-in/ cut-out/ rated speeds, respectively, and *s* typically equals 1,2, or higher values depending on the WTS type. *s* is chosen to be 1 throughout this study. The above probability is conditional upon the availability of the WTS. If the WTSs are close to each other, then wake effect must be considered in this model. In this work, the wake effect is not considered as the WF under study is located in mountainous areas with sufficient separation that wake effect is not a major factor.

4.2 Mathematical Formulation of WF Power Output PDF computation

Three alternative methods are used to compute the WF power PDF as follows:

4.2.1 Analytical Probabilistic Method

The WTS is modeled as a 2-state model: available or unavailable. In other words, either the unit is available with capacity equal to $p_{WTS.rated}$ or unavailable with capacity equal to zero, as shown in Figure 4-2. Note that more complicated models are available where each component of a WTS has a two-state Markov model.

The probability that the i^{th} WTS is unavailable is denoted by q_{WTSi} and calculated as explained in [3]:

$$q_{WTS_i} = \frac{MTTR_{WTS_i}}{MTTF_{WTS_i} + MTTR_{WTS_i}} \tag{4.3}$$

where $MTTR_{WTS}$ is the WTS mean time to repair and $MTTF_{WTS}$ is the WTS mean time to failure. Both $MTTR_{WTS}$ and $MTTF_{WTS}$ are exponentially distributed. Note that q_{WTSi} is assumed identical for all WTSs.

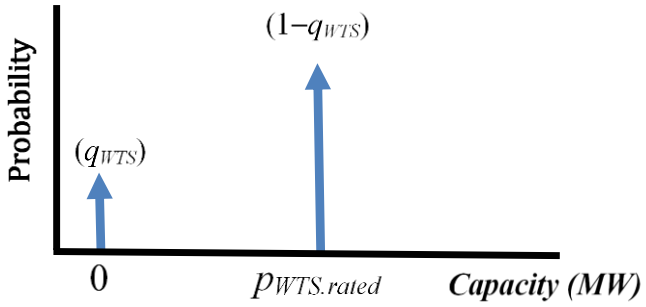

Figure 4-2. The WTS two-state availability model.

To find the probability of all possible cases, Figure 4-3 and Figure 4-4 could be helpful. The law of total probability is used to account for all cases:

$$\begin{aligned} \rho_{TG}\left(p_{WTS}\right) = {} & \rho_{TG}\left(p_{WTS} \mid WTS\ is\ UP\right)\left(1\text{-}q_{WTS}\right) \\ & + \rho_{TG}\left(p_{WTS} \mid WTS\ is\ DOWN\right)\left(q_{WTS}\right) \end{aligned} \tag{4.4}$$

where $\rho_{TG}\left(p_{WTS}\right)$ is the PDF of a single WTS power output.

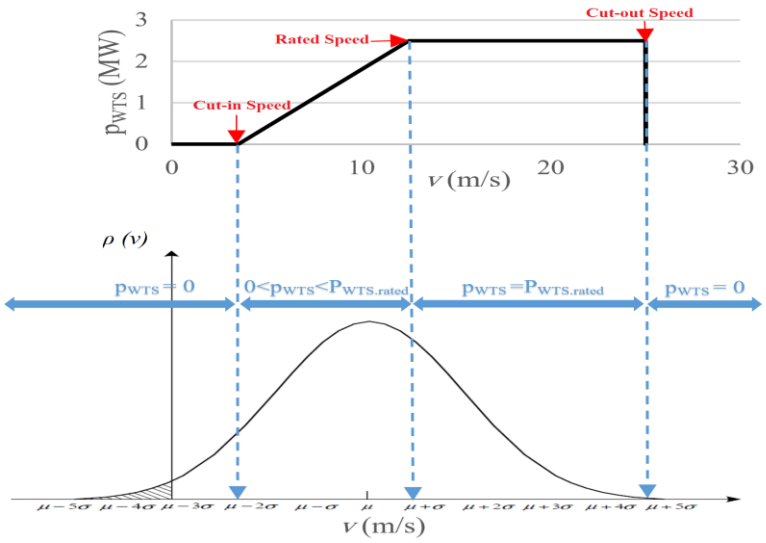

Figure 4-3. WTS power curve and wind speed PDF relationship.

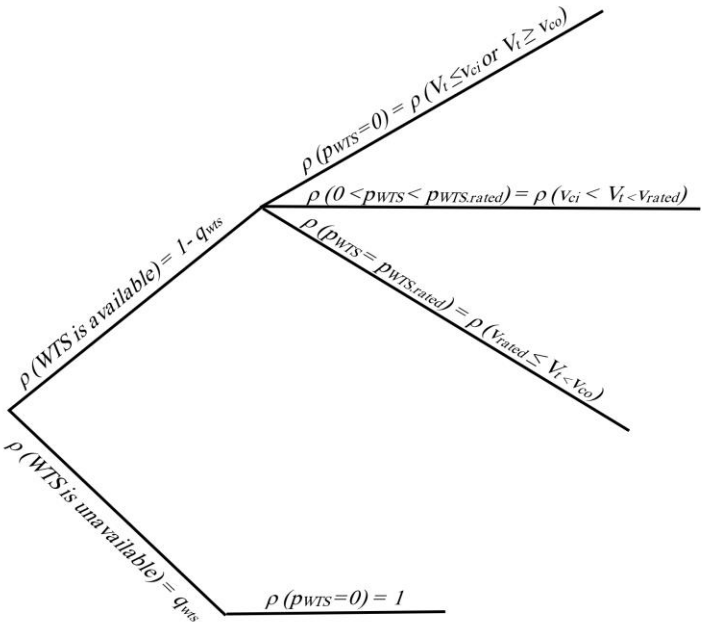

Figure 4-4. Probability tree for single WTS possible outcomes.

For $p_{WTS} = 0$, there are three possibilities: either the WTS is failed, $V_t \le v_{ci}$, or $V_t \ge v_{co}$, thus a single WTS power output pdf $\rho_{TG}(p_{WTS})$:

$$\rho_{TG}(0) = (q_{WTS} + (1 - q_{WTS})(A))\delta(p_{WTS}) \quad (4.5)$$

where $A = \int_{-\infty}^{v_{ci}} \rho_V(v)dv + \int_{v_{co}}^{\infty} \rho_V(v)dv = F_V(v_{ci}) + 1 - F_V(v_{co})$

For $0 < p_{WTS} < p_{WTS.rated}$, it is a continuous region that can be expressed mathematically as follows:

$$\rho_{TG}(p_{WTS}) = (1 - q_{WTS})\rho_V(V_t) \quad \forall V_t \in (v_{ci}, v_{rated}) \quad (4.6)$$

For $p_{WTS} = p_{WTS.rated}$, the wind speed ranges $v_{rated} < V_t < v_{co}$. This is expressed mathematically as follows:

$$\rho_{TG}(p_{WTS.rated}) = (1 - q_{WTS})(B)\delta(p_{WTS} - p_{WTS.rated}) \quad (4.7)$$

where $B = \int_{v_{rated}}^{v_{co}} \rho_V(v)dv = F_V(v_{co}) - F_V(v_{rated})$

In the case of a WF, there are N_{WTS} WTSs. The probability mass function (PMF) of WF availability ($\rho_{WFA}(c_{WF})$) is expressed using the binomial distribution as follows:

$$\rho_{WFA}(c_{WF}) = \sum_{r=0}^{N_{WTS}} \binom{N_{WTS}}{r} (1 - q_{WTS})^r (q_{WTS})^{N_{WTS} - r} \delta(c_{WF} - r\, rp_{WTS.rated}) \quad (4.8)$$

where r is number of operational WTS in the WF. $\rho_{WFA}(c_{WF})$ is shown in Figure 4-5.

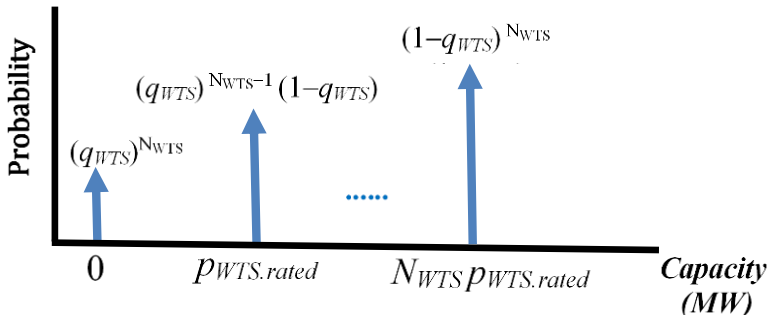

Figure 4-5. The WF availability PMF ($\rho_{WFA}(c_{WF})$).

The $\rho_{WFG}(p_{WF})$ is generalized for N_{WTS} WTSs as follows:

For $p_{WF} = 0$,

$$\rho_{WFG}(0)=\left(q_{WTS}{}^{N_{WTS}}+\left(\sum_{r=1}^{N_{WTS}}\binom{N_{WTS}}{r}(1-q_{WTS})^{r}(q_{WTS})^{N_{WTS}-r}\right)A\right)\delta(p_{WF}) \qquad (4.9)$$

For $0 < p_{WF} < r\,p_{WTS.rated}$,

$$\rho_{WFG}(rp_{WTS})=\binom{N_{WTS}}{r}(1-q_{WTS})^{r}(q_{WTS})^{N_{WTS}-r}\,\rho_{v}(V_{t}) \qquad (4.10)$$

where p_{WTS} as in eq.(4.2) $\quad \forall V_t \in (v_{ci}, v_{rated})$

For this case, $\rho_{WFG}(rp_{WTS})$ should be calculated for all possible values of $rp_{WTS} \in [0, r\,p_{WTS.rated}]$ for all r, and eventually sum up all probabilities resulting from equal rp_{WTS} values.

For $p_{WF} = r\, p_{WTS.rated}$,

$$\rho_{WFG}\left(r\, p_{WTS.rated}\right) = \binom{N_{WTS}}{r}\left(1-q_{WTS}\right)^{r}\left(q_{WTS}\right)^{N_{WTS}-r}\left(B\right)\delta\left(p_{WF} - r\, p_{WTS.rated}\right) \quad \forall r \in [1,2,...,N_{WTS}] \tag{4.11}$$

4.2.2 Non-Sequential Monte Carlo Simulation

In this method, the state sampling is non-chronological, i.e., specific $MTTF_{WTS}$ and $MTTR_{WTS}$ do not have direct effect. Rather, any combination of $MTTF_{WTS}$ and $MTTR_{WTS}$ based on equation (4.3) with equal availability would have similar results. The states of the WTSs availability are modeled as uniform distribution random variable (*Y)* where *Y*~unif*(0,1)*. Subsequently, the availability states for each WTS are calculated as follows [12]:

$$Q_{WTSi,m} = \begin{cases} 0\ , & Y_{i,m} \le q_{WTS} \\ 1\ , & Y_{i,m} > q_{WTS} \end{cases} \quad \forall i \in \{1,2,..N_{WTS}\}, \forall m \in \{1,2,..M\} \tag{4.12}$$

where $Q_{WTSi,m}$ represents the availability state of WTS *i* at sample *m*, and $Y_{WTSi,m}$ is the random number uniformly distributed between 0 and 1 for WTS *i* at state *m*. Afterwards, *M* wind speed samples are generated by duplicating the available wind speed data. Note that *M* in this study is chosen to be multiple of the available wind speed data size, e.g., *M* = 10×the size of the wind speed data. Finally, under the assumption that all WTSs are subject to the same wind speed at each sample *m*, the power output values for the WF is generated as shown in equation (4.13).

$$p_{WF} = \begin{cases} \sum_{i=1}^{N_{WTS}} Q_{WTS_i,m} \left(p_{WTS.rated} \left(\dfrac{V_m^s - v_{ci}^s}{v_{rated}^s - v_{ci}^s} \right) \right) & \forall V_m \in \left(v_{ci}, v_{rated} \right) \\ \sum_{i=1}^{N_{WTS}} Q_{WTS_i,m} p_{WTS.rated} & \forall V_m \in \left[v_{rated}, v_{co} \right) \\ 0 & \text{Otherwise} \\ & \forall m \in \{1, 2, \ldots, M\} \end{cases} \quad (4.13)$$

Subsequently, $\rho_{WFG}(p_{WF})$ is calculated similar to the method used to find $\rho_V(v)$.

4.2.3 Sequential Monte Carlo Simulation

In this method, the state sampling is chronological, i.e., $MTTF_{WTS}$ and $MTTR_{WTS}$ are used in the state duration samples [12]. This is explained as follows: *M* is the size of the samples, as in the non-sequential case. *M* could be interpreted as the length of multiple cycles; each cycle has the length of the original wind speed data size. For each cycle, there are sub-cycles when the WTS is either UP or DOWN as explain next:

When WTS is UP, it transitions to the DOWN state with rate equals to:

$$\lambda_{WTS} = \frac{1}{MTTF_{WTS}} \quad (4.14)$$

When WTS is DOWN, it transitions to the UP state with rate equals to:

$$\mu_{WTS} = \frac{1}{MTTR_{WTS}} \quad (4.15)$$

The failure and repair processes are assumed to be exponentially distributed. These processes are modeled as a continuous time Markov chain. The following two equations describe being in either UP/ DOWN State and transitioning to either DOWN/UP:

$$\frac{dP_{UP}(t)}{dt} = \mu_{WTS}\ P_{DOWN}(t) - \lambda_{WTS}\ P_{UP}(t)$$

$$\frac{dP_{DOWN}(t)}{dt} = \lambda_{WTS} P_{UP}(t) - \mu_{WTS} P_{DOWN}(t)$$

Solving for the previous equations gives:

$$P_{DOWN}(t) = p_{DOWN}(0)\left(\frac{\lambda_{WTS} + \mu_{WTS} e^{-(\lambda_{WTS}+\mu_{WTS})t}}{\lambda_{WTS}+\mu_{WTS}}\right) + p_{UP}(0)\left(\frac{\lambda_{WTS} - \lambda_{WTS} e^{-(\lambda_{WTS}+\mu_{WTS})t}}{\lambda_{WTS}+\mu_{WTS}}\right)$$

$$P_{UP}(t) = p_{DOWN}(0)\left(\frac{\mu_{WTS} - \mu_{WTS} e^{-(\lambda_{WTS}+\mu_{WTS})t}}{\lambda_{WTS}+\mu_{WTS}}\right) + p_{UP}(0)\left(\frac{\mu_{WTS} + \lambda_{WTS} e^{-(\lambda_{WTS}+\mu_{WTS})t}}{\lambda_{WTS}+\mu_{WTS}}\right)$$

Assuming $p_{DOWN}(0) = 0$ and $p_{UP}(0) = 1$, and as $t \to \infty$:

$$P_{UP} = \frac{\mu_{WTS}}{\lambda_{WTS} + \mu_{WTS}} = 1 - q_{WTS} \qquad (4.16)$$

$$P_{DOWN} = \frac{\lambda_{WTS}}{\lambda_{WTS} + \mu_{WTS}} = q_{WTS} \qquad (4.17)$$

For each sub-cycle (UP or DOWN), a uniform random number is generated, $U \sim \text{unif}(0,1)$. The duration sample is calculated using the inverse transform method, as follows:

$$T_{Up} = -MTTF_{WTS}(\ln(U)) \tag{4.18}$$

$$T_{Down} = -MTTR_{WTS}(\ln(U)) \tag{4.19}$$

When the WTS is DOWN for period of T_{Down}, the WTS contribution to WF generated power equals zero. On the other hand, when the WTS is UP, the output is computed as has been discussed earlier: WF power output is the summation of the power generated of the UP units. Finally, $\rho_{WFG}(p_{WF})$ is evaluated similar to the method used to find $\rho_V(v)$.

4.3 Reliability Assessment Based on WF Generated Power PDF

The original PPC method is slightly modified to account for the addition of WF generation. In this case, the load duration is the combination of the actual load minus the WFs generation output. We refer to this as the equivalent load duration, ELDC. The ELDC is computed from the WF probabilistic model and the actual load probabilistic model. The ELDC is computed as follows:

$$\text{ELDC} = \text{Forecasted Load} - \text{Expected WF Power} \tag{4.20}$$

WF expected power output is computed from the three probabilistic methods used to compute $\rho_{WFG}(p_{WF})$: first, hourly Gaussian distributions with means $\hat{\mu}_h$ and standard deviations $\hat{\sigma}_h$ (h = 1,2,…,24) are estimated from the historical wind data. Afterwards, all possible wind speed values are found and converted to power using equation (4.2) with N_{WTS} number of WTSs. Then, the probabilistic expectation is found using the sample WF

power found and their corresponding probability, i.e., $\rho_{WFG}(p_{WF})$. Subsequently, the ELDC is computed using the forecasted load minus the expected values of WF power output. The resultant curve is converted to an IPDF as required by the PPC method. The vertical axis of the IPDF is probability and horizontal axis is the total load (l). Note that all reliability and cost indices are calculated as in mentioned previously in section 3.1.2.

4.4 Case Study

The hourly wind speeds for a year is collected from the System Advisory Model (SAM) [38]. The location under study is at a rolling hills area in AZ, USA. The wind speed data PDF, $\rho_V(v)$, and CDF, $F_V(v)$, of this site are found as described before and is shown in Figure 4-6 and Figure 4-7, respectively. Under the assumption that all WTSs are subject to the same wind regime and have the same specifications, $\rho_{WFG}(p_{WF})$ can be found using one of the three methods described previously. Siemens Wind Turbine (SWT-2.5-120) specification is utilized to perform the analysis of different cases [39]. Theses specifications are: $p_{WTS.rated}$ = 2.5 MW, v_{ci} = 3 m/s, v_{rated} = 11 m/s, and v_{co} = 22 m/s. q_{WTS} is assumed to be 0.15, $MTTF_{WTS}$ = 950 hrs. and $MTTR_{WTS}$ = 167.7 hrs. N_{WTS} in the WF under study is 10. The reliability test system consists of the following: (1) two CG units each has capacity of 58 MW and FOR = 0.05, (2) the WF mentioned previously, and (3) load with the p.u. data taken from the RTS test system considering a base of 100 MW [40], described in details in APPENDIX A. The test system topology is shown in Figure 4-8.

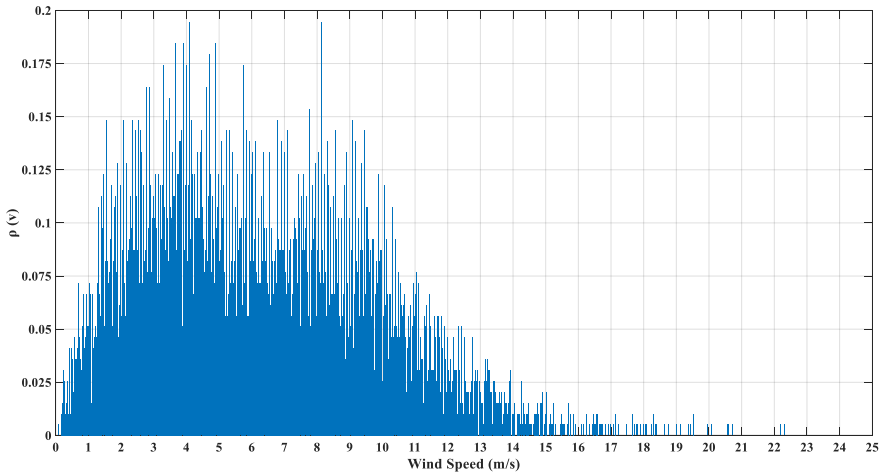

Figure 4-6. The wind speed PDF.

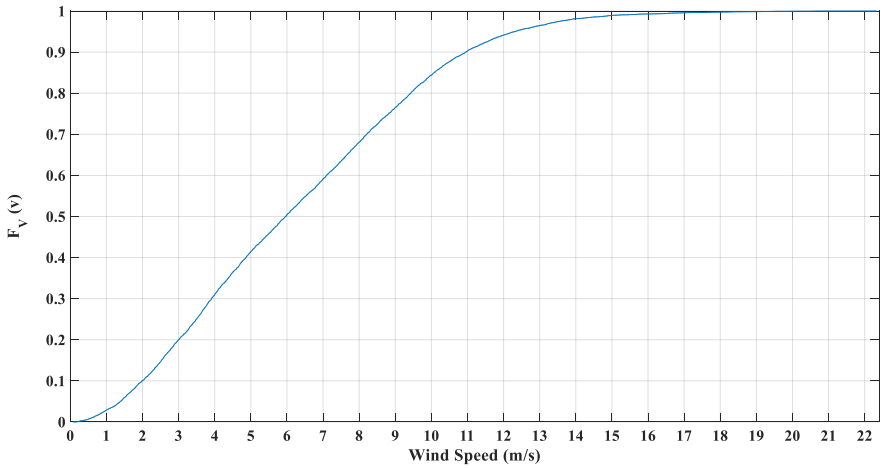

Figure 4-7. The wind speed CDF.

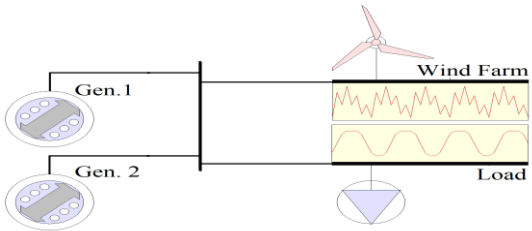

Figure 4-8. The reliability test system.

4.4.1 Analytical Probabilistic Method Results

Equations (4.9), (4.10) and (4.11) were used to find $\rho_{WFG}(p_{WF})$ for a WF that consists of 10 WTSs. Figure 4-9 shows $\rho_{WFG}\ (p_{WF})$ found using the analytical approach. The probability at 0 MW is 0.1987. Equation (4.9) shows that $p_{WF} = 0$ is because either all WTSs are at a failure state or wind speeds are out of the generation region of the operational WTSs. Since $(q_{WTS}=0.15)^{10} \approx 0$, having r operational WTSs out of N_{WTS}, given that the wind speeds are out of the generation region of the WTSs, contributes most to ρ_{WFG} ($p_{WF} = 0$). On the other hand, the probability at 25 MW (WF rated power) equals to 0.0193, which gives indication that the cumulative probability of wind speeds above v_{rated} and within the generation range of the WTS is small. Because in this case, $(1\text{-}q_{WTS})^{10} \approx 0.1969$ multiplied by $F_V\ (v_{rated} < V_t < v_{co})$. Note that there are impulses at $r\ p_{WF.rated}$, where $r = 0, 1,\ldots, 10$, generated mostly from equations (4.9) and (4.10) and small contribution small contribution from equation (4.11).

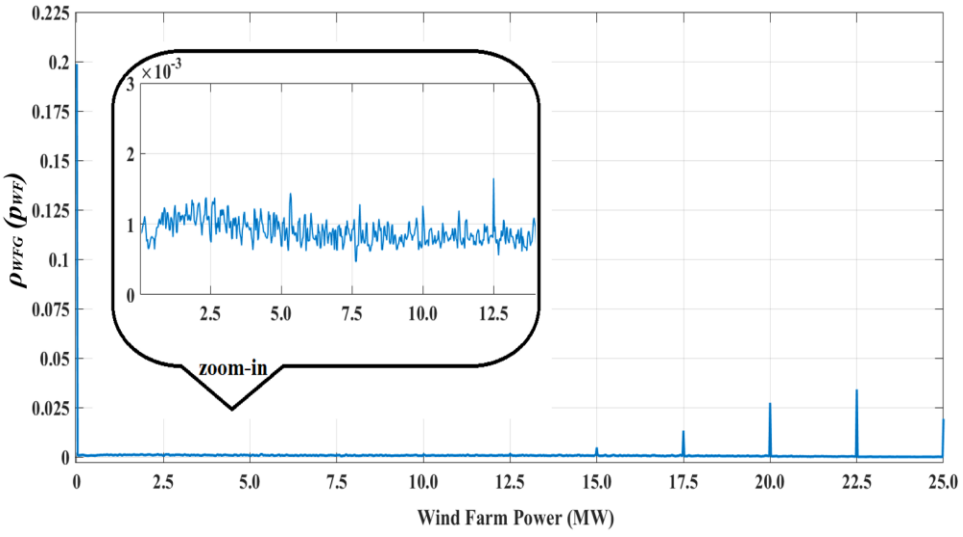

Figure 4-9. $\rho_{WFG}\ (p_{WF})$ using the analytical method.

4.4.2 Non-Sequential Monte Carlo Simulation Results

The state sampling was used to non-chronologically generate hourly UP and DOWN states. *M* is chosen to be 10 times the wind speed data size, i.e., *M* simulates 10 years of the WTSs UP and DOWN states. Equation (4.13) was used to evaluate p_{WF} and subsequently $\rho_{WFG}(p_{WF})$. Figure 4-10 shows $\rho_{WFG}(p_{WF})$. The probability at 0 MW is 0.2001, compared to 0.1987 in the analytical case. On the other hand, the probability at 25 MW equals to 0.0191 compared to 0.0193 in the analytical case. The comparison is favorable.

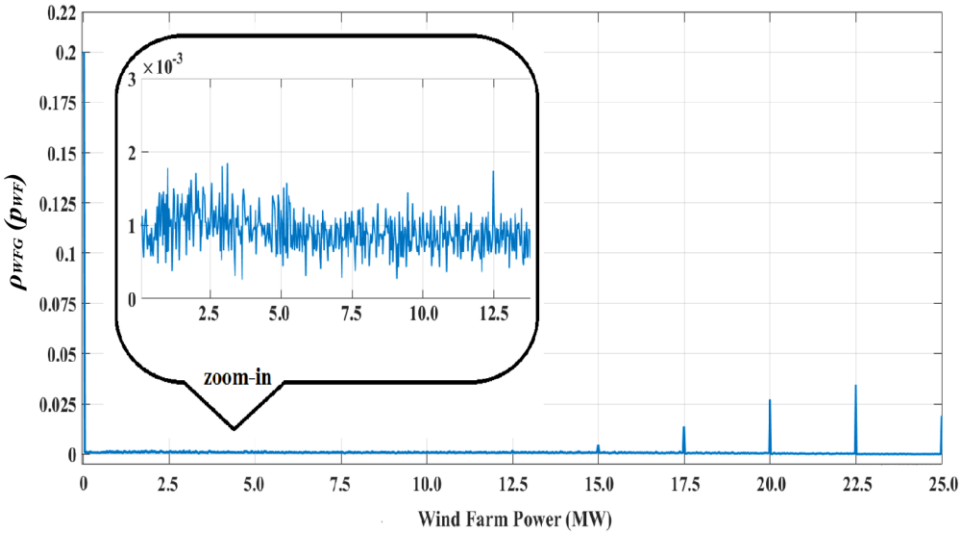

Figure 4-10. $\rho_{WFG}(p_{WF})$ using the NSMCS.

4.4.3 Sequential Monte Carlo Simulation Results

As explained earlier, UP and DOWN sub-cycles are chronologically generated with *M* equals 10 times the wind speed data size. For each year, sub-cycles of UP and DOWN are generated using equation (4.18) and (4.19). The probability at 0 MW is 0.2001, compared to 0.1987 in the analytical case. On the other hand, the probability at 25 MW equals to 0.0185 compared to 0.0193 in the analytical case. Figure 4-11 shows $\rho_{WFG}(p_{WF})$.

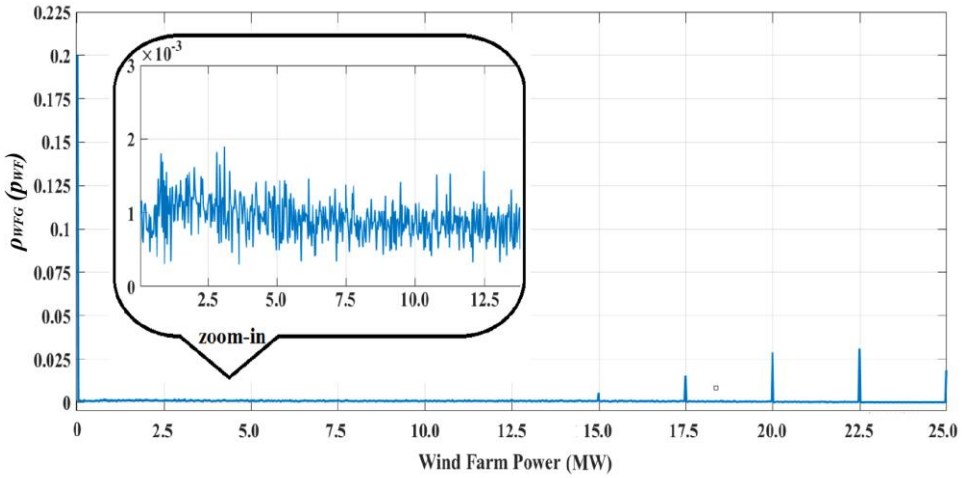

Figure 4-11. $\rho_{WFG}(p_{WF})$ using the SMCS.

The numerical values off all three methods are shown in Table 4-1. A comparison of the WF generated power CDF ($F_{WFG}(p_{WF})$) found using all three methods is shown in Figure 4-12. All three methods could be used to evaluate $\rho_{WFG}(p_{WF})$. However, an advantage of the MCS method over the analytical solution is the capability to simulate complex systems without the need for complex derivations. An example is when FORs are not identical across simulated WTSs or there are derated states. It would be computationally challenging to derive all possible events. Further, SMCS has an advantage over the two other methods because of its ability to preserve the chronology of the process under study, e.g., failure or repair. This could be crucial, for example, when WTS is coupled with a storage system.

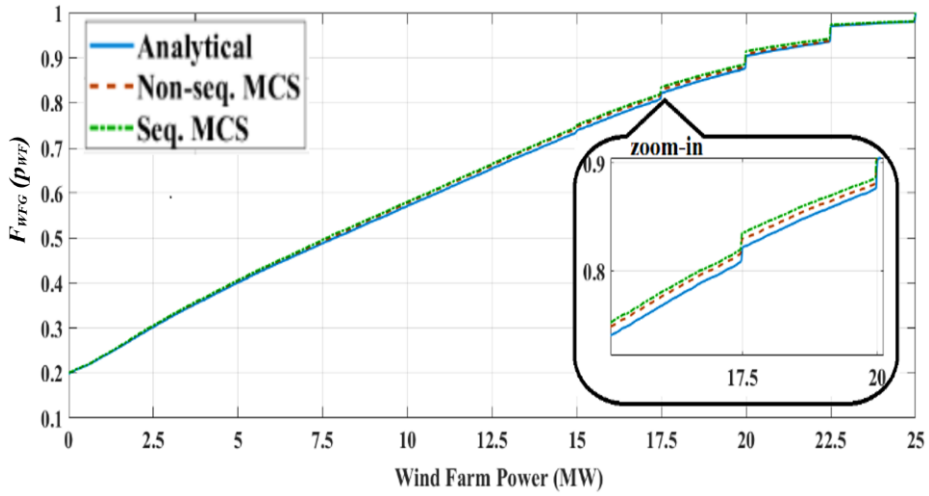

Figure 4-12. F_{WFG} (p_{WF}) for all three methods.

Table 4-1. $\rho_{WFG}(p_{WF})$ values at 0 ~10 $p_{WTS.reated}$.

p_{WF} (MW)	Analytic	NSMCS	SMCS
0	0.1987	0.2001	0.2001
2.5	0.0008	0.0012	0.0011
5	0.0006	0.0012	0.0011
7.5	0.0009	0.0012	0.0014
10	0.0013	0.0012	0.0010
12.5	0.0017	0.0017	0.0010
15	0.0048	0.0048	0.0054
17.5	0.0134	0.0137	0.0153
20	0.0274	0.0273	0.0287
22.5	0.0342	0.0347	0.0311
25	0.0193	0.0191	0.0185

4.4.4 Reliability Assessment Results

Table 4-2 shows the reliability assessment using the PPC method of all cases. When there was no wind generation the LOLP = 0.05495. After the addition of the WF to the test system, the LOLP was lowest when the WF farm output was deterministic (WTSs

unavailability is ignored). In this case, it was reduced by 34.8%. When using the inverse transform sampling (F^{-1}_{WFG} *(random generated numbers from a uniform distribution)*), the averages of running the PPC 10 years (each with 8760 samples) of all indices were close to the deterministic forecast results. The reduction in this case ranged 32.1% ~ 33.1%. Whereas the results of using the Gaussian distribution sampling gave higher LOLPs values since it computed the probabilistic expectation of the hourly WF power output. The LOLP was reduced 21.4% ~23.5%. The EUE and expected CG results followed the same pattern as the LOLP did.

Table 4-2. PPC results of all cases.

Case	LOLP	EUE (MWh)	Expected CG (MWh)
Base case (No WF generation)	0.05495	7,577.1	533,999.7
Deterministic WF output (WTSs FORs ignored)	0.03582	4,370.5	442,457.8
Analytical (Inverse Transform Sampling)	0.03675	4,545.3	455,347.8
Analytical (Gaussian)	0.04304	5,243.4	486,763.8
NSMCS (Inverse Transform Sampling)	0.03730	4,577.9	456,428.1
NSMCS (Gaussian)	0.04320	5,261.9	486,0523.2
SMCS (Inverse Transform Sampling)	0.03708	4,561.0	455,866.6
SMCS (Gaussian)	0.04205	5,093.8	482,687.0

4.5 Conclusions

Three different probabilistic methods were presented in this chapter to compute the power output PDF of a WF consisting of multiple WTSs. The three methods were discussed in detail, and a case study on a WF that consists of 10 WTSs has been presented. First the power output PDF was computed analytically. In addition, both NSMCS and SMCS were

used to simulate WTSs failures non-chronologically and chronologically, respectively. The resulting PDFs computed with all three methods were found to be very close. Subsequently, the PPC method was used to compute the system reliability by combining the WF power outputs PDFs and the electric load probabilistic model. The probabilistic WF power output model and the electric load model were combined to provide an equivalent load duration model which was inputted to the PPC method. The results of the PPC provided reliability indices for the system. These indices quantified the impact of wind farms on the reliability of the system.

CHAPTER 5. PROBABILITY CHARACTERIZATION OF SOLAR FARM POWER OUTPUT AND IMPACT ON SYSTEM RELIABILITY

The chapter presents a computational procedures of generated power probability distribution function of a SF ($\rho_{SFG}(p_{SF})$) consisting of N_{SCG} SCGs. Probabilistic methods are utilized to compute $\rho_{SFG}(p_{SF})$ in a certain location and assumed FORs of the SCGs. Three methods have been investigated: (1) analytical, (2) SMCS and (3) NSMCS. The study aims to draw a comparison of these alternate methods. $\rho_{SFG}(p_{SF})$ is dependent on the solar radiation historical data, FOR of individual SCGs and operating constraints of SCGs. Once $\rho_{SFG}(p_{SF})$ has been computed, using any of the three probabilistic methods mentioned previously, the PPC method is used to assess the reliability of the overall system. Specifically, the SF power output probabilistic model and the electric load probabilistic model are combined to create an ELDC model. The CG system must supply the equivalent load. The PPC simulates the operation of the CG system and the main operational constraints (mainly economic dispatch) to determine the expected production from the conventional units, the LOLP, the EUE, etc. For comparison purposes, the system is also simulated assuming that the operation of SF is deterministic, i.e. forced outages of the SCGs are ignored. An overview of reliability assessment procedure in precedence of solar generation is shown in Figure 5-1.

.

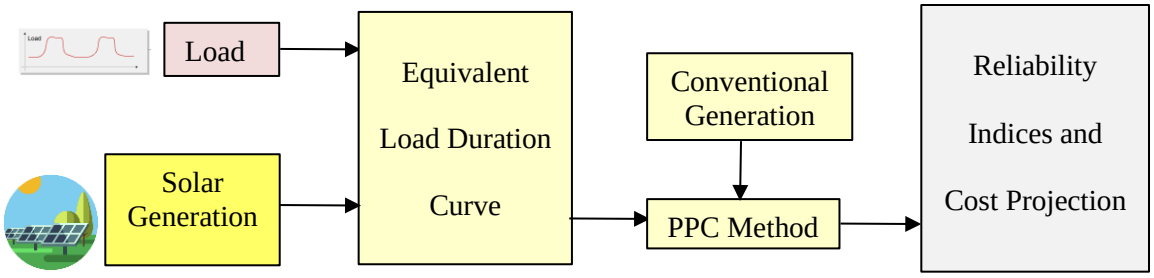

Figure 5-1. Reliability assessment procedure in presence of solar generation.

5.1 Problem Statement and Basic Calculations

Given a number of SCGs $i = 1,\ldots,N_{SCG}$, each SCG has FOR q_{SCGi} and availability $1-q_{SCGi}$. The solar radiation over period of time $t = 1,\ldots,T$ is assumed given as a forecast. Also, each SCG capacity is known. Moreover, SCG power (p_{SCG}) versus solar radiation (G) curve is known, given that the SCG is available. It is desired to find the PDF of individual SCG power ($\rho_{SG}(p_{SCG})$). Subsequently, the PDF of the power output of N_{SCG} SCGs is found. Moreover, it is desirable to compute the ELDC probabilistically and to perform reliability assessment using the PPC method. The reliability assessment is performed on a test system that incorporates a SF or multiple SFs to compute LOLP and EUE, and other indices. The reliability indices computed with this procedure account for the SCG forced outages and solar radiation variability.

The first step is to use the solar radiation historical data of a specific location to find pdf of the solar radiation ($\rho_G(g)$). One method to find $\rho_G(g)$ is to construct a histogram with appropriate number of bins. To convert the histogram to a PDF, the fact that $\int_{-\infty}^{\infty}\rho_G(g)dg = 1$ is used. The counts of occurrences on the horizontal axes of the histogram for each step (bin) are normalized by dividing them by the histogram total area, similar to

finding the pdf of wind speed. Once $\rho_G(g)$ is known, the solar power versus solar radiation curve, conditional upon the availability of the SCG, can be utilized to find the SCG power PDF, $\rho_{SG}(p_{SCG})$. p_{SCG} can be mathematically expressed as follows [5]:

$$p_{SCG} = \begin{cases} p_{SCG.rated}\left(\dfrac{G_t^2}{G_{std}R_C}\right) & \forall G_t \in [0, R_C) \\ p_{SCG.rated}\left(\dfrac{G_t}{G_{std}}\right) & \forall G_t \in [R_C, G_{std}] \\ p_{SCG.rated} & \forall G_t \in (G_{std}, \infty) \end{cases} \quad (5.1)$$

Where R_c is a certain radiation point set usually at 150 W/m^2 and G_{std} the solar radiation in the standard environment , measured in W/m^2.

5.2 Probabilistic Evaluation of SF Generated Power PDF

Three probabilistic methods, analytical, NSMCS and SMCS for evaluating $\rho_{SFG}(p_{SF})$ are described next in detail.

5.2.1 Analytical Probabilistic Method

The SCG is modeled as a 2-state model: either the unit *i* is available with capacity equal to $p_{SCG.rated}$ or unavailable with capacity equal to zero, as depicted in Figure 5-2. The probability that the i^{th} SCG is unavailable, q_{SCGi}, is calculated as in [3]:

$$q_{SCGi} = \frac{MTTR_{SCGi}}{MTTF_{SCGi} + MTTR_{SCGi}} \quad (5.2)$$

where $MTTR_{SCG}$ is the unit mean time to repair and $MTTF_{SCG}$ is the mean time to failure of a SCG. Both $MTTR_{SCG}$ and $MTTF_{SCG}$ are exponentially distributed. Note that q_{SCGi} is assumed to be identical for all SCGs.

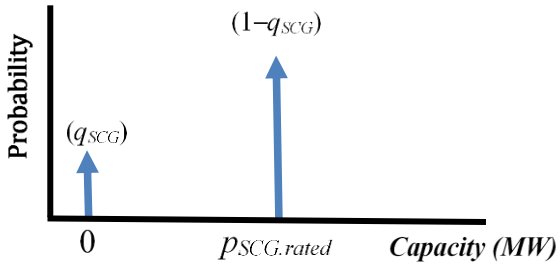

Figure 5-2. The SCG two-state availability model.

Figure 5-3 and Figure 5-4 are important to derive all the cases analytically. To find the probability of all possible cases, the law of total probability is used:

$$\begin{aligned}\rho_{SG}\left(p_{SCG}\right) = {} & \rho_{SG}\left(p_{SCG} \mid SCG\ is\ UP\right)\left(1\text{-}q_{SCG}\right) \\ & + \rho_{SG}\left(p_{SCG} \mid SCG\ is\ DOWN\right)\left(q_{SCG}\right)\end{aligned} \tag{5.3}$$

For $p_{SCG} = 0$, there are two possibilities: either the unit is in a failure state, or $G_t = 0$:

$$\rho_{SG}\left(0\right) = \left(q_{SCG} + \left(1 - q_{SCG}\right) F_G\left(G_t = 0\right)\right)\delta\left(p_{SCG}\right) \tag{5.4}$$

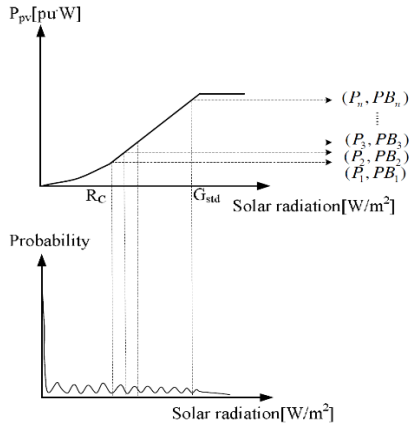

Figure 5-3. SCG power and solar irradiance PDF relationship [16].

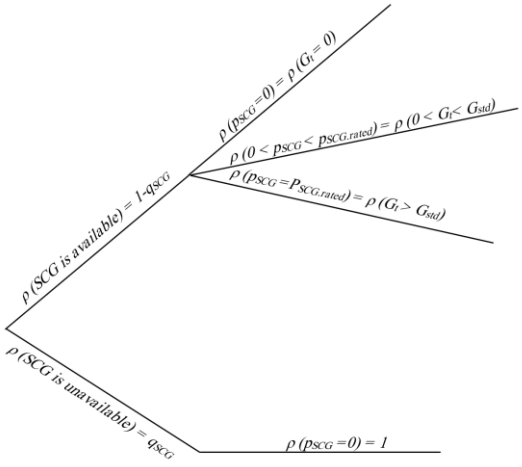

Figure 5-4. Probability tree for SCG possible outcomes.

For $0 < p_{SCG} < p_{SCG.rated}$, it is a continuous region. There are two regions as follows: $0 \le G_t < R_c$, and $R_c \le G_t \le G_{std}$. In this case, $\rho_{SG}(p_{SCG})$ can be expressed mathematically as follows:

$$\rho_{SG}\left(p_{SCG}\right) = \left(1 - q_{SCG}\right)\rho_G\left(G_t\right) \qquad \forall G_t \in (0, G_{std}] \tag{5.5}$$

For $p_{SCG} = P_{SCG.rated}$, the solar radiation ranges $G_t \ge G_{std}$. $\rho_{SG}(p_{SCG.rated})$ in this case can be expressed mathematically as follows:

$$\rho_{SG}\left(p_{SCG.rated}\right)=\left(1-q_{SCG}\right)\left(\int_{G_{std}}^{\infty}\rho_{G}\left(g\right)dg\right)\delta\left(p_{SCG}-p_{SCG.rated}\right) \tag{5.6}$$

Or equivalently:

$$\rho_{SG}\left(p_{SCG.rated}\right)=\left(1-q_{SCG}\right)\left(1-F_{G}(G_{std})\right)\delta\left(p_{SCG}-p_{SCG.rated}\right) \tag{5.7}$$

In the case of a SF, there are N_{SCG} SCGs. The PMF of SF availability ($\rho_{SFA}(c_{SF})$), shown in Figure 5-5, can be expressed using the binomial distribution as follows:

$$\rho_{SFA}\left(c_{SF}\right)=\sum_{r=0}^{N_{SCG}}\binom{N_{SCG}}{r}\left(1-q_{SCG}\right)^{r}\left(q_{SCG}\right)^{N_{SCG}-r}\delta\left(c_{SF}-r\,p_{SCG.rated}\right) \tag{5.8}$$

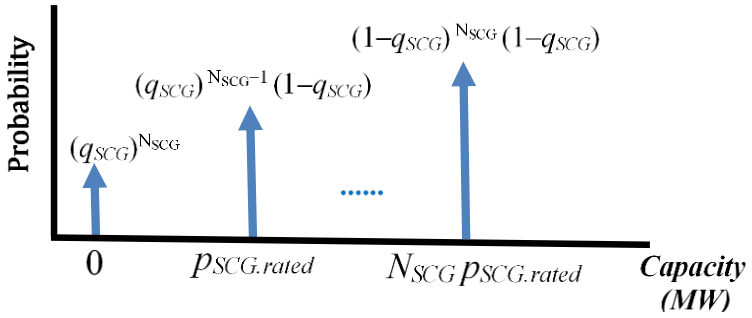

Figure 5-5. The SF availability PMF ($\rho_{SFA}(c_{SF})$).

The $\rho_{SFG}(p_{SF})$ can be generalized for N_{SCG} number of SCGs as follows:

For p_{SF} = 0,

$$\rho_{SFG}(0)=\left(q_{SCG}{}^{N_{SCG}}+\left(\sum_{r=1}^{N_{SCG}}\binom{N_{SCG}}{r}(1-q_{SCG})^{r}(q_{SCG})^{N_{SCG}-r}\right)F_G(G_t=0)\right)\delta(p_{SF}) \qquad (5.9)$$

For $0 < p_{SF} < r\,p_{SCG.rated}$,

$$\rho_{SFG}(rp_{SCG})=\binom{N_{SCG}}{r}(1-q_{SCG})^{r}(q_{SCG})^{N_{SCG}-r}\,\rho_{G}(G_t) \qquad (5.10)$$

where p_{SCG} as in eq.(5.1) $\quad \forall G_t \in [0, G_{std}]$

For this case, $\rho_{SFG}(r\,p_{SCG.rated})$ should be calculated for all possible values of $rp_{SCG} \in [0, r\,p_{SCG.rated}]$ for all r, and eventually summing up all probabilities resulting from equal rp_{SCG} values.

For $p_{SF} = r\,p_{SCG.rated}$,

$$\rho_{SFG}(r\,p_{SCG.rated})=\binom{N_{SCG}}{r}(1-q_{SCG})^{r}(q_{SCG})^{N_{SCG}-r}(1-F_G(G_{std}))\delta(p_{SF}-r\,p_{SCG.rated}) \qquad (5.11)$$

5.2.2 Non-Sequential Monte Carlo Simulation

In this method, the state sampling is non-chronological. This means if the SCG is UP/Down, it could be UP/Down in the following state and the $MTTF_{SCG}$ or the $MTTR_{SCG}$ do not affect the length of the transition from UP state to DOWN state, or vice versa. In other words, any combination of $MTTF_{SCG}$ and $MTTR_{SCG}$ based on equation (5.2) with equal availability would have similar results. The states of the SCGs availability are

modeled as uniform distribution random variable (Y) where Y~unif(0,1). Subsequently, the availability states for each SCG are converted to binary numbers as follows:

$$Q_{SCGi,m} = \begin{cases} 0 \ , \ Y_{i,m} \le q_{SCG} \\ 1 \ , \ Y_{i,m} > q_{SCG} \end{cases} \quad \forall i \in \{1,2,..N_{SCG}\}, \forall m \in \{1,2,..M\} \qquad (5.12)$$

where $Q_{i,m}$ is a binary vector that represents the availability state of SCG i at sample m, and $Y_{i,m}$ is the random number uniformly distributed between 0 and 1 for SCGi at state m. Afterwards, M solar radiation samples are generated by duplicating the available solar radiation data. Note that M in this study is chosen to be multiple of the available solar radiation data size, e.g., M = 10×the size of the solar radiation data. Finally, under the assumption that all SCGs are subject to the same solar radiation at sample m, the power output values for the SF is generated as shown in equation (5.13).

$$p_{SF} = \begin{cases} \sum_{i=1}^{N_{SCG}} Q_{N_{SCG}i,m}\, p_{SCG.rated} \left(\dfrac{G_m^2}{G_{std} R_C} \right) & \forall G_m \in [0, R_C) \\ \sum_{i=1}^{N_{SCG}} Q_{N_{SCG}i,m}\, p_{SCG.rated} \left(\dfrac{G_m}{G_{std}} \right) & \forall G_m \in [R_C, G_{std}] \\ \sum_{i=1}^{N_{SCG}} Q_{N_{SCG}i,m}\, p_{SCG.rated} & \forall G_m \in (G_{std}, \infty) \\ \\ \forall m \in \{1,2,...,M\} \end{cases} \qquad (5.13)$$

Once p_{SF} is calculated for all samples, $\rho_{SFG}(p_{SF})$ is calculated with a method similar to that for finding $\rho_G(g)$.

5.2.3 Sequential Monte Carlo Simulation

As discussed in the WF case, in this method the state sampling is chronological, i.e., $MTTF_{SCG}$ and $MTTR_{SCG}$ are randomly used to compute the state duration samples [12]. This is explained as follows: *M* is the size of the samples, as in the non-sequential case. *M* could be interpreted as the length of multiple cycles; each cycle has the length of the original solar radiation data size. For each cycle, there are sub-cycles when the SCG is either UP or DOWN as explained next:

(1) when the SCG is UP, it transitions to the DOWN state with rate:

$$\lambda_{SCG} = \frac{1}{MTTF_{SCG}} \tag{5.14}$$

(2) when the SCG is DOWN, it transitions to the UP state with rate:

$$\mu_{SCG} = \frac{1}{MTTR_{SCG}} \tag{5.15}$$

The failure and repair processes are assumed to be exponentially distributed. As derived for the WTS case, the following equations are derived:

$$P_{UP} = \frac{\mu_{SCG}}{\lambda_{SCG} + \mu_{SCG}} = 1 - q_{SCG} \tag{5.16}$$

$$P_{DOWN} = \frac{\lambda_{SCG}}{\lambda_{SCG} + \mu_{SCG}} = q_{SCG} \tag{5.17}$$

For each sub-cycle (UP or DOWN), a uniform random number is generated, *U*~unif*(0,1)*. The duration sample is calculated using the inverse transform method, as follows:

$$T_{Up} = -MTTF_{SCG}(\ln(U)) \tag{5.18}$$

$$T_{Down} = -MTTR_{SCG}(\ln(U)) \tag{5.19}$$

When the SCG is DOWN for period of T_{Down}, the SCG has no contribution to SF generated power. On the other hand, when the SCG is UP, the SF generated power is the summation of the power generated of the UP units. Finally, $\rho_{SFG}(p_{SF})$ is evaluated with a method similar to that for finding $\rho_G(g)$.

5.2.4 Reliability Assessment Based on SF Power Output PDF

The PPC method, described previously in CHAPTER 3 is used to assess the reliability when adding SF to a power system. In this case, the net load is the forecasted load minus the SFs generation output. The ELDC is computed from the SF probabilistic model and the actual load probabilistic model. The ELDC is computed as follows:

$$\text{ELDC} = \text{Forecasted Load} - \text{Expected SF Power} \tag{5.20}$$

Similar to the WF case, SF expected power output is computed from $\rho_{FG}(p_{SF})$: first, a Gaussian distribution with mean $\hat{\mu}_h$ and standard deviation $\hat{\sigma}_h$ (h = 1,2,…,24) is estimated from the historical solar radiation data. Subsequently, using equation (5.1), all possible solar radiation values are converted to power with N_{SCG} number of SCGs. Then, the sampled

SF power outputs multiplied by their corresponding probability represents the probabilistic expectation. Subsequently, the ELDC is computed using the forecasted load and the expected values of SF power output. Finally, the resultant curve is converted to an IPDF.

5.3 Case Study

The hourly solar radiation for a year is used in this study. The data was collected from the System Advisory Model (SAM) [38]. The location under study is in Phoenix, AZ (TMY2). Next, the solar radiation PDF, $\rho_G(g)$, and CDF $F_G(g)$, are found as described in section II, shown in Figure 5-6 and Figure 5-7, respectively. All SCGs are assumed to be subject to the same solar radiation and have the same specifications. Each SCG has $p_{SCG.rated}$ = 0.5 MW, G_{std} = 1000 W/m^2, and R_C = 150 W/m^2. The unavailability (q_{SCG}) = 0.15, $MTTF_{SCG}$ = 950 hrs., and $MTTR_{SCG}$ = 167.7 hrs. The number of SCGs, n, in the SF under study is 10. Finally, the reliability test system consists of the following: (1) two CG units of capacity 35 MW and FOR = 0.05 each, (2) the SF with the parameters provided earlier, and (3) load with the p.u. data taken from the RTS test system considering a base of 60 MW [40]. The test system is shown in Figure 5-8.

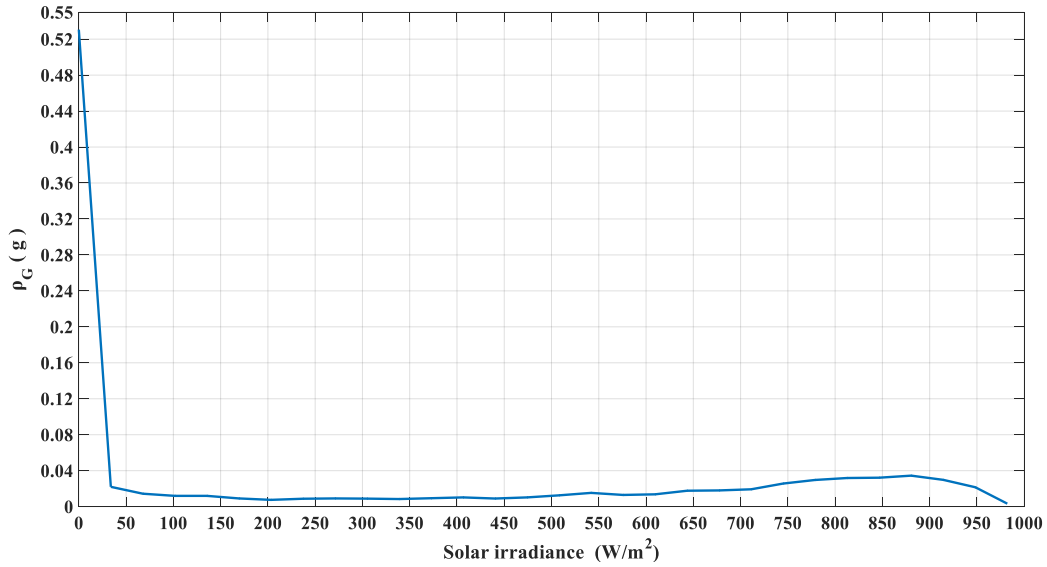

Figure 5-6. Solar radiation PDF.

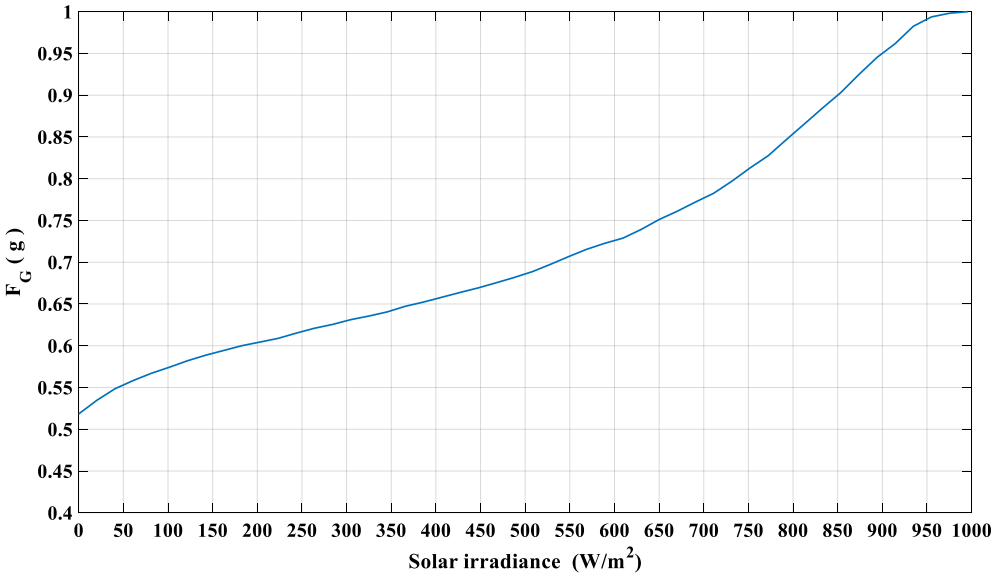

Figure 5-7. Solar radiation CDF.

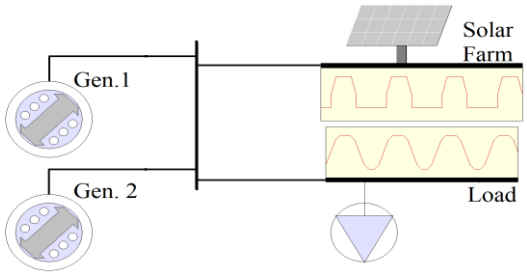

Figure 5-8. The example test system.

5.3.1 Analytical Probabilistic Method Results

ρ_{SFG} (p_{SF}) of the SF that consists of 10 SCGs was computed using the steps illustrated previously in equations (5.9), (5.10) and (5.11). Figure 5-9 shows ρ_{SFG} (p_{SF}) found using the analytical method. The probability at 0 MW is 0.5306. Equation (5.9) shows that the probability that the SF produces 0 MW comes from either all SCGs are experiencing a failure, or solar radiation is 0 W/m^2 given r out of are available. Since $(q_{SCG}=0.15)^{10} \approx 0$, having r operational SCGs out of N_{SCG} while the solar radiation is 0 W/m^2 contributes most to ρ_{SFG} ($p_{SF} = 0$). On the other hand, the probability at 5 MW (SF rated power) = 0.0002 ≈ 0, which indicates that the cumulative probability of the solar radiation above G_{std} is very close to 1. Note that the values at r $p_{SF.rated}$, where r = 0, 1,…,10, were generated mostly from equations (5.9), (5.10) and a small contribution from equation (5.11) since $F_G(G_{std}) \approx 1$ or $1-F_G(G_{std}) \approx 0$.

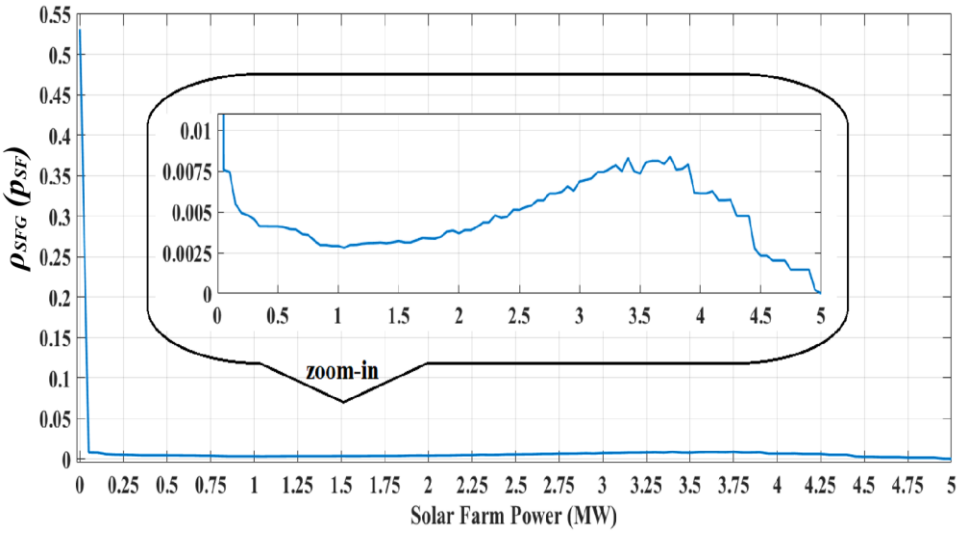

Figure 5-9. ρ_{SFG} (p_{SF}) using the analytical method.

5.3.2 Non-Sequential Monte Carlo Simulation Results

The state sampling in the case of the NSMCS is non-chronological. *M* number of hourly UP and DOWN states were generated. *M* is chosen to be 10 times the solar radiation data size, i.e., *M* simulates 10 years of the SCGs UP and DOWN states. p_{SF} was computed using equation (5.13). Subsequently, $\rho_{SFG}(p_{SF})$ was computed as mentioned before. Figure 5-10 shows $\rho_{SFG}(p_{SF})$. The probability at 0 MW is 0.5360, compared to 0.5306 in the analytical case. On the other hand, the probability at 5 MW equals to 0.0003 compared to 0.0002 In the analytical case.

5.3.3 Sequential Monte Carlo Simulation Results

In the case of the SMCS, UP and DOWN sub-cycles are chronologically generated with *M* equals 10 times the solar radiation data size. For each year, sub-cycles of UP and DOWN are generated using equations (5.18) and (5.19). The probability at 0 MW is 0.5363, compared to 0.5306 in the analytical case. On the other hand, the probability at 5 MW was

found to be 0.0004 compared to 0.0002 in the analytical case. Figure 5-11 shows $\rho_{SFG}(p_{SF})$ for this case.

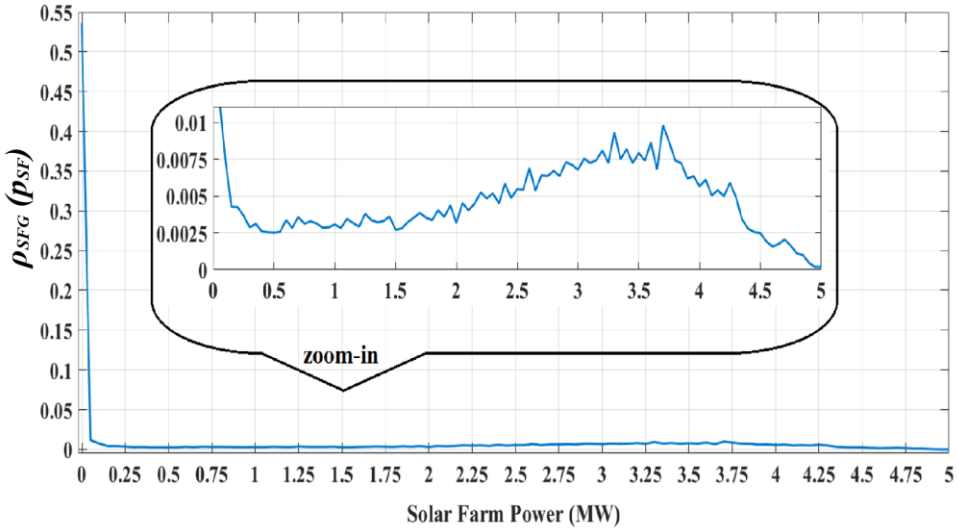

Figure 5-10. $\rho_{SFG}(p_{SF})$ using NSMCS.

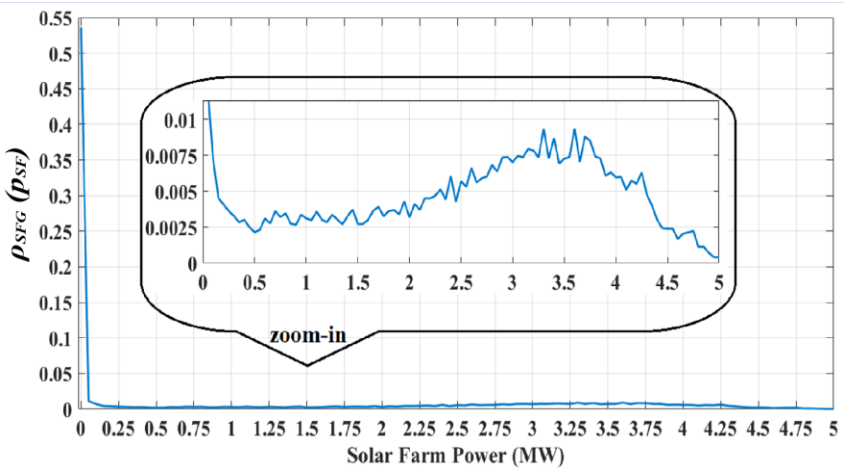

Figure 5-11. $\rho_{SFG}(p_{SF})$ using SMCS.

The numerical values of the resultant probabilities of all three cases are summarized in Table 5-1. Figure 5-12 shows a comparison between the SF generating capacity cumulative probability functions ($F_{SFG}(p_{SF})$) found using all three methods. As shown previously, three methods can be used to evaluate $\rho_{SFG}(p_{SF})$. However, the analytical method

required complex derivations that are needed to weigh in all the possible outcomes whereas both MCS methods did not. If, for example, the FORs of SCGs are not identical, or under the existence of derated states, it would be computationally challenging to mathematically derive all possible events in order to perform the analytical method. Further, the SMCS method simulates the failure and repair process chronologically.

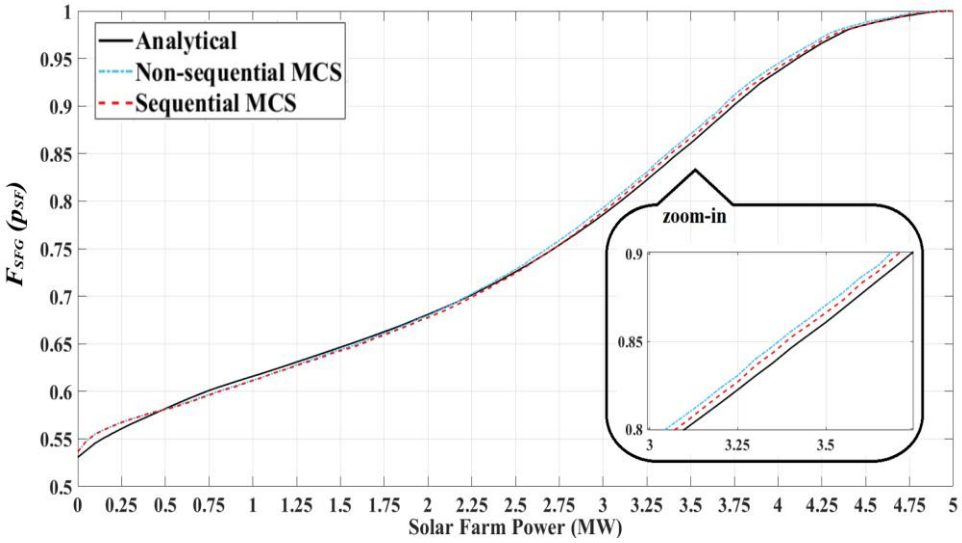

Figure 5-12. $F_{SFG}(p_{SF})$ for all three methods.

Table 5-1. ρ_{SFG} (p_{SF}) values in the range 0 ~10 $p_{SCG.reated}$.

p_{SF} (MW)	Analytical	NSMCS	SMCS
0	0.5306	0.5360	0.5363
0.5	0.0041	0.0024	0.0022
1	0.0029	0.0030	0.0031
1.5	0.0032	0.0025	0.0027
2	0.0037	0.0030	0.0032
2.5	0.0051	0.0059	0.0057
3	0.0069	0.0070	0.0070
3.5	0.0073	0.0079	0.0073
4	0.0061	0.0059	0.0060
4.5	0.0023	0.0025	0.0024
5	0.0002	0.0003	0.0004

5.3.4 Reliability Assessment Results

Table 5-2 shows the reliability assessment using the PPC method of all cases. The LOLP improved the most when the SCGs forced outages were ignored, 9.7%. Using the transform inverse sampling method ((F^{-1}_{SFG} *(random generated numbers from a uniform distribution)*), gave LOLP results higher than the deterministic SF output forecast case. The LOLP improvement range was 6.2% ~ 6.7%. On the other hand, the LOLP results were highest when SF power outputs sampled from the Gaussian distribution. In this case, the LOLP improvements were in the range of 3.8% ~ 4.6%. The EUE and the expected conventional generation of all cases followed similar pattern as the LOLP did.

Table 5-2. PPC results of all cases.

Case	LOLP	EUE (MWh)	Expected CG (MWh)
Base case (No SF generation)	0.06016	5,330.3	336,269.1
Deterministic SF output (SCGs FORs ignored)	0.05433	4,419.9	323,785.2
Analytical (Inverse Transform Sampling)	0.05644	4,792.7	326,475.7
Analytical (Gaussian)	0.05790	4,739.2	328,732.3
NSMCS (Inverse Transform Sampling)	0.05610	4,750.5	325,805.6
NSMCS (Gaussian)	0.05740	4,663.4	327,729.7
SMCS (Inverse Transform Sampling)	0.05622	4,758.5	325,919.6
SMCS (Gaussian)	0.05740	4,628.9	326,819.6

5.4 Conclusions

Three probabilistic methods were presented to evaluate SF power generation probability distribution functions. The three methods were used to find the $\rho_{FG}(p_{SF})$of an

example SF that consists of ten 0.5 MW SCGs. Based on the historical solar radiation data of a specific location, $\rho_G(g)$ was found and subsequently $\rho_{FG}(p_{SF})$ was analytically computed. The SCGs forced outages were simulated non-chronologically and chronologically using NSMCS and SMCS, respectively. The results extracted from all three methods were found to be very close. Subsequently, the PPC method was used to compute the system reliability by combining the SF power outputs PDFs and the electric load probabilistic model. By combining the probabilistic SF power output model and the electric load model, an equivalent load duration model was computed. The equivalent load duration model was inputted to the PPC method to assess the overall system reliability. The results of the PPC in terms of reliability indices quantify the impact of SF on system reliability.

CHAPTER 6. UNIT COMMITMENT AND PROBABILISTIC RELIABILITY ASSESSMENT OF POWER SYSTEMS WITH VARIABLE GENERATION

This Chapter presents a reliability assessment framework for power systems with VG and considering UC schedules and startup/shut down constraints as well as ramp limits. The VG chosen for illustration is SCGs, however, similar analysis can be applied when adding combinations of SCGs and WTSs. The aim is to compute distributions of SCG generated output by taking into account: (1) SCGs FORs, (2) solar radiation forecast, and (3) the CGs ramping, maximum and minimum limits and startup/shutdown period limits. To compute the expected generation contribution of SCGs, G-1 (G is the number of CGs) is applied, i.e., a single CG unit contingency is applied. At every iteration, a UCED model is solved. In total, there are G+1 cases: the base case is when all CGs are in UP state and G cases by taking a single CG out at a time. Once the expected SCGs power output is known, assessing reliability is performed using the probabilistic production costing, PPC, method.

6.1 Problem Statement

Given a number of SCGs $i = 1,\ldots, N_{SCG}$, each with a FOR of q_{SCGi}; a forecast of the solar radiation over period of time $t = 1,\ldots,T$; and the capacity of each SCG. The SCG power, p_{SCG}, versus solar radiation curve is known, given that the SCG is available. The number of SCGs that are subject to the same solar radiation in a SF is known; the solar farm consists of N_{SCG} SCGs. It is desired to find the expected SCGs generated power by

formulating a UCED optimization problem, as explained in detail later in this chapter. The expected SCGs output subtracted from the expected demand, i.e., the net equivalent load, is then inputted to the PPC to find the projected cost and reliability metrics when adding the SCGs.

6.2 Unit Commitment Economic Dispatch Incorporating Solar Generation

In this section, the UCED formulation is discussed in detail. The goal of performing a UCED is to determine the optimal schedule of CGs. The UCED aims to minimize the production cost over a period of time. The UCED problem is a complex problem. Integrating VGs, e.g., renewables, increases the degree of complexity due to VG uncertainty. In general, the UCED should consider the following set of constraints: minimum and maximum production limits, CGs minimum up/down times, ramp up/down limits and demand and reserve requirements. The UCED in this work has been proposed in [20] and explained in [21]. The set of constraints are as follows:

$$x_{g,t} - x_{g,t-1} = s_{g,t} - z_{g,t} \qquad \forall g \in G, \forall t \in T \tag{6.1}$$

Where $x_{g,t}$ is a binary variable the represents the g^{th} CG status (1: ON, 0: OFF), $s_{g,t}$ is a binary variable of the g^{th} CG startup status (1: turned on, 0: otherwise), and $z_{g,t}$ is a binary variable of the g^{th} CG shutdown status (1: turned off, 0: otherwise) at time t. The constraint in (6.1) captures changes in CG status (ON→OFF or OFF→ ON) at time t and a time step before t, i.e., $t-1$. Variables $s_{g,t}$ and $z_{g,t}$ capture CG transitions. Both $s_{g,t}$ and $z_{g,t}$ are known once $x_{g,t}$ and $x_{g,t-1}$ are determined and cannot be both 1 at the same time, either all 0 (no transition) or one of them is 1.

The second constraint is the minimum generation limit which is zero if a CG is off and P_g^{min} otherwise.

$$p_{g,t} \geq P_G^{min} \; x_{g,t} \qquad \forall g \in G, \forall t \in T \tag{6.2}$$

Where $p_{g,t}$ is the g^{th} CG produced power at time t.

The constraint in (6.3) insures that the generated power does not exceed P_g^{max} when it is ON and does not exceed the shutdown rate (SD_g) when it is OFF at t+1.

$$p_{g,t} \leq \bar{p}_{g,t} \leq P_G^{max} x_{g,t} + (SD_g - P_G^{max}) \, z_{g,t+1} \qquad \forall g \in G, \forall t \in T \tag{6.3}$$

Note that $\bar{p}_{g,t} = p_{g,t} + r_{g,t}$, where $\bar{p}_{g,t}$ is the g^{th} CG provided power and reserve, and $r_{g,t}$ is the g^{th} CG reserve provision at time t.

The reserve (R), which is calculated as percentage of the peak load plus the largest CG unit capacity, this constraint is formulated as follows:

$$\sum_{g \in G} \bar{p}_{g,t} \geq D_t + R \qquad \forall t \in T \tag{6.4}$$

Next, the CGs and the SF available generation at time t must meet the demand (D):

$$\sum_{g \in G} p_{g,t} + p_{SF,t} = D_t \quad \forall t \in T \tag{6.5}$$

The SF power output at time t ($p_{SF,t}$) is dependent on the forecasted solar radiation, G_t, and the number of operational SCGs in the SF at time t. The SMCS is used to find the UP/DOWN states of the SCGs. In this method, the state sampling is chronological, i.e., $MTTF_{SCG}$ and $MTTR_{SCG}$ are randomly used to compute the state duration samples [12]. For each sub-cycle (UP or DOWN), a uniform random number is generated, U~unif($0,1$). A sub-cycle represents the time a SCG is either UP or DOWN. Thus, the simulation time, T, consists of a sequence of UP and DOWN sub-cycles. The duration of each sub-cycle is calculated using the inverse transform method, as introduced earlier in section 5.2.3:

$$T_{Up} = -MTTF_{SCG}(\ln(U)) \tag{5.18}$$

$$T_{Down} = -MTTR_{SCG}(\ln(U)) \tag{5.19}$$

When the SCG is DOWN for period of T_{Down}, the SCG has no contribution to SF generated power. $Q_{i,t}$ in (6.6) represents the UP/DOWN status of the i^{th} SCG at instance t, and its summation is the number of the operational SCGs in the SF at time t. To find the upper bound of SF power at time t, the number of operational SCGs is multiplied by the corresponding power output in the SCG power versus solar radiation curve at time t. The detailed derivation is as previously introduced in when discussed SMCS in section 5.2.3.

$$0 \le p_{SF,t} \le \begin{cases} \sum_{i=1}^{N_{SCG}} Q_{i,t}\, p_{SCG.rated} \left(\dfrac{G_t^2}{G_{std} R_C} \right) & \forall G_t \in [0, R_C) \\ \sum_{i=1}^{N_{SCG}} Q_{i,t}\, p_{SCG.rated} \left(\dfrac{G_t}{G_{std}} \right) & \forall G_t \in [R_C, G_{std}] \\ \sum_{i=1}^{N_{SCG}} Q_{i,t}\, p_{SCG.rated} & \forall G_t \in (G_{std}, \infty) \\ & \forall t \in T \end{cases} \tag{6.6}$$

The minimum up time (UT_g) and minimum down time (DT_g) constraints are respectively as follows:

$$\sum_{i=t-UT_g+1}^{t} s_{g,i} \le x_{g,t} \quad \forall t \in T, \forall g \in G \tag{6.7}$$

$$\sum_{i=t-DT_g+1}^{t} s_{g,i} \le 1 - x_{g,t-DT_g} \quad \forall t \in T,\ \forall g \in G \tag{6.8}$$

The constraint in (6.7) insures that there has been at most one transition from ON→OFF in the UT_g period. Similarly, while (6.8) insures that there has been at most one transition in DT_g period.

The ramp up and ramp down constraints ((6.9) and (6.10), respectively) follow that the maximum ramp rate up/down is RU_g / RD_g if a CG is on at t and t+1. Whereas, it is shutdown rate/startup limit SD_g / SU_g if the CG status changes ON→OFF/OFF→ ON on t and t+1.

$$\bar{p}_{g,t} - p_{g,t-1} \leq SU_g \; s_{g,t} + RU_g \; x_{g,t-1} \tag{6.9}$$

$$p_{g,t-1} - p_{g,t} \leq SD_g \; z_{g,t} + RD_g \; x_{g,t} \tag{6.10}$$

The objective function is linear and is in the form of:

$$min \sum_{t \in T} \sum_{g \in G} (y_{g,t} + SU\,cost_{g,t} + z_{g,t} SD\,cost_g) \tag{6.11}$$

The objective function is to minimize operation cost ($y_{g,t}$), start-up ($SUcost_{g,t}$) and shutdown ($SDcost_{g,t}$) costs. While the shutdown cost computation is straightforward because the shutdown cost is constant, the production (fuel) and the start-up cost are not. The production cost is quadratic and is in the form of:

$$a_g p^2_{g,t} + b_g p_{g,t} + c_g$$

Where a_g, b_g and c_g are respectively the fuel quadratic, linear, and constant cost coefficients of the g^{th} CG unit. This cost function can be approximated and linearized as in [41]. The quadratic cost function is divided into segments (J number of segments). Each segment has minimum, maximum, and slope values as shown in Figure 6-1. The slop m_j of the j^{th} segment is the difference between the maximum and the minimum costs (c values on the vertical axis) divided by their corresponding MW values (x values on the horizontal axis). Once the slope is known, $y_{g,t}$ can be computed as follows:

$$y_{g,t} \geq m_j(p_{g,t} - x_j) + c_j \qquad j = 1,2,\ldots,J \tag{6.12}$$

Variable $y_{g,t}$ is nonnegative. The constraint in (6.12) ensures that the generated power belongs to the appropriate cost segment. For every time instance, cost of generating $p_{g,t}$ is calculated J times and the corresponding cost is the highest, which is determined by the slope m_j and upper limits of each segment x_j. Since the objective is minimized, $y_{g,t}$ strictly equals to this cost.

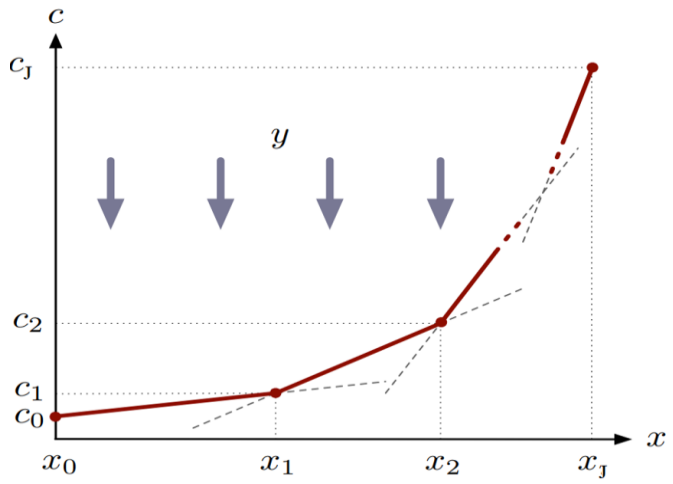

The piecewise production cost [41].

Similarly, the start-up cost is non-linear. However, it can be represented as staircase function as in Figure 6-2 [42],[43]. Assuming there are s segments, each segment has cost k_τ (τ=1,2,…,s), the constraint in (6.13) represents the staircase linearized start-up cost computation for each CG at time t. the more time a CG remains off, the higher the start-up cost incurred to turn it on. Obviously, $SUcost_{g,t}$ is nonnegative. If a CG is ON after it has been OFF for time $\geq t_g^\tau$, $SUcost_{g,t}$ is incurred depending on the length of the OFF period.

The maximum cost is when a CG has been OFF for a time that equals the cold start time (*CT*).

$$SU\,cost_{g,t} \geq k_{\tau}\left(x_{g,t} - \sum_{i=1}^{t_g^{\tau}} x_{g,t-i}\right) \quad \tau=1,2,\ldots,s \tag{6.13}$$

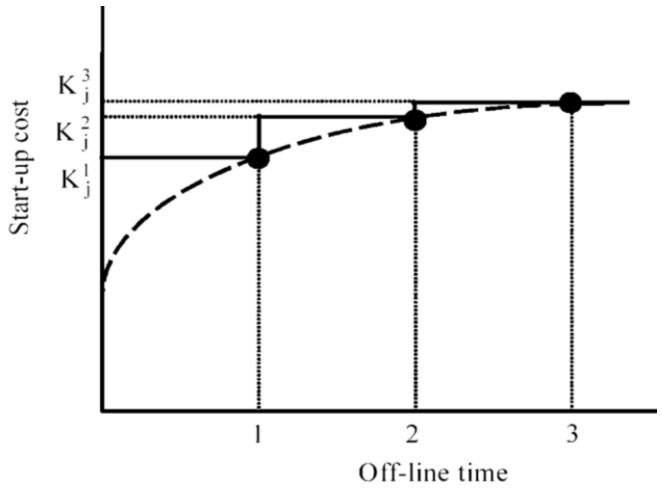

Figure 6-2. Staircase start-up cost function [42].

An important note is that the analysis is applied *G*+1 times: one time with all CGs up and reserve requirement, the constraint in (6.4), is imposed, and *G* times with a single CG outage in each iteration, and (6.4) is relaxed because it is a contingency. Then, the power output of the SF is computed at each iteration and averaged. The UCED is applied for all cases: normal operation and contingencies to calculate the expected SF utilized generation. Due to computation limitation, 4 weeks (672 hrs.) are chosen to represent every season, i.e., the year is represented using the data of 16 weeks. The average power output of the SF will be inputted to the PPC as explained next.

6.3 Reliability Assessment Using the Probabilistic Production Costing

The PPC method, described previously in CHAPTER 3 is used to assess reliability when adding SF to a power system.

6.3.1 Conventional Generation Units

A CG unit is modeled as a 2-state model as explained earlier in 3.1.2.1: available with probability q_g and capacity equals to P_g^{max} or unavailable with probability $1 - q_g$ and capacity equals to zero.

6.3.2 Equivalent Load/SF Representation

The ELDC is computed as explained earlier in CHAPTER 5:

$$\text{ELDC} = \text{Forecasted Load} - \text{Expected SF Power} \tag{5.20}$$

The ELDC is computed using the forecasted load and the expected values of SF power output from the contingency and normal operation cases.

6.3.3 Reliability Assessment

The PPC method is used to assess reliability when adding SF to a power system. The LOLP and EUE are calculated as before. Once LOLP is computed, another index can be computed, loss of load expectation, LOLE, as follows: LOLE=LOLP x 8760 (hrs. /year). Lastly, it is desired to compute the capacity credit (CC), which is the capacity of a CG unit (dispatchable) that would provide the same reliability improvement that the VG (non-dispatchable) provides. To compute CC, the effective load carrying capacity (ELCC) is

computed first. ELCC in this work is defined as load increase that the power system may carry when adding SF generation with LOLP equals the LOLP before adding the SF to the system [44]. The CC, which represents a single SCG capacity credit, is computed once the ELCC is known as in (6.14):

$$CC = \frac{ELCC}{N_{SCG}} \tag{6.14}$$

6.4 Case Study

The annual hourly solar radiation data is obtained from Phoenix, AZ (TMY2) [45]. For the example system, all SCGs are assumed to be subject to the same solar radiation and have the same specifications. Each SCG has specifications as shown in Table 6-1. The number of SCGs in the SF, N_{SCG}, under study is dependent on the penetration level. The penetration levels are 5% to 30% of the total CG installed capacity. Finally, the reliability test system consists of the following:

(1) 10 CGs with specifications in Table 6-2, cost coefficients in Table 6-3 [46] with assumed FORs in Table 6-4.

(2) The SF with the parameters provided earlier,

(3) Load with the p.u. data taken from the IEEE-RTS with a base of 1,200 MW [40].

Table 6-1. SCG specifications.

$p_{SCG.rated}$	10 MW
G_{std}	1,000 W/m^2
R_C	150 W/m^2
q_{SCG} (assumed)	0.15
$MTTF_{SCG}$	950 hrs.
$MTTR_{SCG}$	167.7 hrs.

Table 6-2. The 10 CGs specifications.

g	Pmax (MW)	Pmin (MW)	DT (h)	UT (h)	Hot start cost ($)	Cold start cost ($)	Cold start time (h)	Ramp Rate (MW)
1	455	150	8	8	4500	9,000	5	264
2	455	150	8	8	5000	10,000	5	264
3	130	20	5	5	550	1,100	4	110
4	130	20	5	5	560	1,120	4	110
5	162	25	6	6	900	1,800	4	137
6	80	20	3	3	170	340	2	60
7	85	25	3	3	260	520	2	60
8	55	10	1	1	30	60	0	45
9	55	10	1	1	30	60	0	45
10	55	10	1	1	30	60	0	45

Table 6-3. The 10 CGs cost coefficients.

g	*a* ($/MW^2)	*b* ($/MWh)	*c* ($/h)
1	4.80E-04	16.19	1,000
2	3.10E-04	17.26	970
3	0.002	16.6	700
4	0.00211	16.5	680
5	0.00398	19.7	450
6	0.00712	22.26	370
7	7.90E-04	27.74	480
8	0.00413	25.92	660
9	0.00222	27.27	665
10	0.00173	27.79	670

Table 6-4. The 10 CGs FORs.

g	MTTF (hrs.)	MTTR (hrs.)	FOR
1,2	967	33	0.0033
3,4,5	960	40	0.04
6,7	1,960	40	0.02
8,9,10	969	31	0.031

6.4.1 UCED Results

The UCED solutions for normal operation and contingencies were different, as expected. For instance, Table 6-4 shows the difference between the SF generated power at 30% penetration between normal operation and when *CG* 1 is out. Also, for the purpose of calculating the ELCC, the same analysis was applied on different loads peaks.

Table 6-5. P_{SF} Utilization Example.

	Unit	Hours of the year						
		325	**326**	**327**	**328**	**329**	**330**	**331**
All units are UP	1	175	167	167	175	258	455	455
	2	150	150	150	150	151	150	150
	3	20	20	20	20	20	43.6	68.8
	4	20	20	20	20	20	56.6	83.0
	5	25	25	25	25	25	25	25
	6	0	0	0	0	20	20	20
	7-10	0	0	0	0	0	0	0
	p_{SF}	338	330	322	313	241	60	0
Gen. 1 out	1							
	2	365	351	385	390	442	455	455
	3	0	0	0	0	0	0	0
	4	0	0	0	0	28	130	130
	5	0	0	0	0	250	145	162
	6-10	0	0	0	0	0	0	0
	p_{SF}	363	361	346	313	241	60	0

6.4.2 Reliability Assessment and Capacity Credit

Table 6-6 shows the reliability assessment and cost projection of different penetration levels, and different peaks (needed to compute CC and ELCC). The improvement range was 20% to 52% in LOLP and LOLE. However, the rate of improvement decreased as the penetration increased. The EUE decreased from 19% to 54.6% as the penetration level increased and with same rate of improvement as the LOLP and LOLE. On the other hand, Figure 6-3 shows the ELCC of all cases. To compute the ELCC, the UCED and the PPC analysis were applied to different load peaks. The dotted line in Figure 6-3 shows the criterion in the ELCC computation. The ELCC increased from 24 to 90 MW as penetration increased, while the CC decreased from 30 to 18.75 MW as shown in Figure 6-4.

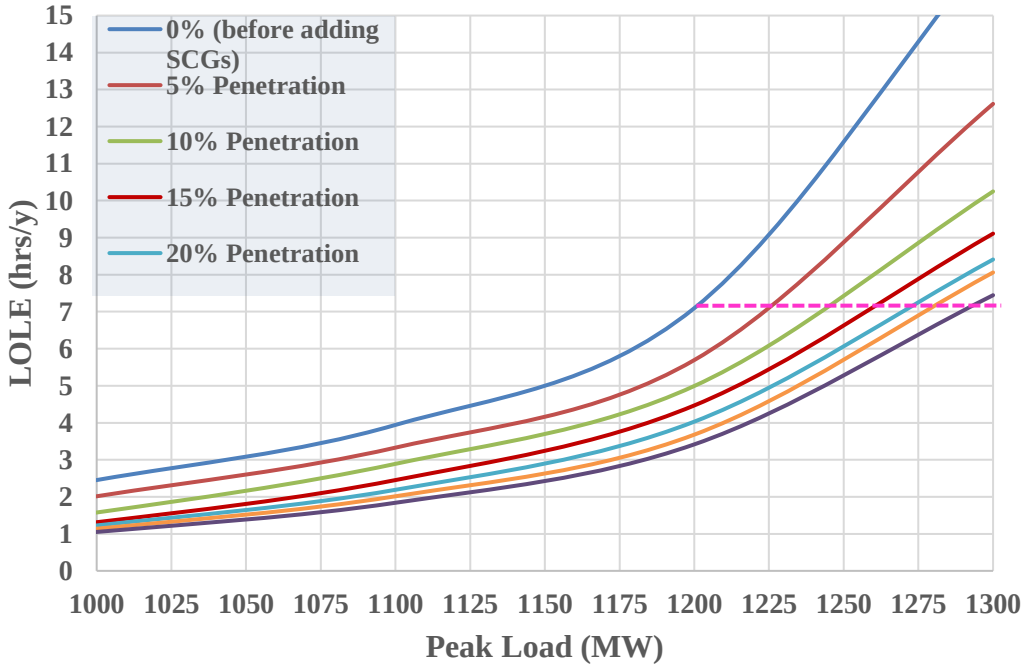

Figure 6-3. The ELCC of all penetration levels.

Table 6-6. Reliability assessment results.

Peak (MW)	Penetration level	LOLP	LOLE (h/year)	EUE (MWh)	Total Cost (k$)
1,100	0%	0.00045	3.942	456.61	116,165
	5%	0.00038	3.3288	360.83	112,679
	10%	0.00033	2.8908	294.59	109,695
	15%	0.00028	2.4528	248	106,698
	20%	0.00025	2.19	221.73	103,888
	25%	0.00023	2.0148	212	100,594
	30%	0.00021	1.8396	197.5	98,282
1,000	0%	0.00028	2.4528	212.6	105,073
	5%	0.00023	2.0148	153.26	102,223
	10%	0.00018	1.5768	119.9	99,342
	15%	0.00015	1.314	101.48	96,274
	20%	0.00014	1.2264	93.03	93,235
	25%	0.00013	1.1388	89.99	89,887
	30%	0.00012	1.0512	84.98	87,275
1,200	0%	0.00081	7.096	863.04	126,947
	5%	0.00065	5.694	697.58	123,733
	10%	0.00057	4.993	589.69	120,478
	15%	0.00051	4.468	508.56	117,140
	20%	0.00046	4.030	452.69	114,242
	25%	0.00042	3.679	424.8	111,162`
	30%	0.00039	3.416	391.53	108,890
1,300	0%	0.00193	16.9068	1,747	137,738
	5%	0.00144	12.6144	1,354	134,390
	10%	0.00117	10.2492	1,144	131,247
	15%	0.00104	9.1104	1,003	127,913
	20%	0.00096	8.4096	907	124,774
	25%	0.00092	8.0592	852	121,544
	30%	0.00085	7.446	785.70	119,103

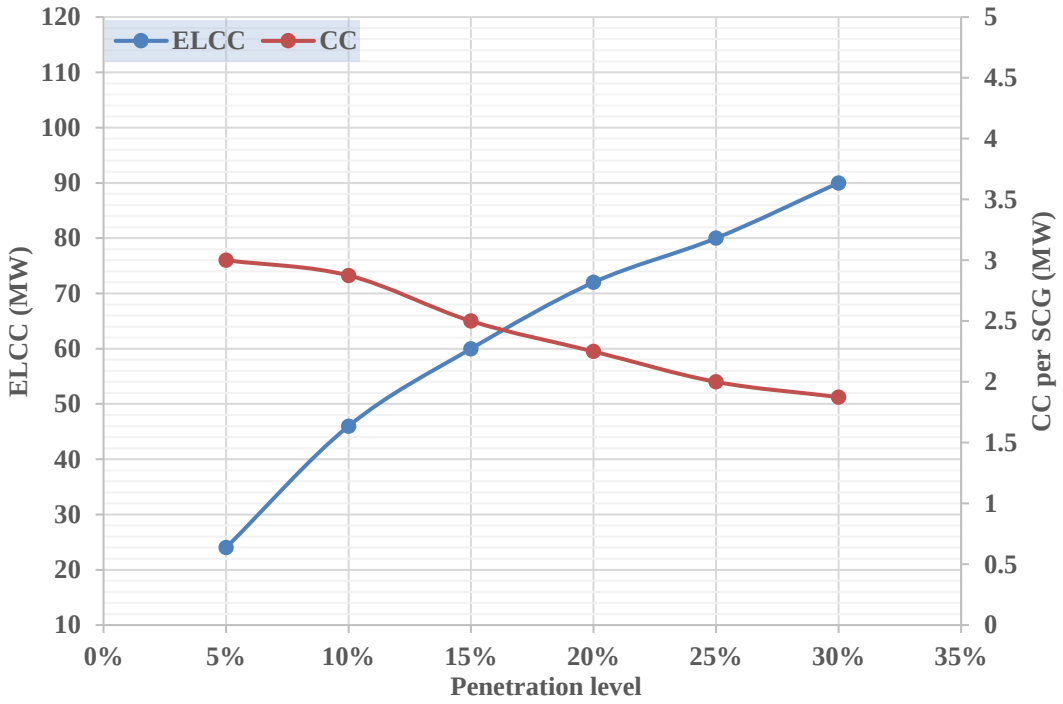

Figure 6-4. The ELCC and CC of all penetration levels.

6.5 Conclusions

This chapter presented a reliability assessment for systems with different levels of penetration of SCGs. A unit commitment economic dispatch model is used to compute the expected CGs output at different penetration levels and the output of SF given the probabilistic model of solar radiation. The probabilistic load and SF output model were inputted to the PPC method to compute reliability indices. The proposed model used solar radiation prediction based on historical data and took into consideration random outages of both SCGs and CGs. The model also provided the capacity credit of the SFs. The study showed that reliability improvement lessened as the solar generation penetration increased.

CHAPTER 7. ENERGY STORAGE SIZING AND RELIABILITY ASSESSMENT FOR POWER SYSTEMS WITH VARIABLE GENERATION

This chapter formulates the energy storage system, ESS, sizing problem in the presence of both WTSs and SCGs at different penetration levels as a mixed integer linear programing, MILP. The method takes into account: (1) SCGs and WTSs FORs, (2) solar radiation and wind speed forecasts, and (3) the CGs ramping, max./min. limits and startup/shutdown period limits, as in the previous chapter. The ESS sizing problem is formulated as a UCED with an objective function of minimizing CGs costs in addition to the cost associated with the ESS. Once the ESS size is computed, reliability assessment is performed to quantify the ESS impact on reliability. Reliability assessment is performed using the probabilistic production costing (PPC) method with appropriate modification to account for VG and ESS. Figure 7-1 illustrates the flow chart of the proposed computational procedure. Moreover, Figure 7-2 shows the reliability assessment procedure using the PPC method in presence of VGs and ESS.

7.1 Problem Statement

The following data is assumed given: a number of SCGs $i = 1,\ldots, N_{SCG}$, each with FOR of $q_{SCGi.}$, rated power equals to $p_{SCG.rated,}$ and a forecast of the solar radiation, G_t, over a period of time $t = 1,\ldots,T$. Also, the SCG power, p_{SCG}, versus solar radiation curve is known. A solar farm, SF, consists of N_{SCG} number of SCGs and they are assumed to be exposed to the same solar radiation. Similarly, a number of WTSs $i = 1,\ldots, N_{WTS}$, each with

FOR of q_{WTSi}, rated power equals to $p_{WTS.rated}$, and a forecast of the wind speed over period of time $t = 1,\ldots,T$. The WTS power as a function of the wind speed is also given. A wind farm, WF, consists of N_{WTS} WTSs and they are exposed to the same wind speed. Also, the energy and power costs of ESS of a certain ESS technology are given. It is desired to optimally size the needed ESS as to minimize the overall cost of the power system with the VG. Once the optimal ESS size is known, the net equivalent load is computed and inputted to the PPC to find the projected cost and reliability metrics.

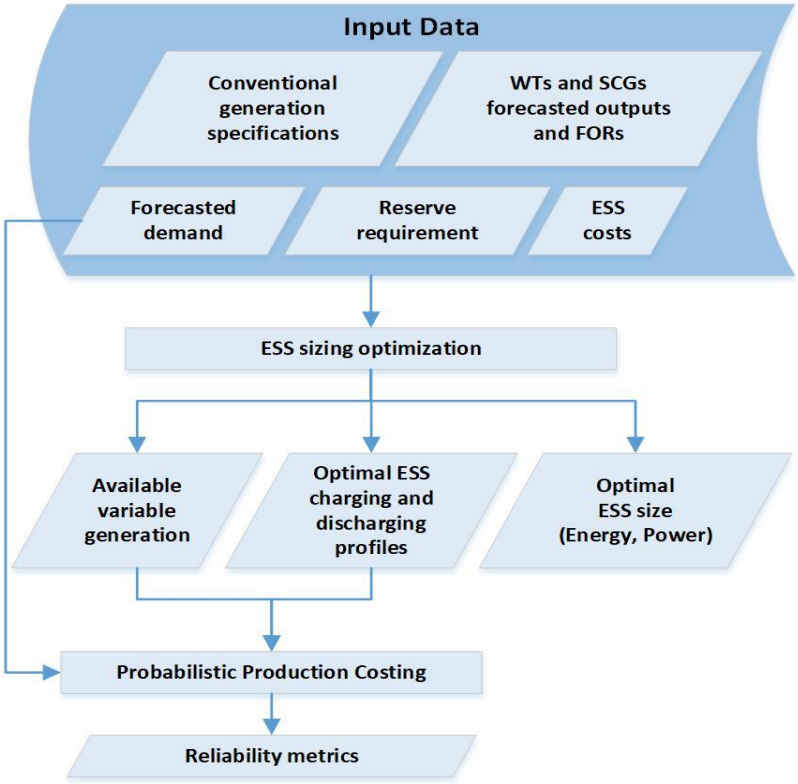

Figure 7-1. Proposed computational procedure.

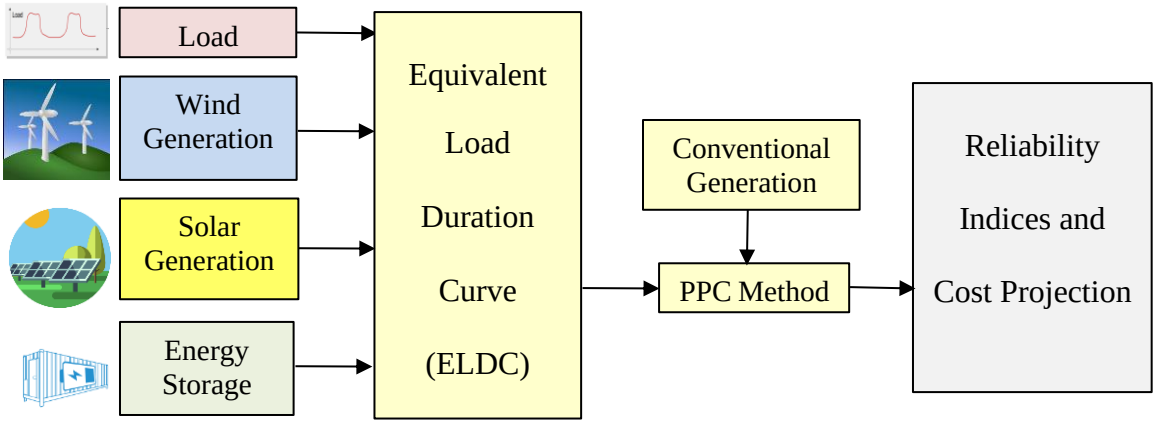

Figure 7-2. Reliability assessment procedure in presence of VG and ESS.

7.2 Energy Storage Sizing Optimization Formulation

In this section, the method for finding the optimal ESS size is discussed in detail. The ESS sizing is formulated as a MILP problem which can be viewed as a modified UCED problem. The constraints are similar to the ones introduced in section 6.2. The complete set of constraints is as follows:

$$x_{g,t} - x_{g,t-1} = s_{g,t} - z_{g,t} \qquad \forall g \in G, \forall t \in T \mid t = 1 \tag{6.1}$$

$$p_{g,t} \geq P_G^{min} \, x_{g,t} \qquad \forall g \in G, \forall t \in T \tag{6.2}$$

$$p_{g,t} \leq \bar{p}_{g,t} \leq P_G^{max} x_{g,t} + (SD_g - P_G^{max}) \, z_{g,t+1} \qquad \forall g \in G, \forall t \in T \tag{6.3}$$

Where $\bar{p}_{g,t} = p_{g,t} + r_{g,t}$.

$$\sum_{g \in G} \bar{p}_{g,t} \geq D_t + R \quad \forall t \in T \tag{6.4}$$

$$\sum_{i=t-UT_g+1}^{t} s_{g,i} \leq x_{g,t} \quad \forall t \in T, \forall g \in G \tag{6.7}$$

$$\sum_{i=t-DT_g+1}^{t} s_{g,i} \leq 1 - x_{g,t-DT_g} \quad \forall t \in T, \ \forall g \in G \tag{6.8}$$

$$\bar{p}_{g,t} - p_{g,t-1} \leq SU_g \ s_{g,t} + RU_g \ x_{g,t-1} \tag{6.9}$$

$$p_{g,t-1} - p_{g,t} \leq SD_g \ z_{g,t} + RD_g \ x_{g,t} \tag{6.10}$$

Next, the CGs, the VG (SF and WF) and ESS available at time *t* must meet the demand a in (7.1):

$$\sum_{g \in G} p_{g,t} + p_{SF,t} + p_{WF,t} + p_{dis,t} = D_t + p_{ch,t} \quad \forall t \in T \tag{7.1}$$

Where $p_{ch,t}$ is the power injected (charging) into ESS and $p_{dis,t}$ Power drawn (discharging) from ESS at time *t*.

The VG set of constraints determines the expected output of SCGs and WTSs taking into consideration G_t and V_t, respectively, and random outages of SCGs and WTSs. Starting with SCGs in a SF, $p_{SF,t}$ is dependent on the forecasted solar radiation, G_t, and the number of operational SCGs in the SF at time *t*. SMCS is used to find the UP/DOWN states of the

SCGs. In this method, the state sampling is chronological as described earlier. consists of a sequence of UP and DOWN sub-cycles. The duration of each sub-cycle is calculated using the inverse transform method, as follows:

$$T_{Up} = -MTTF_{SCG}(\ln(U)) \tag{5.18}$$

$$T_{Down} = -MTTR_{SCG}(\ln(U)) \tag{5.19}$$

$QS_{i,t}$ in (7.2) represents the UP/DOWN status of the i^{th} SCG at instance t, and its summation is the number of the operational SCGs in the SF at time t. To find the upper bound of SF power at time t ($p_{SFmax,t}$), the number of operational SCGs is multiplied by the corresponding power output in the SCG power versus solar radiation curve at time t.

$$0 \le p_{SF,t} \le p_{SF\,max,t} \tag{7.2}$$

where

$$p_{SF\,max,t} = \begin{cases} \sum_{i=1}^{N_{SCG}} QS_{i,t}\, p_{SCG.rated} \left(\dfrac{G_t^2}{G_{std} R_C} \right) & \forall G_t \in [0, R_C) \\ \sum_{i=1}^{N_{SCG}} QS_{i,t}\, p_{SCG.rated} \left(\dfrac{G_t}{G_{std}} \right) & \forall G_t \in [R_C, G_{std}] \\ \sum_{i=1}^{N_{SCG}} QS_{i,t}\, p_{SCG.rated} & \forall G_t \in (G_{std}, \infty) \\ & \forall t \in T \end{cases}$$

Similarly, $p_{WF,t}$ is dependent on the forecasted wind speed ,V_t, and the number of operational WTSs in the WF at time t. Chronological sampling using $MTTF_{WTS}$ and

$MTTR_{WTS}$, as in the SF case, is applied. The duration of each sub-cycle is calculated using the inverse transform method, as follows:

$$T_{Up} = -MTTF_{WTS}(\ln(U)) \tag{4.18}$$

$$T_{Down} = -MTTR_{WTS}(\ln(U)) \tag{4.19}$$

$QW_{i,t}$ in constraint (7.3) represents the UP/DOWN status of the i^{th} WTS at instance t, and its summation is the number of the operational WTSs in the WF at time t. To find the bound of WF power at time t ($p_{WFmax,t}$), the number of operational WTSs is multiplied by the corresponding power output in the WTS power versus wind speed curve at time t.

$$0 \le p_{WF,t} \le p_{WF\,max,t} \tag{7.3}$$

where

$$p_{WF\,max,t} = \begin{cases} \sum_{i=1}^{N_{WTS}} QW_{i,t}\left(p_{WTS.rated}\left(\dfrac{V_t^s - v_{ci}^s}{v_{rated}^s - v_{ci}^s} \right) \right) & \forall V_t \in \left(v_{ci}, v_{rated}\right) \\ \sum_{i=1}^{N_{WTS}} QW_{i,t}\ p_{WTS.rated} & \forall V_t \in \left[v_{rated}, v_{co}\right) \\ 0 & \text{Otherwise} \\ & \forall t \in T \end{cases}$$

Where The WF power output at time t ($p_{WF,t}$) s is chosen to be 1 throughout this model.

It is important to add a variable that represents the unutilized VG generation ($p_{u,t}$) at time *t*. This variable represents the VG power which is available but not used because there is no demand and the ESS is fully charged:

$$p_{u,t} = p_{SF\max,t} - p_{SF,t} + p_{WF\max,t} - p_{WF,t} \tag{7.4}$$

The constraints in (7.5) to (7.12) dictate the operation of ESS energy resources and they are important for optimal ESS sizing. The constraint in (7.5) provides the relationship of the state of charge (SOC) between two consecutive time intervals, i.e., the dynamics of the ESS. The constraints in (7.6), (7.7) and (7.8) limit the operation of ESS within its ratings (maximum storage limit and charging/discharging limits). Notably, E_{ESS} and P_{ESS} (the ESS energy and power optimal sizing, respectively), are decision variables. The two constraints in (7.9) and (7.10) ensure that charging and discharging cannot occur simultaneously. *M* is a large number, e.g., 1000 MW. While it is not necessary in this work, P_{ESS} is restricted to be less than or equal one third E_{ESS}, as represented with constraint (7.11).

$$E_{t+1} = E_t + \eta_{ch} p_{ch,t} - \frac{p_{dis,t}}{\eta_{dis}} \qquad \forall t \in T \tag{7.5}$$

$$0 \le E_t \le E_{ESS} \qquad \forall t \in T \tag{7.6}$$

$$0 \le P_{ch,t} \le P_{ESS} \qquad \forall t \in T \tag{7.7}$$

$$0 \le P_{dis,t} \le P_{ESS} \quad \forall t \in T \tag{7.8}$$

$$0 \le P_{ch,t} \le \alpha_t M \quad \forall t \in T \tag{7.9}$$

$$0 \le P_{dis,t} \le (1-\alpha_t) M \quad \forall t \in T \tag{7.10}$$

$$p_{ESS} \le \frac{E_{ESS}}{3\Delta t} \tag{7.11}$$

Where E_t is the ESS energy level or the SOC at time t, η_{ch} and η_{dis} are the ESS charging and discharging efficiency, and Δt is the simulation time step (Δt = 1 hr.).

Last ESS constraint is to restrict the ESS charging power to be less than or equal to the unutilized VG power.

$$p_{ch,t} \le p_{u,t} \quad \forall t \in T \tag{7.12}$$

The objective function is linear and is in the form of:

$$\begin{aligned} min \sum_{t \in T} \sum_{g \in G} (y_{g,t} + SU\,cost_{g,t} + z_{g,t} SD\,cost_g) \\ + \pi \Delta t \sum_{t \in T} (P_{u,t} - P_{ch,t}) + dE_{ESS} + eP_{ESS} \end{aligned} \tag{7.13}$$

Where *d* is ESS energy capacity capital cost in $/MWh, *e* is the ESS power capacity capital cost in $/MW, and π is a penalty on utilized VG as VG reduces the greenhouse emissions.

The objective function is to minimize fuel cost, startup and shutdown costs, the ESS energy and power capital capacity costs, and a penalty for the unutilized VG (SF+WF) power. While the shutdown cost computation is straightforward (constant), the production (fuel) and the startup cost are linearized as discussed earlier in section 6.2.

For simplicity, 4 weeks (672 hrs.) are chosen for this study. Once the ESS optimization problem is solved, the expected power output of the SF, WF and ESS is inputted to the PPC to assess production costs and reliability.

7.3 Reliability Assessment Using the Probabilistic Production Costing

The PPC method is described earlier is applied to assess the reliability when adding ESS. The CG model stays the same. However, the equivalent load model is modified to account for the ESS addition as follows:

7.3.1 Equivalent Load Representation

The ELDC is computed as follows:

$$\text{ELDC} = \text{Load} - \text{Expected VG Power} - \text{ESS power} \tag{7.14}$$

The ELDC is computed using the forecasted load, the expected values of SF and WF power output consumed directly by the demand, and ESS power. Subsequently, the resultant curve is converted to IPDF.

Once the IPDF is constructed, reliability indices are calculated as explained earlier.

7.4 Case Study

The hourly solar radiation data is obtained from Phoenix, AZ (TMY2) [45]. For the test system, all SCGs are assumed to be subject to the same solar radiation and have the same specifications. Each SCG has specification as shown in Table 7-1. The number of SCGs in the SF (N_{SCG}) under study is dependent on the solar penetration level. For instance, if the penetration level is 30 %, 15% is solar generation and 15 % is wind generation. The penetration levels are 10% to 30% of the total CGs installed capacity. Similarly, the wind speed hourly data of the same location is collected [45]. All WTSs in the WF are assumed to be subject to the same wind patterns and have the same specifications. The Areva Multibird M5000 WT specifications are utilized to perform the analysis of the case study [45]. Theses specifications are listed in Table 7-2. The ESS technology chosen for the study is lead-acid with following specification shown in Table 7-3 [47]. Note that the study is for 672 hrs. and e and d are calculated to reflect the cost of the ESS over the study period. With the assumption that the ESS lifetime is 20 years and the discount rate is 5%, e=2,037 \$/MWh and d = 2,469 \$/MW. The price penalty on unutilized VG, π, equals 80 \$/MWh. Finally, the test system consists of the following:

(1) The 10 CGs as introduced earlier in Table 6-2,Table 6-2 and Table 6-3.

(2) The SF with the data provided earlier.

(3) The WF with the data provided earlier.

(4) Load with the p.u. data taken from the IEEE-RTS considering a base of 1,150 MW [40].

Table 7-1. SCG specifications.

$p_{SCG.rated}$	5 MW
G_{std}	1,000 W/m^2
R_C	150 W/m^2
q_{SCG} (assumed)	0.15
$MTTF_{SCG}$	950 hrs.
$MTTR_{SCG}$	167.7 hrs.

Table 7-2. WTS specifications.

Type	Areva Multibird M5000 WT
$p_{WTS.rated}$	5 MW
v_{ci}	4 m/s
v_{rated}	12.5 m/s
v_{co}	25 m/s
q_{WTS} (assumed)	0.15
$MTTF_{WTS}$	950 hrs.
$MTTR_{WTS}$	167.7 hrs.

Table 7-3. ESS specifications.

ESS technology	lead-acid
η_{ch} / η_{dis}	80%
Energy capital cost	330 k$/MWh
Power capital cost	400 k$/MW
Lifetime	20 years
Discount rate	5%
e	26480.05 $/MWh
d	32,097.03 $/MW

7.4.1 ESS Sizing Results

The proposed ESS optimal sizing method was applied to the test system for three VG penetration levels as follows: 10%, 20% and 30 %. SCGs and WTSs contributed equally to each penetration level. Table 7-4 shows the optimal P_{ESS}, E_{ESS} and ESS cost for all cases.

Notably, when the penetration level was 10%, the optimal decision was not to have ESS rather changing the operation of the CGs and directing most VGs to meet the demand directly. On the other hand, when penetration levels were 20% and 30%, having ESS provided the optimal solution.

For comparison purposes, the same analysis discussed earlier was applied to the test system without ESS. For instance, Figure 7-3 shows that in presence of ESS more VG power was utilized than the case without ESS. Figure 7-4 shows ESS hourly energy and charge/discharge power.

Table 7-4. Optimal sizing and cost of ESS.

VG %	P_{ESS}	E_{ESS}	ESS Cost ($)
30%	53.2	167.50	521,925.9
20%	29.9	89.71	282,400.3
10%	0	0	0

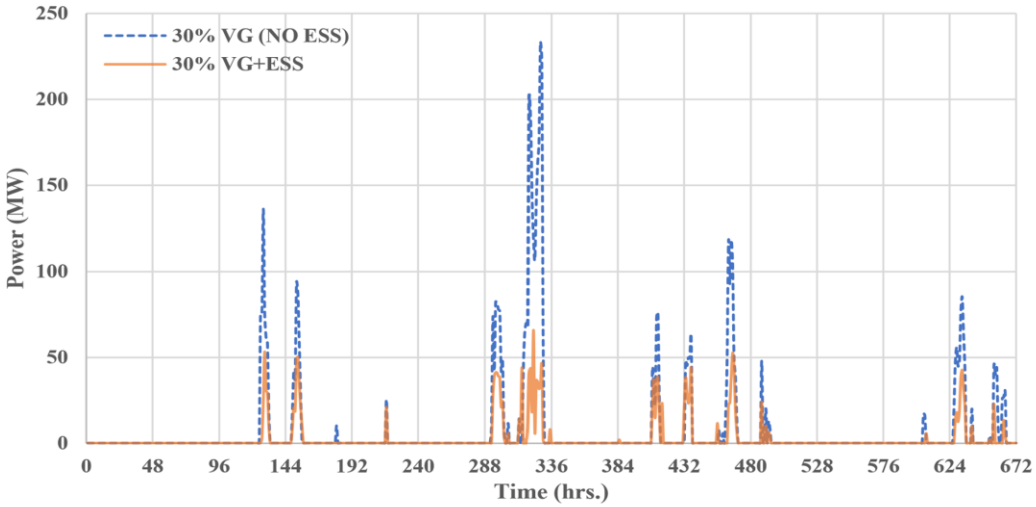

Figure 7-3. Unutilized VG comparison at 30% penetration.

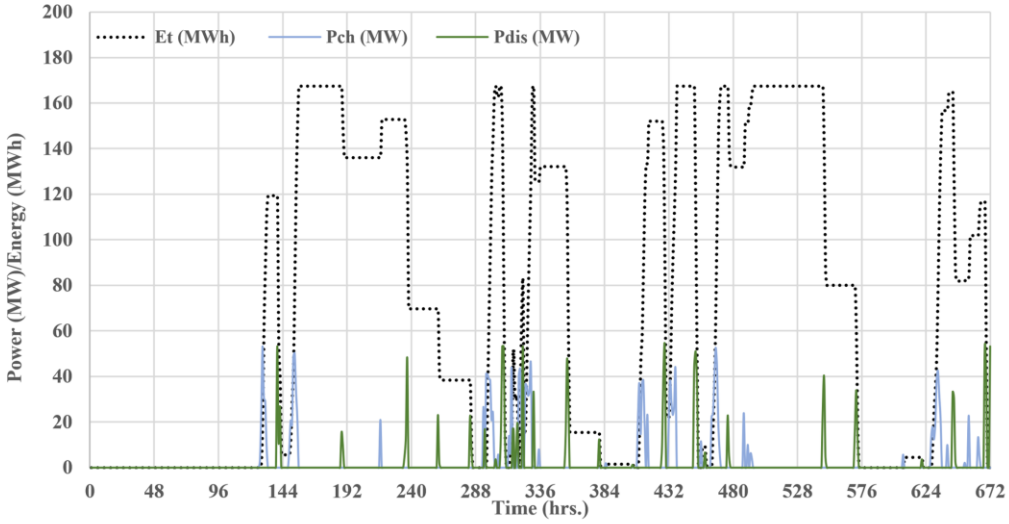

Figure 7-4. ESS power and energy profiles at 30% penetration.

7.4.2 Reliability Assessment

Table 7-5 shows the reliability assessment and cost projection of different penetration with/without ESS. The improvement ranged from 51.5% to 70% in LOLP and LOLE in presence of VG and ESS while it ranged from 42.4% to 66.7% in presence of just VG. All cases are compared to having neither VG nor ESS, base case. The EUE and the total cost followed the same pattern for all cases. Note that even though the 10% VG penetration optimal ESS sizing was zero, the 10% VG penetration affected the reliability of the system as compared to the base case. In this case, avoiding the unutilized VG penalty resulted in utilizing more VG and improved reliability.

Table 7-5. Reliability assessment results.

Case	VG %	LOLP	LOLE (hrs./y)	EUE (MWh)	Total Cost (k$)
Base case	0%	0.00033	2.8908	14.44	8,276
VG only	10%	0.00019	1.6644	7.52	7,827
	20%	0.00013	1.1388	5.14	7,328
	30%	0.00011	0.9636	4.22	6,894
VG+ESS	10%	0.00016	1.4016	6.41	7,561
	20%	0.00013	1.1388	5.02	7,318
	30%	0.00010	0.8760	3.86	6,820

7.5 Conclusions

This chapter presented an optimization model for ESS sizing for systems with VG. Further, a reliability assessment method for power systems with specific VG penetration and available ESS has been proposed. Several cases were analyzed considering different VG penetrations and optimal ESS size. In the case of 10% penetration level, the optimal sizing of ESS was zero. However, as the VG penetration level increased, the optimal ESS size that reduces the total cost increased. The probabilistic load, VG and ESS models as well as the probabilistic models of CG were inputted to the PPC method to compute reliability indices. The proposed model used solar radiation and wind speed predictions based on historical data for a specific area and considered random outages for both SCGs and WTSs. The study shows that reliability improvement rates lessen as the VG penetration level increased indicating that the cost and reliability improvements levels off as the penetration increases.

CHAPTER 8. ANALYTICAL METHOD FOR ENERGY STORAGE SIZING AND RELIABILITY ASSESSMENT FOR POWER SYSTEMS WITH VARIABLE GENERATION

This chapter formulates the ESS sizing in presence of VG at different penetration levels. The problem is formulated as MILP similar to the model in CHAPTER 7, but here the seasonal PDFs of wind speed and solar radiations are considered. Firstly, for specific locations, historical seasonal wind speeds and solar radiation data along with WTSs/SCGs FORs and their generation models are used to find power output PDFs of WTSs/SCGs. The PDFs are computed analytically and integrated into the MILP for finding ESS sizing with objective to minimize CGs production cost, startup and shutdown costs in addition to ESS investment costs. Once the ESS optimal sizing is computed, a reliability assessment is performed, using PPC method, to quantify reliability improvements from the addition of ESS.

8.1 Problem Statement

Assuming that the number of CG units is G and their specifications are given. In addition, the energy and power costs of ESS are given as well as the ESS charging/discharging efficiency. The ESS sizing optimization problem requires the following data: the VG is represented by solar farms, SFs, and wind farms, WFs. There are N_{SF} SFs and N_{WF} WFs in the system under study. A SF consists of N_{SCG} number of SCGs. The number of SCGs in the SF defines the solar generation penetration level. For SCG i, where $i = 1, \ldots, N_{SCG}$, the FOR of SCG_i is denoted by q_{SCGi} and the rated power by $p_{SCG.ratedi}$.

The historical data of the solar radiation (G_h) is given, where h=1,2,…,H. The solar radiation data is partitioned into four different groups depending on the season: winter, spring, summer and fall. Also, p_{SCG} versus solar radiation curve is known. While not necessary, for simplicity all SCGs are assumed to be exposed to the same solar radiation. Also, we assume that the type of SCGs, and N_{SCG} are identical in each SF. Similarly, a WF consists of N_{WTS} WTSs. The number of WTSs in the WF defines the wind generation penetration level. For WTSs i, where i= 1,…, N_{WTS}, the FOR is denoted by q_{WTSi} and the rated power by $p_{WTS.ratedi}$. The historical data of the wind speed (V_h) is given, where h=1,2,…,H. The wind speed data is partitioned into four different seasonal groups as in the solar radiation case. Also, the WTS power as a function of the wind speed is also given. Similar to SCGs, in this study, all WTSs in the WF are assumed to be exposed to the same wind speed. Also, we assume that the type of WTSs and N_{WTS} are identical in each WF.

Given the four partitioned data sets of solar radiation/wind speed of a specific location, it is desired to find the PDF and CDF of solar radiation/wind speed for each season. Then, using these PDFs and CDFs conditioned on the availability of SCGs/WTSs, the SFs/WFs power output PDFs and CDFs are computed for each season. Once the PDFs and CDFs of SFs/WFs power output of all four seasons are computed, SFs/WFs power samples can be integrated into the ESS sizing optimization problem to represent SFs/WFs forecasted outputs. Then, solving for the ESS sizing gives ESS charging/discharging profile and utilized WFs/SFs power to be inputted to the PPC method in addition to the forecasted load to compute the net equivalent load.

8.2 Computation of SFs/WFs Generated Power Probability Distribution Function

8.2.1 SF Power Probability Distribution Function

This section presents the analysis for a single SF, which is repeated for every SF in the study. For simplicity, the subscript s (s=1,…, N_{SF}) in p_{SFs}, N_{SCGs}, …, etc. is omitted. For each season's solar radiation, the PDF of solar radiation is found, subsequently, the PDF/CDF of the SF power output, ρ_{SFG} (p_{SF})/ F_{SFG} (p_{SF}), is computed analytically, as explained earlier in section 5.2.1.

8.2.2 WF Power Probability Distribution Function

This section presents the analysis for a single WF, which is repeated for every WF in the study. For simplicity, w (w=1,…, N_{WF}) in p_{WFw} , N_{WTSw} ,…etc. is omitted. For each season's wind speed, the PDF of wind speed is found, subsequently, the PDF/CDF of the WF power output, ρ_{WFG} (p_{WF})/ F_{WFG} (p_{WF}), is computed analytically, as explained earlier in section 4.4.1.

8.3 Energy Storage Sizing Optimization Formulation

In this section, the method for finding the optimal ESS size considering multiple SFs/WFs and seasonal variation of solar radiation/wind speed is discussed in detail. The ESS sizing is formulated as a MILP problem. The complete set of constraints is as follows:

$$x_{g,t} - x_{g,t-1} = s_{g,t} - z_{g,t} \quad \forall g \in G, \forall t \in T \mid t = 1 \tag{6.1}$$

$$p_{g,t} \geq P_G^{min} \; x_{g,t} \qquad \forall g \in G, \forall t \in T \tag{6.2}$$

$$p_{g,t} \leq \bar{p}_{g,t} \leq P_G^{max} x_{g,t} + (SD_g - P_G^{max}) \, z_{g,t+1} \qquad \forall g \in G, \forall t \in T \tag{6.3}$$

Where $\bar{p}_{g,t} = p_{g,t} + r_{g,t}$.

$$\sum_{g \in G} \bar{p}_{g,t} \geq D_t + R \quad \forall t \in T \tag{6.4}$$

$$\sum_{i=t-UT_g+1}^{t} s_{g,i} \leq x_{g,t} \quad \forall t \in T, \forall g \in G \tag{6.7}$$

$$\sum_{i=t-DT_g+1}^{t} s_{g,i} \leq 1 - x_{g,t-DT_g} \quad \forall t \in T, \; \forall g \in G \tag{6.8}$$

$$\bar{p}_{g,t} - p_{g,t-1} \leq SU_g \; s_{g,t} + RU_g \; x_{g,t-1} \tag{6.9}$$

$$p_{g,t-1} - p_{g,t} \leq SD_g \; z_{g,t} + RD_g \; x_{g,t} \tag{6.10}$$

Next, demand and energy charging into the ESS at time *t* must be met by CGs, SFs, WFs, and ESS:

$$\sum_{g \in G} p_{g,t} + \sum_{s=1}^{N_{SF}} p_{SFs,t} + \sum_{w=1}^{N_{WF}} p_{WFw,t} + p_{dis,t} = D_t + p_{ch,t} \qquad \forall t \in T \tag{8.1}$$

Where $p_{SFs,t}$ is *s* SF power output at time *t*, and $p_{WFw,t}$ is *s* WF power output at time *t*.

The VG (SFs and WFs) set of constraints determine the expected output of SCGs and WTSs taking into consideration the uncertainty associated with this type of generation. Earlier, G_h and V_h, were partitioned to four groups depending on the season. Subsequently, it was shown how to analytically compute $\rho_{SFGs}(p_{SFs})/F_{SFGs}(p_{SFs})$ and $\rho_{WFGw}(p_{WFw})/F_{WFGw}(p_{WFw})$. Samples from these CDFs are used represent the SFs/WFs power output. The number of generated samples for each WF/SF equals *T*, the simulation period. As *T* must represent the four seasons, the samples are divided into 4 groups, each with length equals *T*/4. Each group is sampled from its corresponding WF/SF power output CDF, as discussed next. Starting with SCGs in a SF, once the $F_{SFGs}(p_{SFs})$ of each season is computed, uniform random numbers are generated, U_t ~unif*(0,1)*. Then, these random numbers are used to compute the power using the ITM. The power computed here is the maximum output of every SF ($p_{SFs\ max,\ t}$) at instant *t* as follows:

$$p_{SFs\max,t} = F^{-1}_{SFGs}(U_t) \qquad s = 1,\ldots,N_{SF} \tag{8.2}$$

The constraint in (8.3) represents the SF production limits:

$$0 \le p_{SFs,t} \le p_{SFs\max,t} \qquad s = 1,\ldots,N_{SF} \tag{8.3}$$

Similarly, once $F_{WFGw}(p_{WFw})$ of each season is computed, uniform random numbers are generated, U_t ~unif*(0,1)*. Then, they are used to compute the power using the ITM. The power computed is the maximum output of the WF ($p_{WFw\ max,\ t}$) at instant *t* as follows:

$$p_{WFw\max,t} = F^{-1}_{WFGw}(U_t) \quad w = 1,\ldots,N_{WF} \tag{8.4}$$

Constraint in (8.5) represents the WF production limits:

$$0 \le p_{WFw,t} \le p_{WFw\max,t} \quad w = 1,\ldots,N_{WF} \tag{8.5}$$

It is desirable to utilize all the VG either to serve the load directly or to charge the ESS. However, this may not be always possible. Hence, $p_{u,t}$ is the unutilized VG computed as follows:

$$p_{u,t} = \sum_{s=1}^{N_{SF}} p_{SFs\max,t} - \sum_{s=1}^{N_{SF}} p_{SFs,t} + \sum_{w=1}^{N_{WF}} p_{WFw\max,t} - \sum_{w=1}^{N_{WF}} p_{WFw,t} \tag{8.6}$$

The ESS set of constraints remain the same as in model introduced in the previous chapter:

$$E_{t+1} = E_t + \eta_{ch} p_{ch,t} - \frac{p_{dis,t}}{\eta_{dis}} \quad \forall t \in T \tag{7.5}$$

$$0 \le E_t \le E_{ESS} \quad \forall t \in T \tag{7.6}$$

$$0 \le p_{ch,t} \le P_{ESS} \quad \forall t \in T \tag{7.7}$$

$$0 \le p_{dis,t} \le P_{ESS} \quad \forall t \in T \tag{7.8}$$

$$0 \le p_{ch,t} \le \alpha_t M \quad \forall t \in T \tag{7.9}$$

$$0 \le p_{dis,t} \le (1-\alpha_t) M \quad \forall t \in T \tag{7.10}$$

$$p_{ESS} \le \frac{E_{ESS}}{3\Delta t} \tag{7.11}$$

$$p_{ch,t} \le p_{u,t} \quad \forall t \in T \tag{7.12}$$

The objective function is linear and as introduced earlier in section 7.2:

$$\begin{aligned} min \sum_{t \in T} \sum_{g \in G} (y_{g,t} + SU cost_{g,t} + z_{g,t} SD cost_g) \\ + \pi \Delta t \sum_{t \in T} (P_{u,t} - P_{ch,t}) + dE_{ESS} + eP_{ESS} \end{aligned} \tag{7.13}$$

For simplicity, 4 weeks (672 hrs.) are chosen for this study. Once the ESS optimization problem is solved, the expected power output of the SF, WF and ESS is inputted to the PPC to assess production costs and reliability.

8.4 Reliability Assessment Using the Probabilistic Production Costing

The PPC method is described earlier is applied to assess the reliability when adding ESS. The CG model and the equivalent load model stay the same as in section 7.3.

8.5 Case Study

Hourly solar radiation and wind speed data for 6 years of Texas is collected [48],[49]. The SCGs/WTSs in the SFs/WFs have the same specifications. The VG penetration levels are 20% and 30% of the total CG installed capacity. There are 2 WFs and 2 SFs in the study. The WFs and SFs contribute equally to each penetration level. For instance, if the VG penetration level is 20%, 5% is the contribution of each WF/SF. N_{SCG} and N_{WTS} are dependent on the considered VG penetration level. Starting with the SFs, there are N_{SCG} SCGs in each SF and each SCG has specifications as in Table 7-1 . On other hand, the Areva Multibird M5000 WT specifications are utilized to perform the analysis of the case study [48]. These specifications are shown in Table 7-2. The ESS technology chosen for the study is lead-acid with following specification shown in Table 7-3 [47]. The time of simulation, T, is 672 hrs., Δt = 1 hr. and e and d are computed to reflect the cost of the ESS T, as introduced earlier in section 7.4. The price penalty on unutilized VG, π, equals 80 $/MWh. Finally, the test system consists of:

(1) 10 CGs as introduced earlier in Table 6-2, Table 6-2 and Table 6-3,

(2) 2 SFs and 2 WFs,

and (3) load with the p.u. data taken from the IEEE-RTS with a base of 1,150 MW [40].

8.5.1 SFs/WFs Power Output PDF/CDF Results

SFs and WFs power output PDFs and CDFs were computed for all seasons and for the two penetration levels. Taking 30% penetration level as an example, Figure 8-1-Figure 8-8 show comparison between the two SFs output PDFs and CDFS. These figures show that SF1 has lower zero output probabilities in all seasons than SF2 does. On the other hand, Figure 8-9-Figure 8-16 compare the output of WF1 and WF2 PDFs and CDFs. WF2 has lower probabilities of having zero output in all seasons. The PDFs and CDFs of SF1, SF2, WF1 and WF2 power outputs at 20% penetration level are in APPENDIX B.

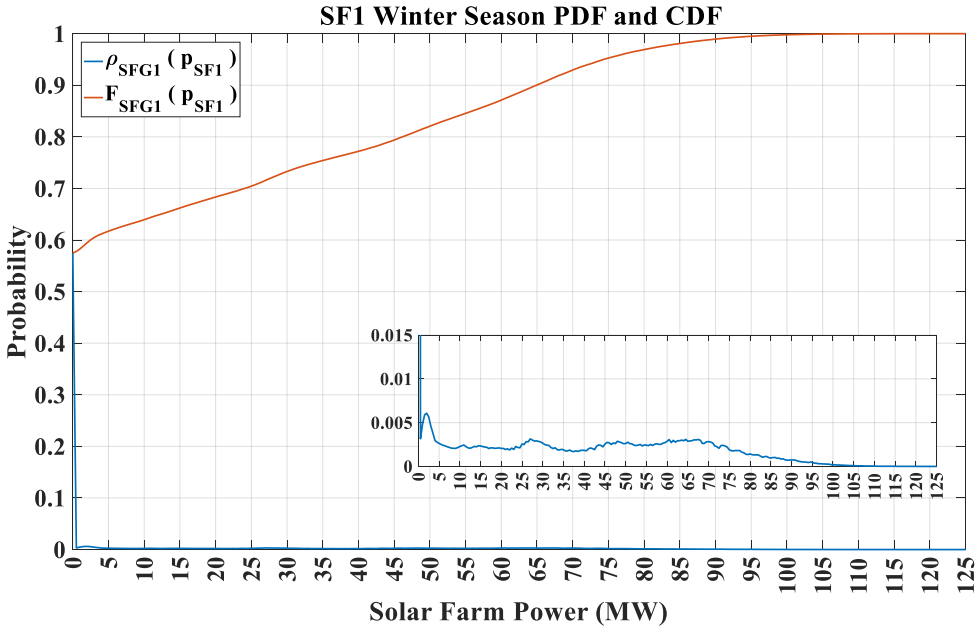

Figure 8-1. Winter season PDF and CDF of SF1 at 30% penetration level.

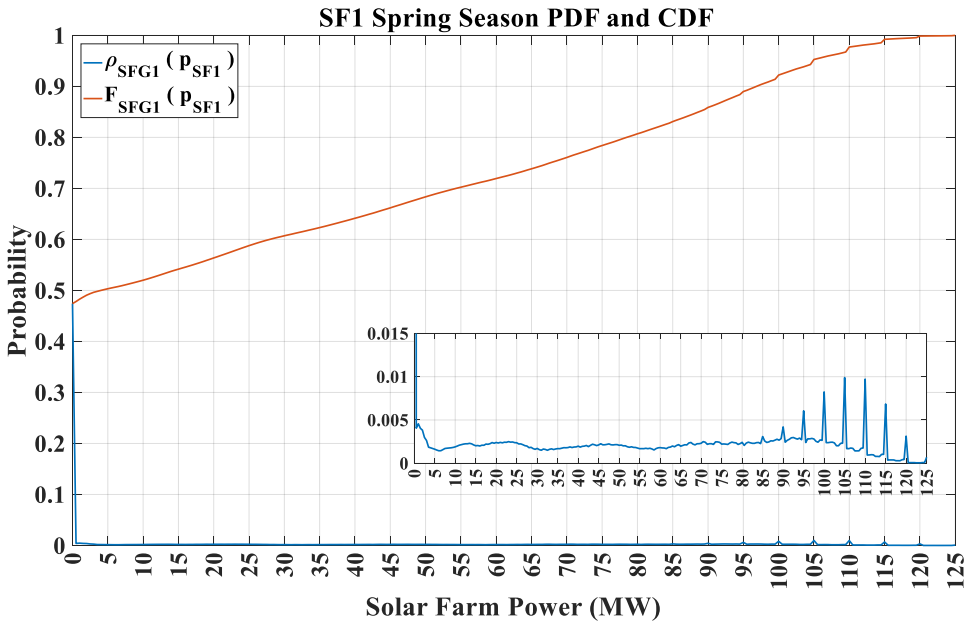

Figure 8-2. Spring season PDF and CDF of SF1 at 30% penetration level.

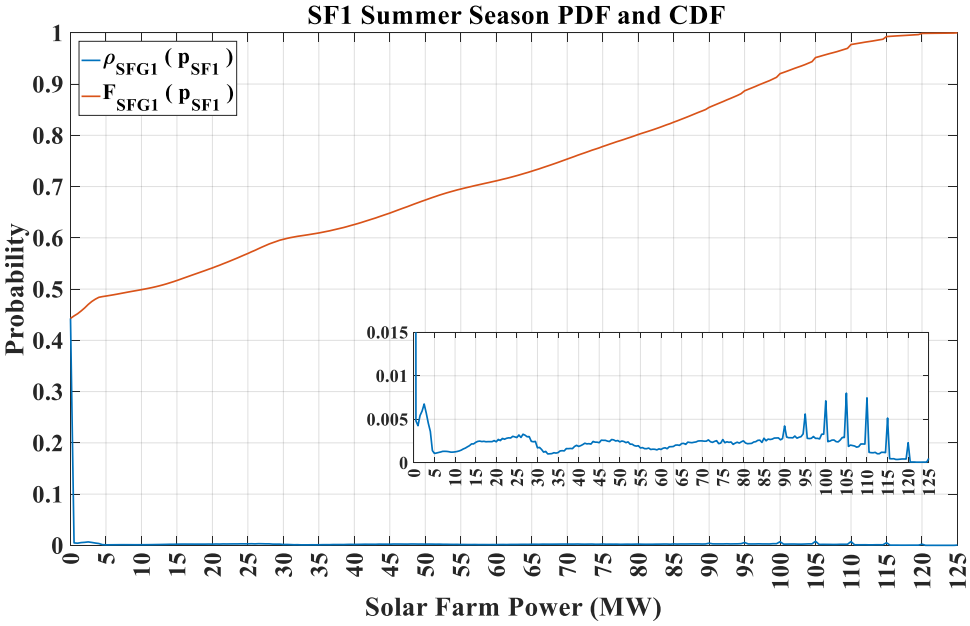

Figure 8-3. Summer season PDF and CDF of SF1 at 30% penetration level.

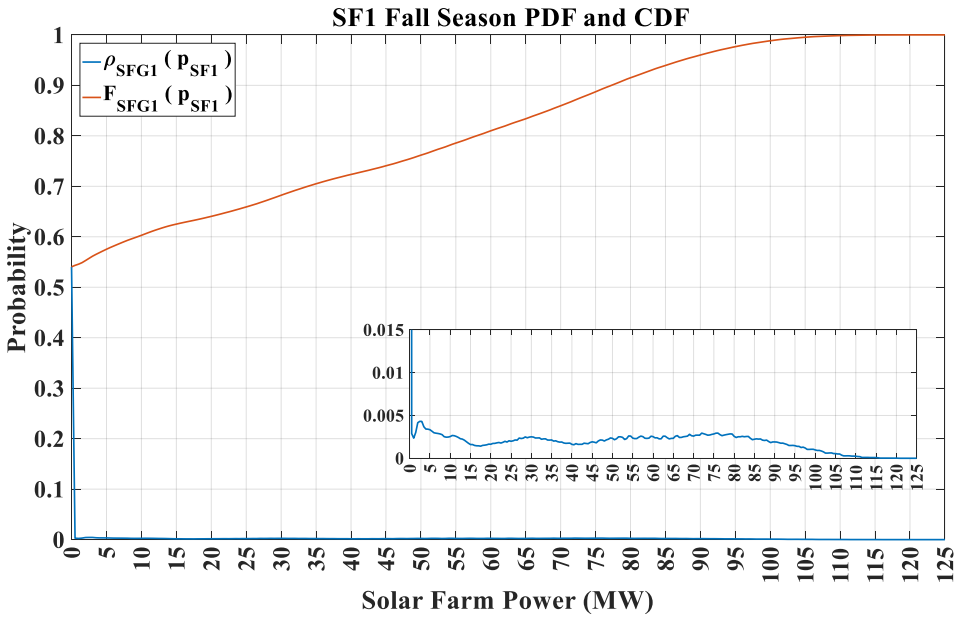

Figure 8-4. Fall season PDF and CDF of SF1 at 30% penetration level.

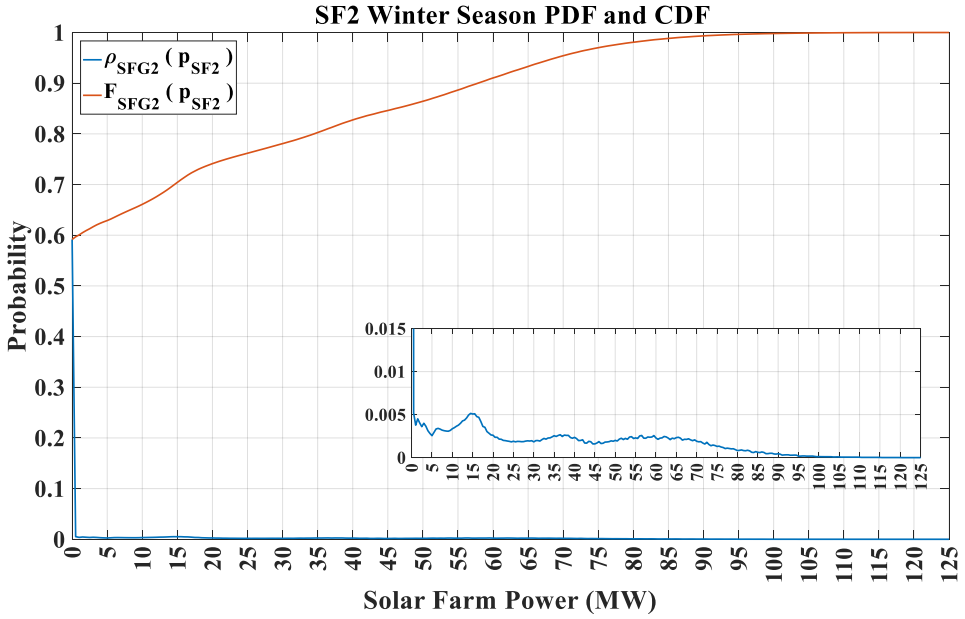

Figure 8-5. Winter season PDF and CDF of SF2 at 30% penetration level.

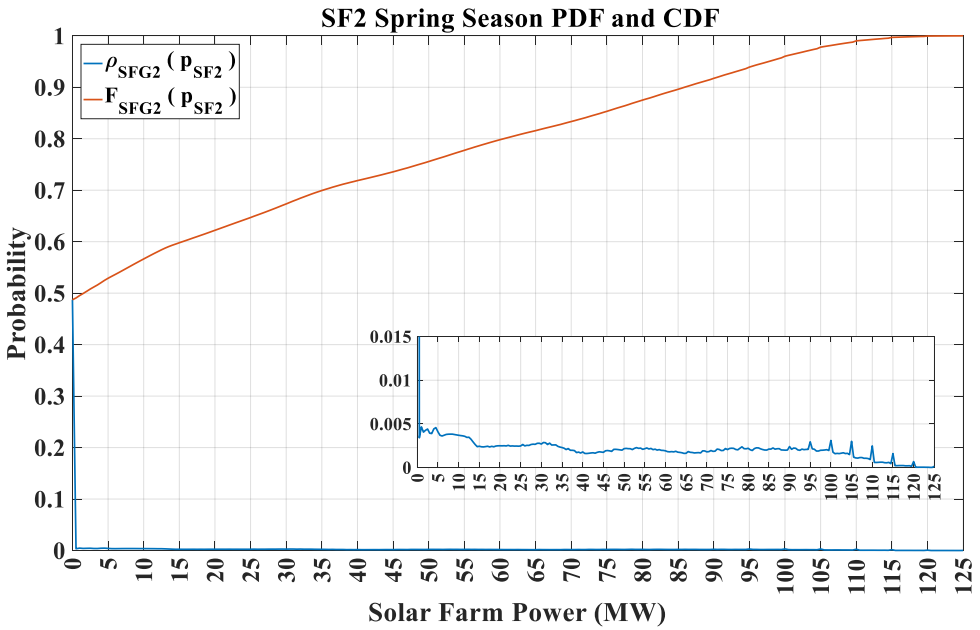

Figure 8-6. Spring season PDF and CDF of SF2 at 30% penetration level.

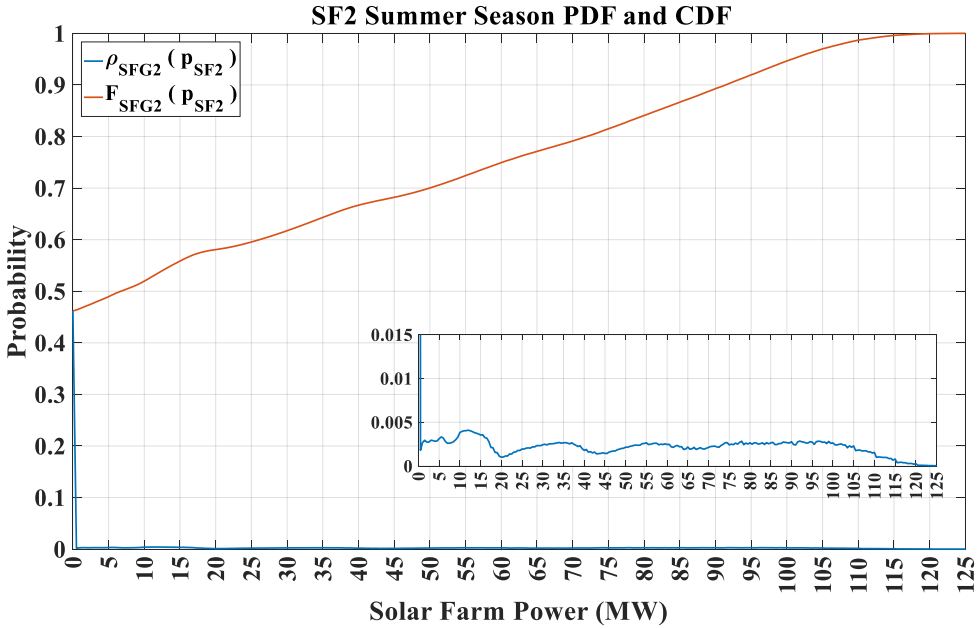

Figure 8-7. Summer season PDF and CDF of SF2 at 30% penetration level.

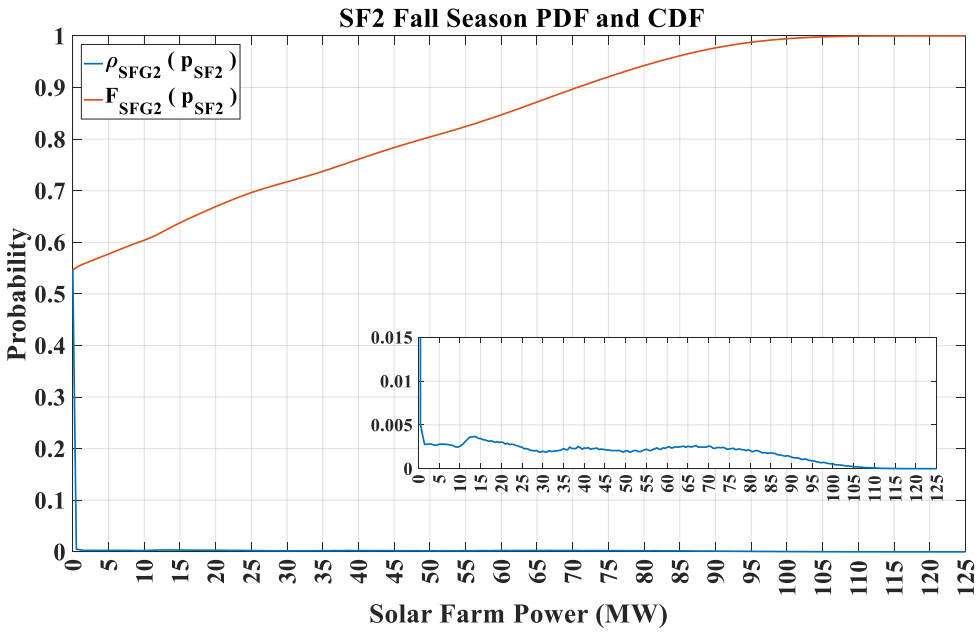

Figure 8-8. Fall season PDF and CDF of SF2 at 30% penetration level.

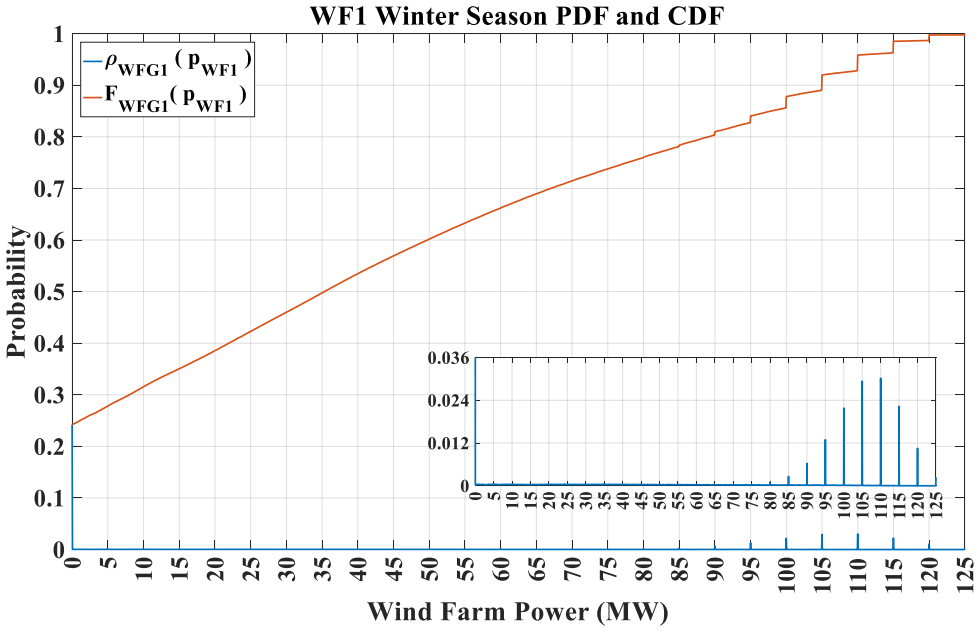

Figure 8-9. Winter season PDF and CDF of WF1 at 30% penetration level.

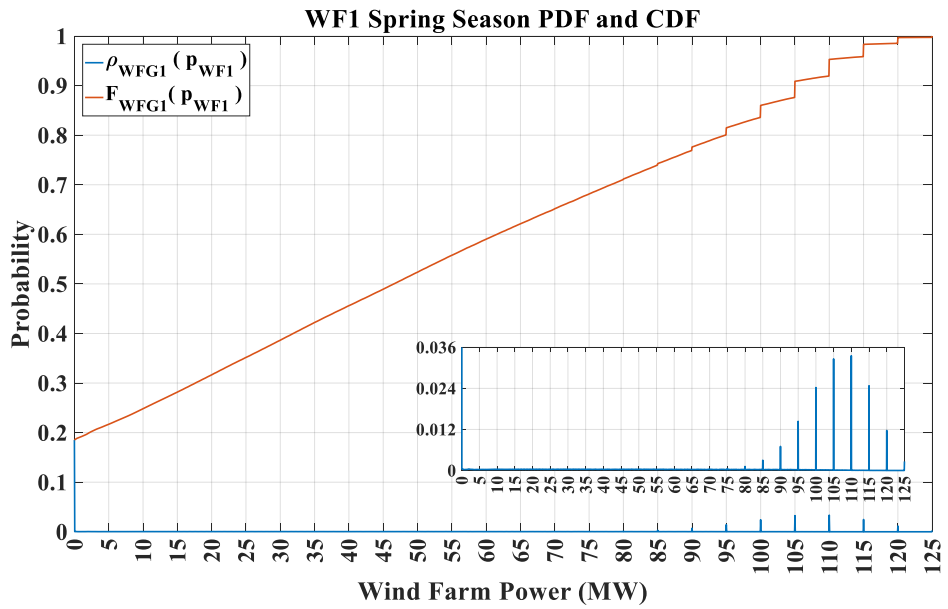

Figure 8-10. Spring season PDF and CDF of WF1 at 30% penetration level.

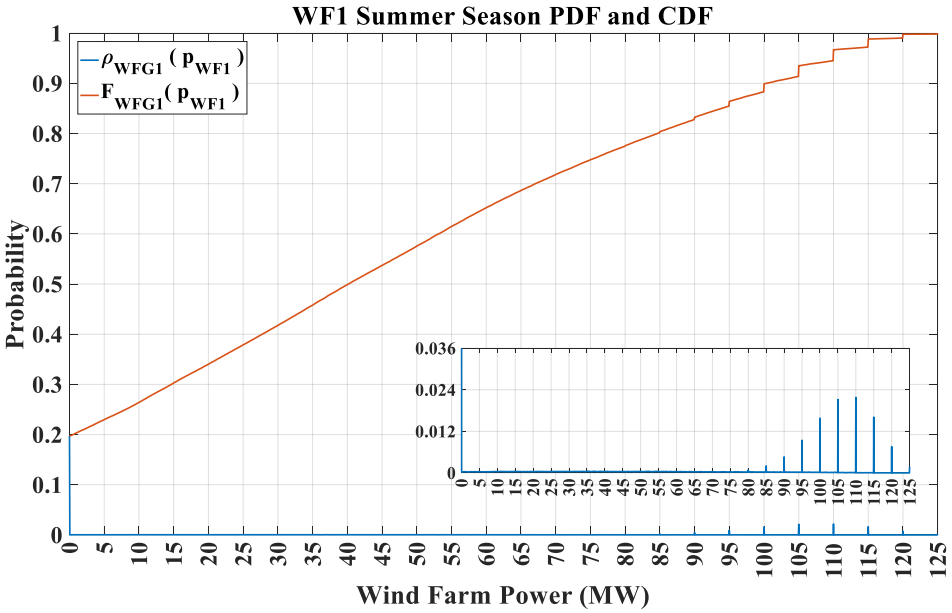

Figure 8-11. Summer season PDF and CDF of WF1 at 30% penetration level.

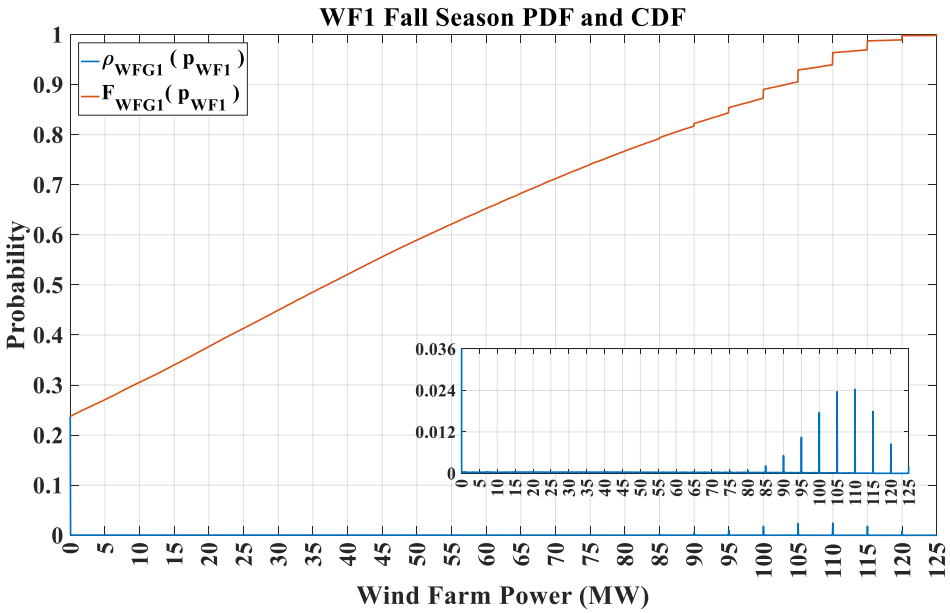

Figure 8-12. Fall season PDF and CDF of WF1 at 30% penetration level.

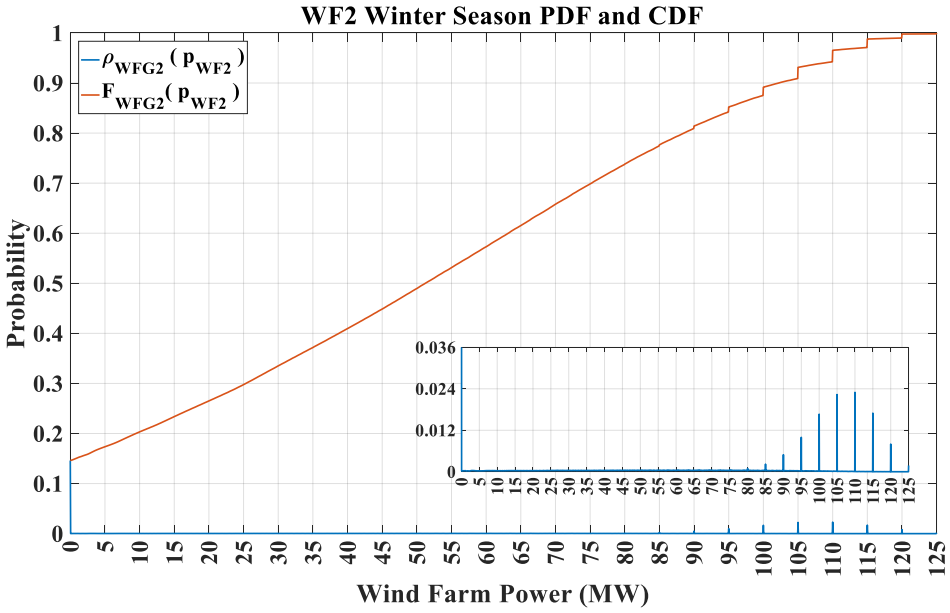

Figure 8-13. Winter season PDF and CDF of WF2 at 30% penetration level.

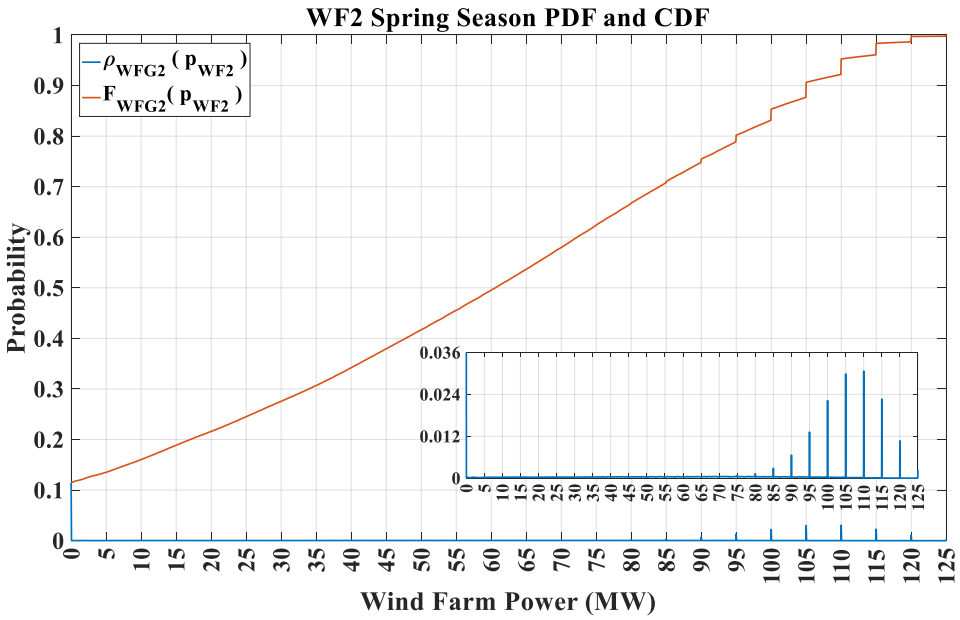

Figure 8-14. Spring season PDF and CDF of WF2 at 30% penetration level.

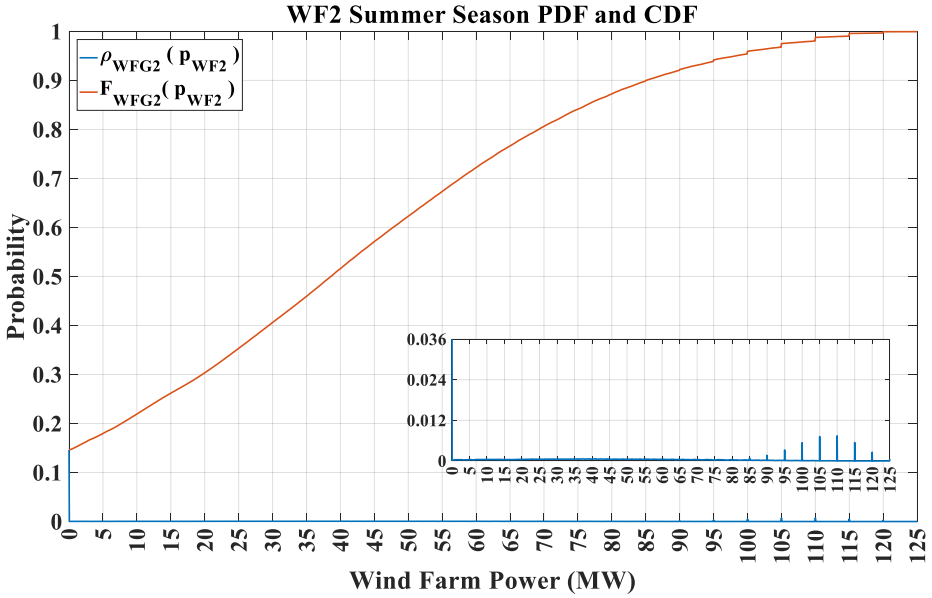

Figure 8-15. Summer season PDF and CDF of WF2 at 30% penetration level.

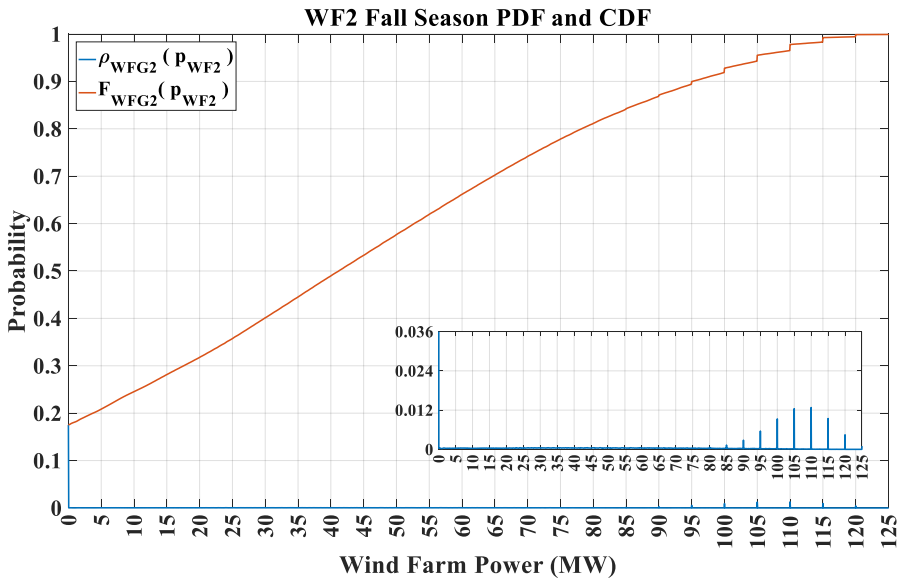

Figure 8-16. Fall season PDF and CDF of WF2 at 30% penetration level.

8.5.2 ESS Sizing Results

Table 8-1 shows the optimal P_{ESS}, and E_{ESS} as well as the resultant ESS cost for the two penetration levels over the simulation period. Comparing the ESS sizing at 30% and 20%, P_{ESS} and E_{ESS} at 30% were significantly larger than P_{ESS} and E_{ESS} at 20%. This might be attributed to the significant increase in penetration (10% more) that resulted in more VG utilized and a change in CGs operation to reduce the overall cost while maintaining the operational constraints.

Table 8-1. ESS sizing results.

VG %	P_{ESS} (MW)	E_{ESS} (MWh)	ESS Cost ($)
30%	52.60	157.79	451,287.60
20%	9.81	29.46	84,230.91

To compute reliability the same analysis was applied first without ESS and VG (base case with just CG) and then with only VG (no ESS). Taking the 30% penetration level as an example, Figure 8-17 shows the charging/discharging and SOC profiles of the ESS. Figure 8-18 shows the unutilized VG power with and without ESS. The ESS clearly decreased the unutilized energy significantly and resulted in reducing the total cost of the system from $ 7,946,000 to $7,341,000 and improved the system reliability as well.

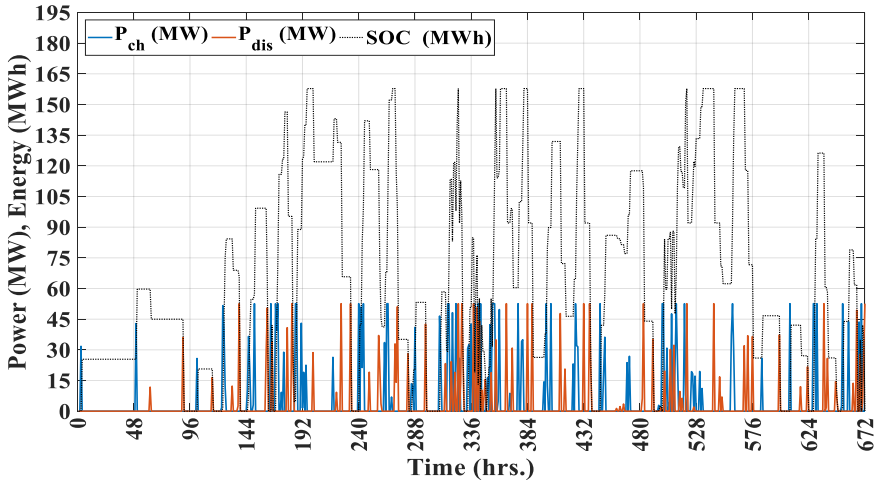

Figure 8-17. ESS power and energy profiles at 30% penetration.

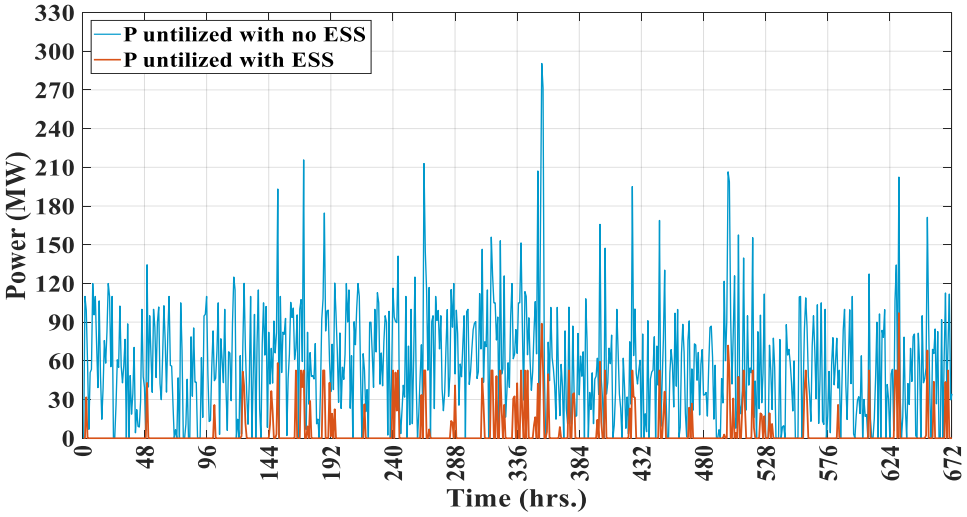

Figure 8-18. Unutilized VG at 30% penetration (with/without ESS).

8.5.3 Reliability Assessment Results

Table 8-2 shows the reliability assessment and cost projection of the two penetration levels with/without ESS. Compared to the base case, the improvement ranged from 35 % to 63% in LOLP and LOLE in the presence of VG and ESS while ranged from 22% to 43% in presence of only VG. similarly, the EUE improvement ranged from 36% to 54% in presence of only VG while the improvement ranged from 54% to 74% in the case of VG and ESS. The total cost followed the same pattern as the EUE and LOLP.

Table 8-2. Reliability assessment results.

Case	VG %	LOLP	LOLE (hrs./y)	EUE (MWh)	Total Cost (k$)
Base case	0%	0.00054	4.73	43.11	9,184
VG only	20%	0.00042	3.68	27.46	8,470
	30%	0.00031	2.72	19.92	7,946
VG+ESS	20%	0.00035	3.07	19.71	8,045
	30%	0.00020	1.75	11.05	7,341

8.6 Conclusions

This Chapter presented a MILP model for optimal ESS sizing that considers VG units forced outages, seasonal and locational variation of wind speed and solar radiation and different penetration levels. Subsequently, the PPC method was used to assess the ESS impact on reliability. The results indicate that for the specific system considered, ESS improved both LOLP index and the EUE index, and reduced the total expected cost.

CHAPTER 9. ENERGY STORAGE SIZING AND PROBABILISTIC RELIABILITY ASSESSMENT FOR POWER SYSTEMS BASED ON COMPOSITE DEMAND

This chapter introduces a comprehensive model for long-term optimal ESS sizing that takes into account VG-load seasonal variations and mutual correlations while also accounts for VG failure and repair rates, CG operational practices and constraints and operational reserve requirements. As the VG and demand are key factors in ESS sizing, the correlation between VG and demand is important for more accurate long-term model for ESS sizing when representing VG and demand. The model formulates the optimal ESS sizing as a MILP problem accounting for different VG penetration levels over time. The proposed ESS optimal sizing model considers the following: (a) WTSs and SCGs FORs, (b) solar radiation and wind speed seasonal variation and uncertainty and their correlation with each other and the demand, (c) CGs operational constraints, and (d) demand and reserve (provided by both CGs and ESS) requirements. First, as introduced before in CHAPTER 8, for a specific location, historical wind speeds and solar radiation data is partitioned into four groups, one for each season. Then, the expected WTSs and SCGs generation is computed based on (a) their generation model, and (b) availability and unavailability model, i.e., the collective WTSs/SCGs availability PDFs based on their FORs. Subsequently, an important step is to compute the correlation between each pair of the WTSs/SGSs expected output and demand. The correlation indicates the tendency of expected VG power outputs and demand to change or vary together and considering it produces more accurate results when representing VG and demand in the ESS sizing

model, as explained later. The objective of the ESS sizing optimization problem is to minimize CGs production (fuel), startup and shutdown costs in addition to ESS investment costs. Once the ESS optimal sizing is computed, a reliability assessment is performed based on the PPC method; these computations are repeated for different penetration levels.

9.1 Problem Statement

Assuming that these the following information are given:

1. There are a number of CG units, *G*, with given specifications.
2. The energy and power costs of ESS and the charging/discharging efficiency.
3. The historical wind speed data (V_h) which is partitioned into four groups depending on the season: winter (V_{Wi}), spring (V_{Sp}), summer (V_{Su}) and fall (V_{Fa}).
4. The historical solar radiation data (G_h) which is partitioned into four groups depending on the season: winter (G_{Wi}), spring (G_{Sp}), summer (G_{Su}) and fall (G_{Fa}).
5. The historical demand data (D_h) for the specific location is collected and partitioned into four groups depending on the season,
6. A SF/WF consists of N_{SCG}/N_{WTS} SCGs/WTSs. The SCGs/ WTSs specifications and FORs are assumed given.

The optimal parameters of the ESS system are obtained with the following procedure. Given the four partitioned data sets of solar radiation/wind speed of a specific location, it is desired to find first the expected WF (p_{WF})/SF (p_{SF}) outputs by convolving the PDF of the WF/SF availability and the WF/SF deterministic power outputs. Subsequently, the correlation coefficients (CC) between the *D* and p_{SF}, the *D* and p_{WF}, and p_{SF} and p_{WF} are computed for every season. The correlation is computed using the least square estimation

(LSE) method. The correlation gives insight of how demand and VG co-vary. Depending on the correlations, the samples composite demand (*CD*) is computed. *CD* in general is the demand minus the VG at every instant of time. Once the *CD* samples of all four seasons are computed, they are inputted into the ESS optimal sizing problem. The solution of this problem provides ESS charging/discharging schedules which, in addition to *CD* are inputted to the PPC method to assess the reliability of the integrated load, VG, ESS and CG model, as explained in detail later.

9.2 Computation of SFs/WFs Expected Power Output

9.2.1 SF Expected Power Outputs

Once the historical solar radiation, G_h, is seasonally partitioned, they can be converted to power using the SCG generation model, using equation (5.1). Also, as explained in 5.2.1, $\rho_{SFA}(c_{SF})$, the PMF of SF availability, is a binomial distribution given by equation (5.8). Subsequently convolving the partitioned G_h of each season and $\rho_{SFA}(c_{SF})$ gives the expected SF output as follows:

$$p_{SF} = \rho_{SFA}\left(c_{SF}\right) * G_{Season} \quad \text{Season= Wi, Sp, Su, and Fa} \tag{9.1}$$

where * is the convolution operator.

9.2.2 WF Expected Power Output

Similarly, Once the historical wind speed, V_h, is seasonally partitioned, they can be converted to power using the WTS generation model, equation (5.1). Also, as explained in

5.2.1, $\rho_{WFA}(c_{WF})$, the PMF of WF availability, is a binomial distribution given by equation (4.8). Subsequently convolving the partitioned V_h of each season and $\rho_{WFA}(c_{WF})$ gives the expected SF output as follows:

$$p_{WF} = \rho_{WFA}\left(c_{WF}\right) * V_{Season} \quad \text{Season= Wi, Sp, Su, and Fa} \tag{9.2}$$

The next step is to find CC between D, p_{SF} and p_{WF} for each season.

9.3 Correlation Coefficient and Composite Demand PDF Computation

9.3.1 Correlation Coefficient Computation

The least squares estimation, LSE, [50] is briefly introduced here. In general, we have a set of observed values (o) and would like to fit a straight line. The LSE minimizes the sum of the squared errors (distances) between the observed values and the line. The model of the line is in the form of:

$$o = \beta_o + \beta_1 p \tag{9.3}$$

p is an independent (predictor) variable and o is dependent (or response) variable. It is desired to find the values of β_0, β_1 that minimize the sum of the squared residuals:

$$S(\beta_o, \beta_1) = \sum_{i=1}^{n} (o_i - \beta_o - \beta_1 p)^2 \tag{9.4}$$

To study the correlation of the two variables, the following are computed:

$$S_{pp} = \frac{1}{n}\sum_{i=1}^{n}(p_i - \bar{p})^2 \tag{9.5}$$

$$S_{oo} = \frac{1}{n}\sum_{i=1}^{n}(o_i - \bar{o})^2 \tag{9.6}$$

$$S_{po} = \frac{1}{n}\sum_{i=1}^{n}(p_i - \bar{p})^2(o - \bar{o})^2 \tag{9.7}$$

Where n equals the size of o and p, and $\bar{p}$ and $\bar{o}$ are averages of p and o, respectively. Once the sums of the squares are computed, CC is calculated as in (9.8):

$$CC = \frac{S_{po}}{\sqrt{S_{pp}S_{oo}}} \tag{9.8}$$

The slope of the line that fits the data best is follows:

$$\hat{\beta}_1 = \frac{S_{po}}{S_{pp}} \tag{9.9}$$

and the intercept is:

$$\hat{\beta}_o = \bar{o} - \hat{\beta}_1\bar{p} \tag{9.10}$$

The fitted line equation is:

$$\bar{\sigma} = \hat{\beta}_o + \hat{\beta}_1 \bar{p} \tag{9.11}$$

This analysis will be applied to find the CC of these pairs: (D, p_{SF}), (D, p_{WF}) and (p_{WF}, p_{SF}), i.e., in each pair, there is a predictor and a response.

9.3.2 Composite Demand PDF and CDF Computation Computation

There are three possible cases, depending on the numerical values of pairwise correlation coefficients among D, p_{SF} and p_{WF}:

1. Small or negligible correlation between all three pairs mentioned before. The variables are treated as statistically independent.

2. D is correlated with p_{SF} and p_{WF}. In this case, $CD = D - p_{SF} - p_{WF}$. Then, the PDF/CDF ($\rho_{CD}(cd)$/ $F_{CD}(cd)$) of CD is computed.

3. D is correlated with either p_{SF} or p_{WF}. In this case, two PDFs/CDFs are computed: *D–correlated VG* (either p_{SF} or p_{WF}) PDF/CDF, and *the uncorrelated VG* (either p_{SF} or p_{WF}) PDF/CDF. Subsequently, CD is *D–correlated VG* sample minus *uncorrelated VG* sample.

Intuitively, case 1 is unlikely to happen at least by examining p_{SF} and D. p_{SF} in general is zero before the sun rises and then peaks during the day and declines till it reaches zero when the sun sets. p_{SF}, roughly speaking, has similar increment and decrement behavior in certain hours of the day as the demand does, hence case 1 is unlikely, and cases 2 and 3 are more likely. However, if one VG is uncorrelated or weakly correlated its variation can be

treated as an independent random variable, providing a computational advantage in planning methods. Once the correlation coefficients are computed and the *CD* is determined according to either case 1, 2 or 3, samples of *CD* are computed from appropriate PDFs and CDFs to be inputted to the optimal ESS sizing problem, as explained next.

9.4 Energy Storage Sizing Optimization Formulation

The optimal ESS sizing is similar to the model introduced in section 8.3. However, here some modifications are introduced. The complete set of the constraints are as follows:

$$x_{g,t} - x_{g,t-1} = s_{g,t} - z_{g,t} \qquad \forall g \in G, \forall t \in T \mid t = 1 \tag{6.1}$$

$$p_{g,t} \geq P_G^{min} \, x_{g,t} \qquad \forall g \in G, \forall t \in T \tag{6.2}$$

$$p_{g,t} \leq \bar{p}_{g,t} \leq P_G^{max} x_{g,t} + (SD_g - P_G^{max}) \, z_{g,t+1} \qquad \forall g \in G, \forall t \in T \tag{6.3}$$

Where $\bar{p}_{g,t} = p_{g,t} + r_{g,t}$.

$$\sum_{i=t-UT_g+1}^{t} s_{g,i} \leq x_{g,t} \qquad \forall t \in T, \forall g \in G \tag{6.7}$$

$$\sum_{i=t-DT_g+1}^{t} s_{g,i} \leq 1 - x_{g,t-DT_g} \qquad \forall t \in T, \ \forall g \in G \tag{6.8}$$

$$\bar{p}_{g,t} - p_{g,t-1} \leq SU_g \; s_{g,t} + RU_g \; x_{g,t-1} \tag{6.9}$$

$$p_{g,t-1} - p_{g,t} \leq SD_g \; z_{g,t} + RD_g \; x_{g,t} \tag{6.10}$$

Both the CGs and ESS provide reserve capacity. The CG units provide reserve, r_g, and the ESS should provide up/down reserve ($\bar{p}_{ESS\_UP}/\bar{p}_{ESS\_DN}$) while both also must meet the demand at any instant *t*. The required reserve, *R*, is calculated as a percentage of the peak *CD* plus the largest CG unit capacity while the ESS reserve provision will be discussed when discussing ESS constraints. The constraint in (9.12) ensures that the CG units and ESS can meet the demand and reserve requirements:

$$\sum_{g \in G} \bar{p}_{g,t} + \bar{p}_{ESS\_UP,t} \geq CD_t + \bar{p}_{ESS\_DN,t} + R \qquad \forall t \in T \tag{9.12}$$

The demand constraint, (9.13), ensures that available CG and discharging ESS power should meet the composite demand and charging ESS power at time *t*:

$$\sum_{g \in G} p_{g,t} + p_{dis,t} = CD_t + p_{ch,t} \qquad \forall t \in T \tag{9.13}$$

Sampling for CD_t depends in which case it falls into. First, the time of the simulation *T*, is divided into 4 equal periods, i.e., *T*/4 per season. CD_t sampling is performed by generating uniform random numbers (~unif(*0,1*)), for every instant of time, *t*, and then applying the Inverse Transform method (ITM) as follows:

Case 1: if D, p_{SF} and p_{WF} are all uncorrelated, CD_t samples are the D sample minus p_{SF} and p_{WF} sample, where these samples are generated from their individual CDFs in this case.

Case 2: in this case D, p_{SF} and p_{WF} are correlated, and $CD = D - p_{SF} - p_{WF}$. Subsequently $\rho_{CD}(cd)/F_{CD}(cd)$ are computed and random CD_t samples are generated. $\rho_{CD}(cd)/ F_{CD}(cd)$ are computed for every season. CD_t sampling is performed by generating uniform random numbers, $U_{1,t}$ ~unif*(0,1)*, for every instant of time, *t*, and then applying using the ITM as in (9.14):

$$CD_t = F_{CD}^{-1}(U_{1,t}) \quad \forall t \in T \tag{9.14}$$

Case 3: when demand is correlated with only one VG, either p_{SF} or p_{WF}. There are two possibilities:

a. if D and p_{SF} are correlated, the PDF/CDF of $D - p_{SF}$ ($\rho_{D-SF}(d)/ F_{D-SF}(d)$) are computed first. Then, the PDF/CDF of p_{WF} ($\rho_{WFG}(p_{WF})/ F_{WFG}(p_{WF})$) is computed. Sampling for CD_t in (9.12) and (9.13), is as follows:

$$CD_t = F_{CD}^{-1}(U_{2,t}) - F_{WFG}^{-1}(U_{3,t}) \quad \forall t \in T \tag{9.15}$$

Where $U_{2,t}$ ~unif(0,1) and U3,t ~unif(0,1). CD_t in this case is the subtraction of WF power samples from the $D - p_{SF}$ samples. This procedure is repeated for every season.

b. if D and p_{WF} are correlated, the PDF/CDF of $D - p_{WF}$ ($\rho_{D-WF}(d)$/ $F_{D-WF}(d)$) are computed first. Then, the PDF/CDF of p_{SF} ($\rho_{SFG}(p_{SF})$/ $F_{SFG}(p_{SF})$) is computed. Sampling for CD_t, in this case, is performed as in (9.16):

$$CD_t = F_{CD}^{-1}(U_{4,t}) - F_{SFG}^{-1}(U_{5,t}) \quad \forall t \in T \tag{9.16}$$

where $U_{4,t}$ ~unif*(0,1)* and $U_{5,t}$ ~unif*(0,1)*. CD_t in this case is the subtraction of SF power samples from the $D - p_{WF}$ samples. This procedure is repeated for every season.

The ESS set of constraints are modified to account for the addition of ESS reserve provision capability The ESS constraints are key factors in determining the optimal ESS size as they dictate the operation of ESS. They determine the ESS charge/discharge schedule and set power and energy limits. Constraint in (7.5) and (7.6) as introduced before. Constraints in, (9.17) and (9.18) are the down reserve and charging, and up reserve and discharging power limits, respectively. Constraints (9.19) and (9.20) ensure no simultaneously ESS charging and discharging nor simultaneously Up and Down reserve provision. Constraints (9.21) and (9.22) ensure that the SOC at time *t* is not exceeded when providing ESS power and reserve.

$$E_{t+1} = E_t + \eta_{ch} p_{ch,t} - \frac{p_{dis,t}}{\eta_{dis}} \quad \forall t \in T \tag{7.5}$$

$$0 \le E_t \le E_{ESS} \quad \forall t \in T \tag{7.6}$$

$$0 \le p_{ch,t} \le \bar{p}_{ESS\_DN,t} \le P_{ESS} \quad \forall t \in T \tag{9.17}$$

$$0 \le p_{dis,t} \le \bar{p}_{ESS\_UP,t} \le P_{ESS} \quad \forall t \in T \tag{9.18}$$

$$0 \le \bar{p}_{ESS\_UP,t} \le \alpha_t M \quad \forall t \in T \tag{9.19}$$

$$0 \le \bar{p}_{ESS\_DN,t} \le (1-\alpha_t) M \quad \forall t \in T \tag{9.20}$$

$$\bar{p}_{ESS\_UP,t} \le \frac{E_t}{\Delta t} \quad \forall t \in T \tag{9.21}$$

$$\frac{E_{ESS} - E_t}{\Delta t} - \bar{p}_{ESS\_DN,t} \ge 0 \quad \forall t \in T \tag{9.22}$$

$$p_{ESS} \le \frac{E_{ESS}}{3\Delta t} \tag{7.11}$$

Where $\bar{p}_{ESS\_UP,t} = p_{dis,t} + r_{ESS\_UP,t}$ and $\bar{p}_{ESS\_DN,t} = p_{ch,t} + r_{ESS\_DN,t}$.

The objective function is linear and as introduced earlier. The objective function minimizes CG production cost, startup and shutdown costs, and ESS power and energy costs as follows:

$$min \sum_{t \in T} \sum_{g \in G} (y_{g,t} + SU\,cost_{g,t} + z_{g,t} SD\,cost_g) + dE_{ESS} + eP_{ESS} \qquad (9.23)$$

9.5 Reliability Assessment Using the Probabilistic Production Costing

The PPC method is described earlier is applied to assess the reliability when adding ESS. The CG model and the equivalent load model is modified as follows:

$$\text{ELDC} = \text{CD} - \text{ESS power} \qquad (9.23)$$

9.6 Case Study

Hourly, solar radiation wind speed and demand data for 6 years in Texas are collected [48],[49],[51] . Note that the historical demand data is scaled down to the test system peak. The test system consists of:

(1) The 10 CGs as introduced earlier in Table 6-2, Table 6-2 and Table 6-3,

(2) A WF with N_{WTS} identical WTSs, the WTS specification shown in Table 7-2.

(3) A SF with N_{SCG} identical SCGs, the SCG specification shown in Table 9-1.

(4) Demand data taken from [51] and scaled to a peak of 1,150 MW.

(5) ESS with specifications as shown in Table 9-2.

The VG penetration levels are 20% and 30% of the total CG installed capacity (1,662 MW). The WF and the SF contribute equally to each penetration level. For instance, if the

VG penetration level is 20%, 10% comes from the WF and 10% from the SF. N_{SCG} and N_{WTS} are dependent on the considered VG penetration level. Specifically, for 20% penetration level: N_{SCG} =33, and N_{WTS} =332; for 30% penetration level: N_{SCG} =50, and N_{WTS} =499. The ESS technology chosen is lead-acid and the time of simulation, T, is 8760 hrs. and Δt = 1 hr. The ESS life expectancy is 20 years and e and d reflect the energy and power capital costs, respectively, over T assuming a discount rate of 5%.

Table 9-1. SCG specifications.

$p_{SCG.rated}$	0.5 MW
G_{std}	1,000 W/m^2
R_C	150 W/m^2
q_{SCG} (assumed)	0.15
$MTTF_{SCG}$	950 hrs.
$MTTR_{SCG}$	167.7 hrs.

Table 9-2. ESS specifications.

ESS technology	lead-acid
η_{ch} / η_{dis}	80%
Energy capital cost	330 k$/MWh
Power capital cost	400 k$/MW
Lifetime	20 years
Discount rate	5%
e	26480.05 $/MWh
d	32,097.03 $/MW

9.6.1 Expected WF/SF Power Outputs Results

The historical demand, wind speed and solar radiation data is partitioned into four seasonal groups. Samples of the partitioned data are shown in Figure 9-1, Figure 9-2 and Figure 9-3. Subsequently, the partitioned wind speed and solar radiation are converted to power using the WTS and SCG generation models respectively. Then, the expected WF power output, p_{WF}, and expected SF power output, p_{SF}, are calculated using the convolution operation explained in section 9.2. Note that this is repeated for every VG penetration level

because N_{SCG} and N_{WTS} are computed from the assumed VG penetration level. For instance, at 30% penetration level, Figure 9-4 and Figure 9-5 show the expected WF and SF power output, respectively. APPENDIX C includes the expected WF and SF power output figures, respectively, for the 20% penetration level case.

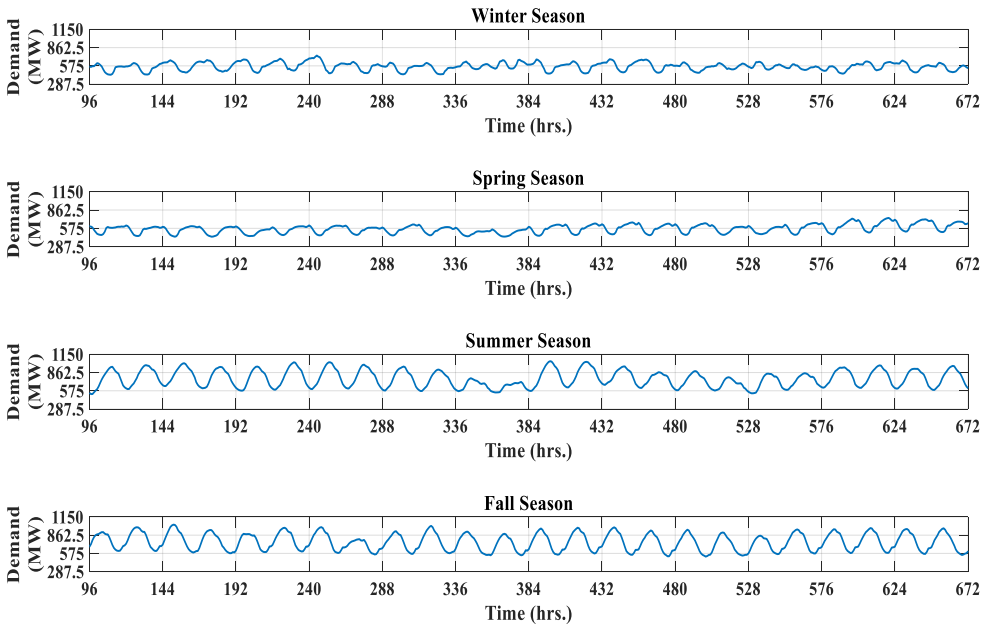

Figure 9-1. Historical demand data.

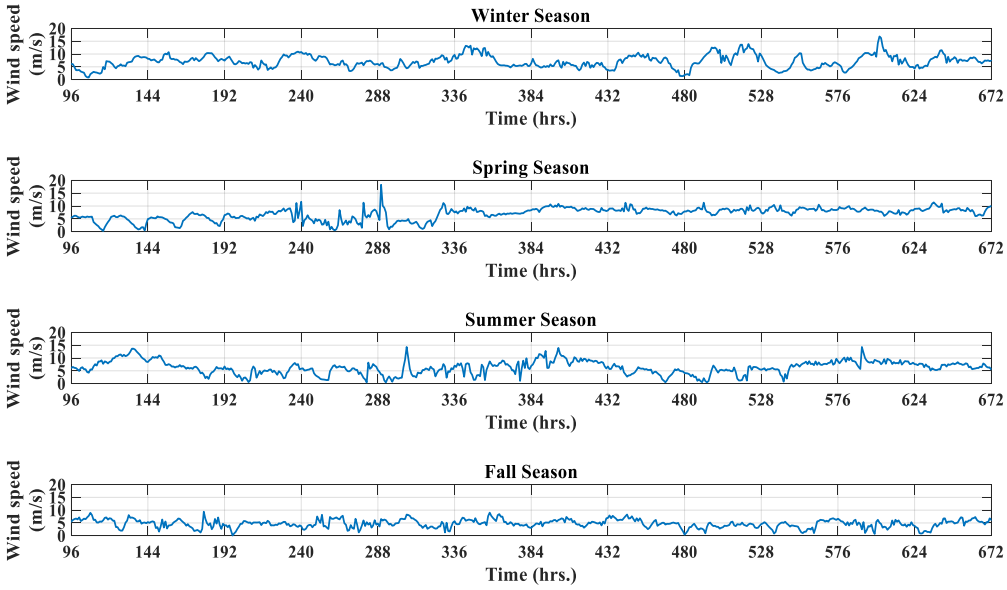

Figure 9-2. Historical wind speed data.

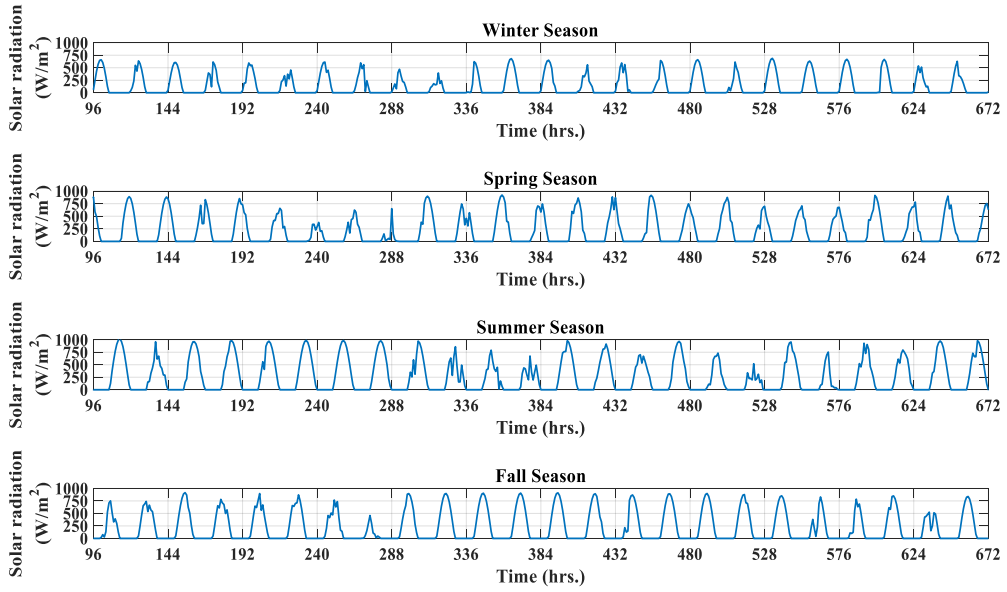

Figure 9-3. Historical solar radiation data.

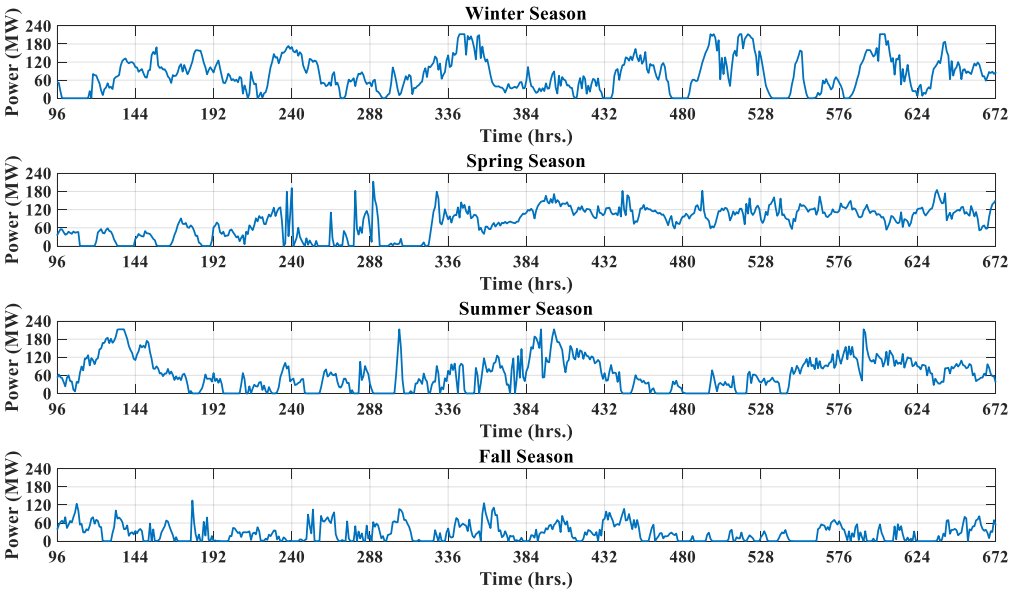

Figure 9-4. Expected WF power output (p_{WF}) at 30% penetration level.

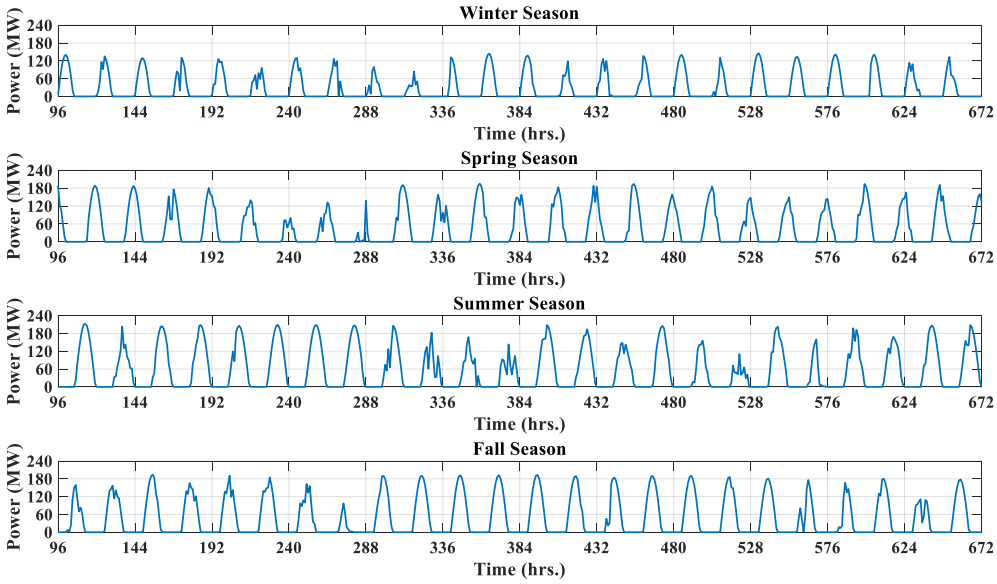

Figure 9-5. Expected SF power output (p_{SF}) at 30% penetration level.

9.6.2 Correlation Coefficients and Composite Demand PDF

The correlation coefficients, CC, were computed for all pairs, (D, p_{SF}), (D, p_{WF}) and (p_{WF}, p_{SF}), for all four seasons. Note that the penetration level has no statistical effect on the CC, i.e., CC at 30% penetration level equals CC at 20% level for the same pair. Table 9-3 shows the CC values between the aforementioned pairs. D and p_{SF} CC values were highest in summer (0.5699) and lowest in winter (0.2552). Examining the CC values of D and p_{SF} indicated that there is strong correlation between D and p_{SF}. On the other hand, D/ p_{WF} and p_{WF}/ p_{SF} CC values indicated that there is negligible correlation. Because of the negligible CC values of p_{WF} and demand/ p_{SF}, p_{WF} varies negligibly when D/ p_{SF} change. For comparative purposes, two cases studied: (a) p_{WF} assumed to be dependent process contributing to the *CD*, i.e., case 2, and (b) as a statistically independent process, i.e., case 3.

Table 9-3. Correlation coefficient values.

Response/predictor	Season	Correlation Coefficient (CC)
D/ p_{SF}	Winter	0.2552
	Spring	0.4507
	Summer	0.5699
	Fall	0.4500
D/ p_{WF}	Winter	0.0226
	Spring	-0.0237
	Summer	0.1562
	Fall	-0.1242
p_{SF} / p_{WF}	Winter	-0.1658
	Spring	-0.0553
	Summer	0.0368
	Fall	-0.1380

For each season, $\rho_{CD}(cd)$ and $F_{CD}(cd)$ were computed according to case 2 and case 3. For case 2, *CD* was found by subtracting p_{WF} and p_{SF} from *D*. Figure 9-6 and Figure 9-7 depict $\rho_{CD}(cd)$ and $F_{CD}(cd)$ respectively for all four seasons at 30% penetration level. Notably, at 30% penetration level, $\rho_{CD}(cd)$ and $F_{CD}(cd)$ has negative values because VG was greater than the demand for few hours. To apply the ESS sampling, 2,190, i.e., 8760/4, samples were generated from each season $F_{CD}(cd)$ using the ITM (equation (9.14)). In total, 8760 samples were generated and inputted to the ESS sizing problem. On the other hand, treating p_{WF} as in case 3, *CD* was computed by subtracting only p_{WF} samples from the *D*- p_{SF} Samples. Figure 9-8 and Figure 9-9 depict $\rho_{D-SF}(d)$ and $F_{D-SF}(d)$, respectively, and Figure 9-10and Figure 9-11 show $\rho_{WFG}(p_{WF})$ and $F_{WFG}(p_{WF})$, respectively. Similar PDFs and CDFs can be found in APPENDIX C for the 20% penetration level. All the aforementioned PDFs and CDFs highlight the demand and VG variabilities for this case. Sampling from each season PDFs/CDFs captures these variabilities and define the ESS sizing problem more accurately.

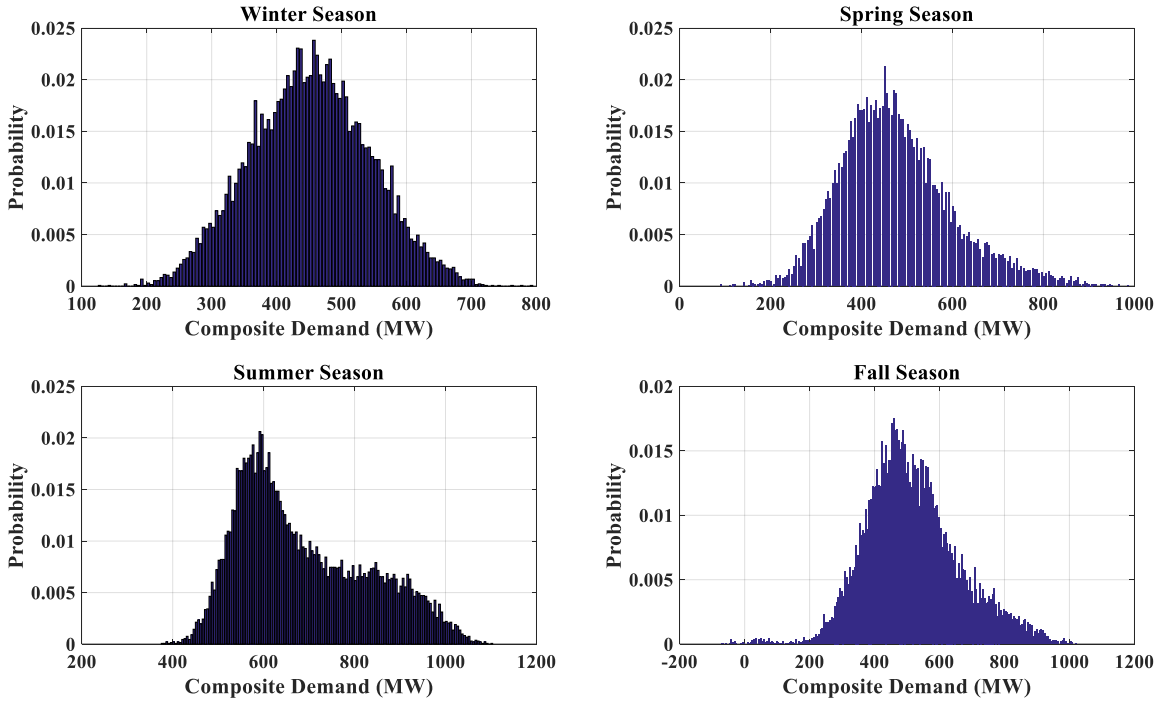

Figure 9-6. Composite demand PDFs ($\rho_{CD}(cd)$) at 30% penetration level (Case 2).

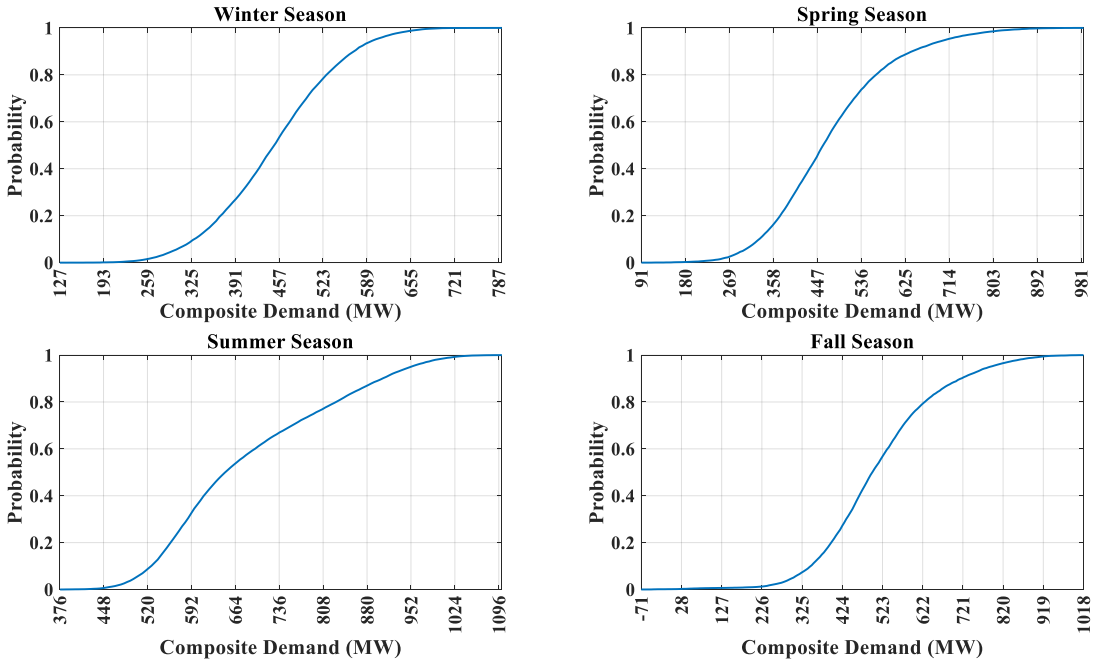

Figure 9-7. Composite demand CDFs ($F_{CD}(cd)$) at 30% penetration level (Case 2).

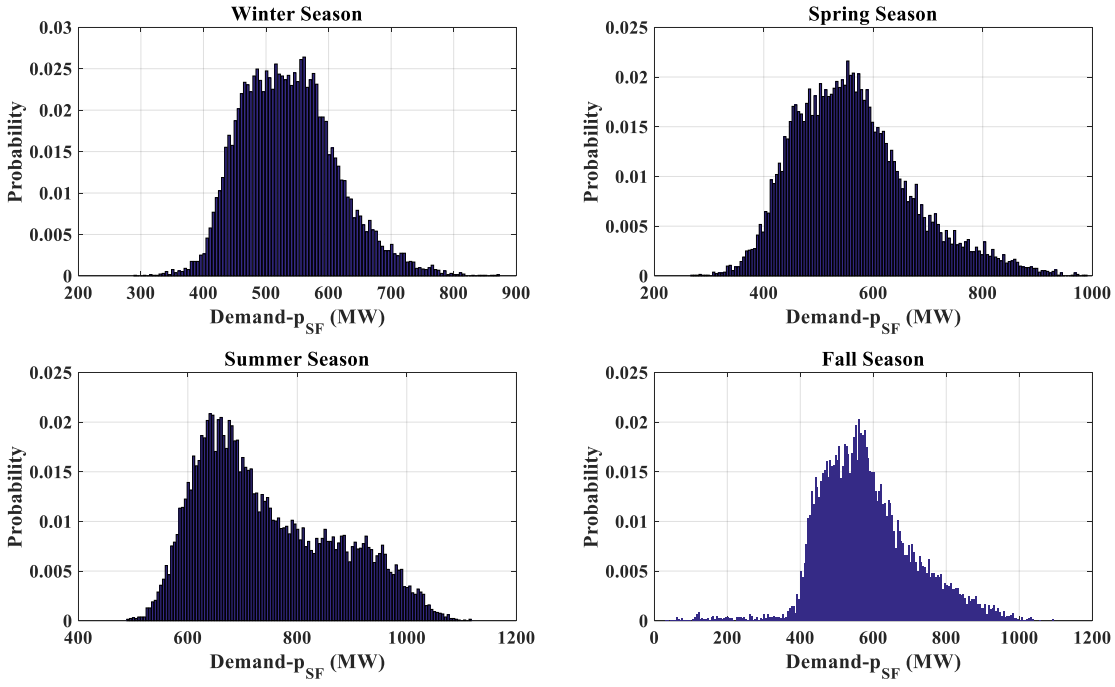

Figure 9-8. *D – SF* PDFs ($\rho_{D-SF}(d)$) at 30% penetration level (Case 3).

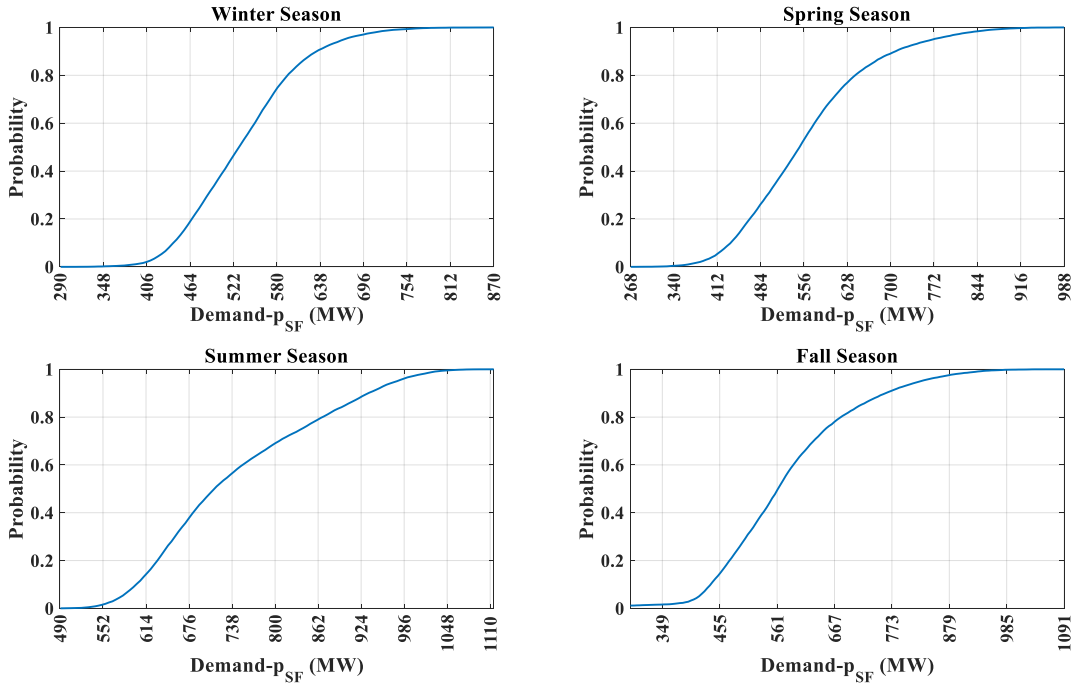

Figure 9-9. *D – SF* CDFs ($\rho_{D-SF}(d)$) at 30% penetration level (Case 3).

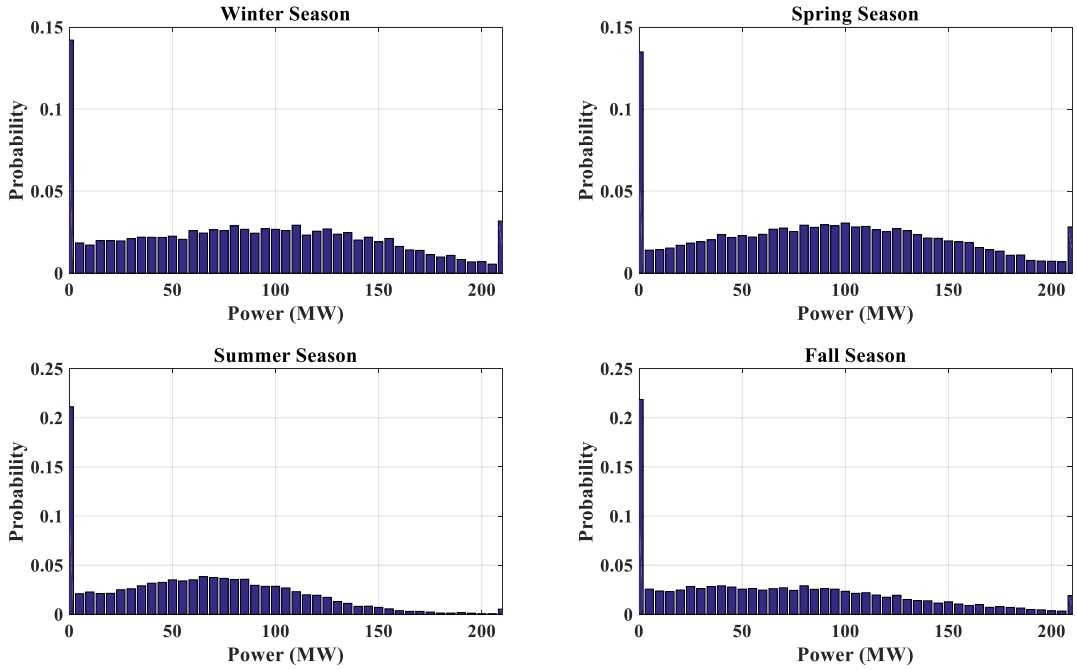

Figure 9-10. WF power output (ρ_{WFG} (p_{WF})) PDFs at 30% penetration (Case 3).

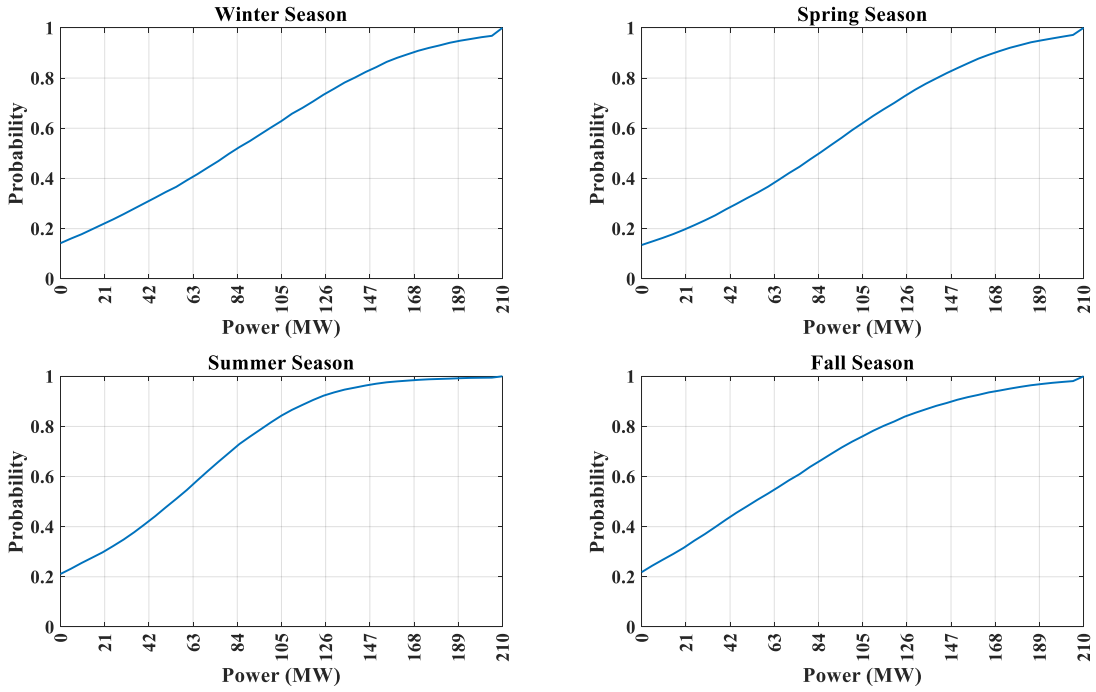

Figure 9-11. WF power output (F_{WFG} (p_{WF})) PDFs at 30% penetration (Case 3).

9.6.3 ESS Sizing Results

Table 9-4 shows the ESS sizing results for cases 2 and 3 for all penetration levels. Case 3 resulted in higher E_{ESS} and P_{ESS} values compared with case 2. Comparing case 3 results to Case 2, ESS costs and optimal sizes found by applying case 3 were 9.5% and 11.7% higher than the one in Case 2 for 20% and 30% penetration levels, respectively. These differences between the two cases results could be attributed to the small correlation between p_{WF} and $D/\ p_{SF}$. Notably, Case 3 ESS sizing results at 30% and 20% were higher than Case 2 at 30%. This could be a result of not considering the small variation between p_{WF} and $D/\ p_{SF}$. On the other hand, Figure 9-12 shows the state of charge ,SOC, of the ESS for both cases at 30% penetration level over the simulation period while Figure 9-13 shows SOC for one day. Figure 9-14 and Figure 9-15 show the CG and ESS reserve provision over the period of the simulation for 30% and 20% respectively. Over the period of the simulation, ESS provided substantial percentage of the reserve.

Table 9-4. ESS sizing and cost results.

	VG %	**P_{ESS} (MW)**	**E_{ESS} (MWh)**	**ESS Cost ($)**
Case 2	30%	387.51	1,162.54	43,222,037
	20%	355.69	1,067.06	39,672,395
Case 3	30%	424.38	1,273.14	47,334,148
	20%	397.26	1,191.78	44,309,260

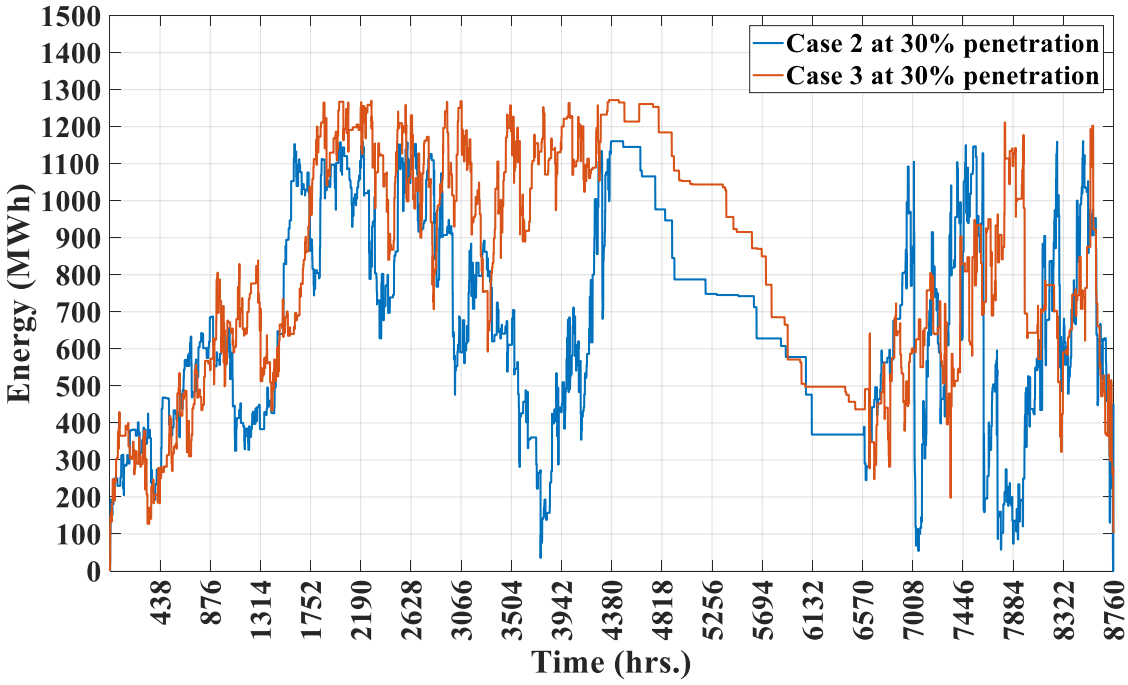

Figure 9-12. ESS SOC for case 2 and 3 at 30% penetration level.

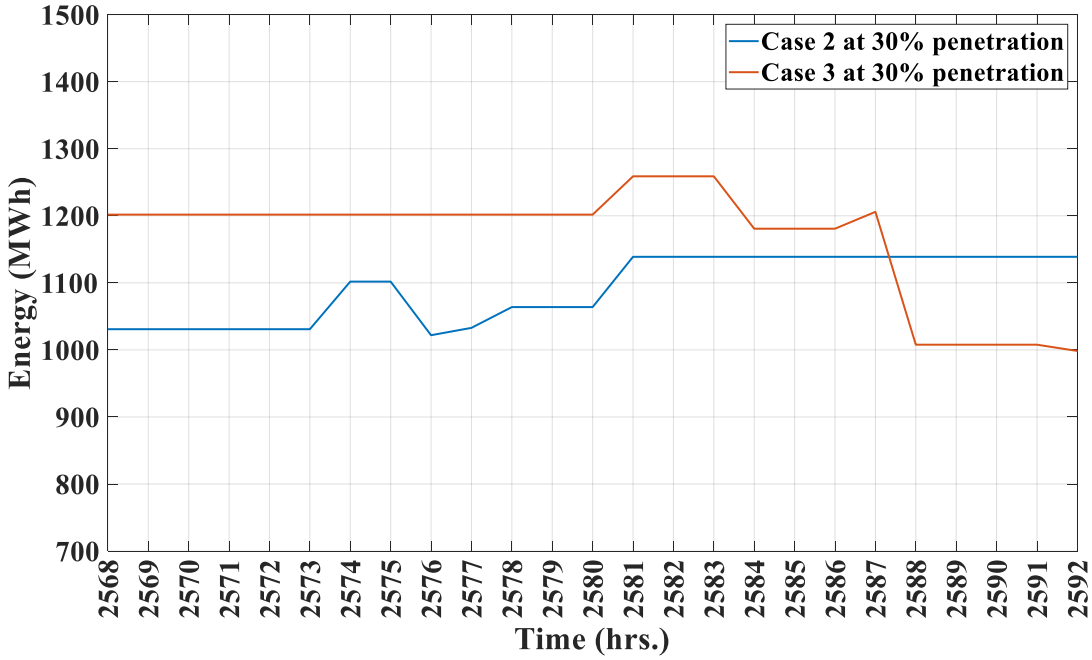

Figure 9-13. ESS SOC for case 2 and 3 at 30% penetration level.

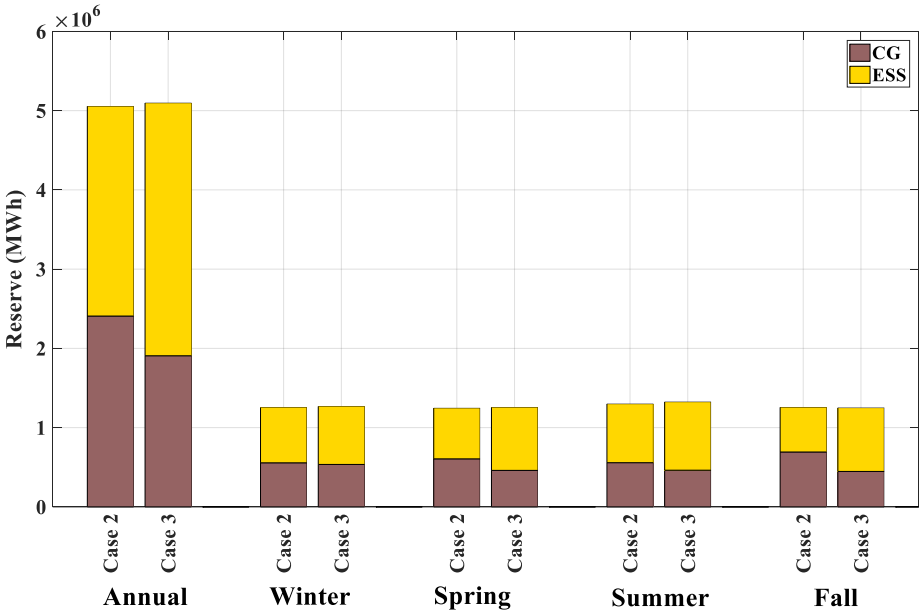

Figure 9-14. ESS and CG reserve comparison between Case 2 and Case 3 at 30% penetration level.

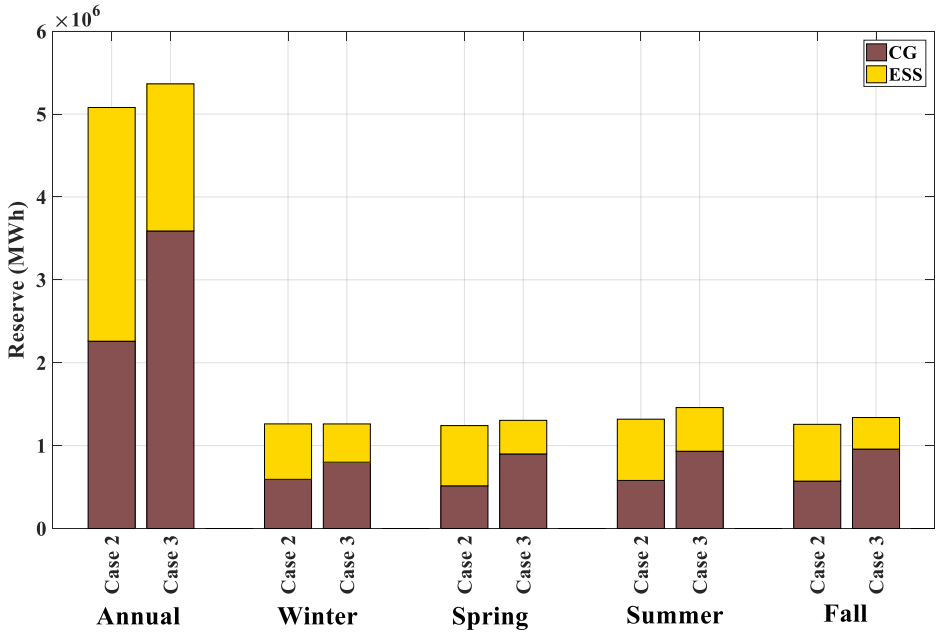

Figure 9-15. ESS and CG reserve comparison between Case 2 and Case 3 at 20% penetration level.

9.6.4 Reliability Assessment Results

Once the ESS optimal size has been computed, the results are fed into the PPC to assess reliability. Table 9-5 shows the reliability assessment results and the projected cost. At both penetration levels, the reliability improvement when considering case 2 was less than case 3. This indicates that ignoring the correlation between WF expected power output and demand/SF expected power output results in slight overestimation of unreliability. However, the expected total costs of the CG were slightly higher in case 3 (WF power output is assumed statistically independent) than case 2 for both penetration levels. It is important to note that these differences are small in this case because the cross-correlation is small (less than 0.16, see Table 9-3).

Table 9-5. Reliability assessment results.

	Penetration Level (%)	**LOLP**	**LOLE (hrs./y)**	**EUE (MWh)**	**Total Cost (k$)**
Case 2	30%	0.00009	0.788	72.94	91,313.53
	20%	0.00013	1.139	113.35	98,092.13
Case 3	30%	0.00008	0.701	66.53	91,968.82
	20%	0.00012	1.051	103.51	98,643.22

9.7 Conclusions

A MILP model for ESS power and energy sizing has been presented. The model takes into account VG and load seasonal correlation, VG unit reliability (modeled as a repairable component with certain FOR), reserve and CG operational constraints. A case study presented which showed that there is considerable correlation between the SF expected power and demand in every season while the correlation between the WF expected power

and demand was small. Because of these correlation results, the composite demand was computed by subtracting the SF expected power from demand while the WF expected power was treated as a statistically independent process. For comparison purposes, the composite demand was also computed by assuming that both WF and SF expected power outputs are correlated to the demand. The two case results were compared in terms of ESS sizing and reliability assessment. The results show that approximating WF power output as statistically independent of demand and SF power output, the error is very small. It is therefore acceptable to treat wind as statistically independent from demand and SF power output if the correlation is below a threshold (recommended threshold value 0.1). For example, for the suggested threshold value and for the example data, the analysis for Spring will assume WF power output to be statistically independent and for other seasons this assumption will not be used.

CHAPTER 10. SUMMARY, CONTRIBUTIONS AND FUTURE RESEARCH DIRECTIONS

10.1 Summary

This thesis introduced models to assess reliability of power systems in presence of VG with and without ESS. The models are focused on generation adequacy and assume reliable and sufficient transmission and distribution networks. The models can be summarized as follows:

1) Three probabilistic models were presented to evaluate WF/SF power generation probability distribution functions. Based on the historical wind speed/solar radiation data of a specific location, the wind speed PDF and the solar radiation PDF were analytically computed. The WTSs/SCGs forced outages were simulated non-chronologically and chronologically using non-sequential and sequential MCS, respectively. Subsequently, the PPC method was used to compute the system reliability by combining the WF/SF power outputs PDFs and the electric load probabilistic model. By combining the probabilistic WF/SF power output model and the electric load model, an equivalent load duration model is computed. The equivalent load duration model was inputted to the PPC method to assess the overall system reliability. The results of the PPC in terms of reliability indices quantify the impact of WF/SF on system reliability.

2) A unit commitment economic dispatch, UCED, model was integrated into the reliability analysis method to compute the expected CG and VG outputs by taking into

account normal and contingency operations of CGs and the forecasted weather and FORs of VGs. The UCED was applied on a test system consisting of *G* CGs and different penetration levels of SCG. Then, the expected VGs power output and the forecasted load probabilistic model was inputted to the PPC method to assess reliability, compute projected production cost, and capacity credit for the VGs. The UCED added constraints such as reserve and minimum up time of CGs, etc. that determined the operation of both CG and VG.

3) A mixed integer linear programing, MILP, model for Energy storage system, ESS, optimal sizing, based on the UCED model was presented. The model determines the optimal parameters (power and energy storage) of ESS taking into account FOR of all generating units and operational practices of CG, mainly economic dispatch. For the specific size of ESSs, the reliability and projected costs were computed in a probabilistic manner. Results were presented using an example test system.

4) Accounting for weather forecast error and VG and demand correlation. The final model in this research work accounts for wind speed and solar radiation forecast errors in ESS optimal sizing and reliability assessment. Also, the correlation between wind speed/solar radiation and load was computed using the least square method.

10.2 Contributions of This Research

This thesis has made the following contributions:

1) Three different models have been developed to characterize the output of WFs/SFs output. The outputs of the three models are comparable and similar, but the

methodology is different, providing confidence that the methods are reliable. The analytical method required complex derivations that are needed to weigh in all the possible outcomes whereas both MCS methods did not. If, for example, the FORs of WTSs/SCGs are not identical, or under the existence of derated states, it would be computationally challenging to mathematically derive all possible events in order to perform the analytical method. Further, the sequential MCS method simulates the failure and repair process chronologically. Any of the three methods could be used to assess power system reliability in presence of VG. The three models are considered the building blocks that can be integrated in more complex models to represent the WFs/ SFs power outputs probabilistic models.

2) Developed a UCED model to compute the expected VGs and CGs output by taking into account normal and contingency operations of CGs, the forecasted weather and forced outages of VG units.

3) The UCED is further developed to find the optimal size of ESS for a power system with VG. The optimal size of ESS was used to study its effect on reliability taking into account FOR of all VG units and operational practices of CG.

4) A further development to account for weather forecast errors and the correlation between WF/SF power outputs and demand in ESS sizing and reliability assessment.

10.3 Publications

Published Papers:

1) A. Alamri and A. P. Meliopoulos, "Reliability Assessment and Capacity Credit of Variable Generation," *2017 North American Power Symposium (NAPS)*, Morgantown, WV, 2017.
2) A. Alamri, M. AlOwaifeer and A. P. S. Meliopoulos, "Probability Characterization of Solar Farm Power Output and Impact on System Reliability," *2018 IEEE International Conference on Probabilistic Methods Applied to Power Systems (PMAPS)*, Boise, ID, 2018.
3) A. Alamri, M. AlOwaifeer and A. P. S. Meliopoulos, "Probability Characterization of Wind Farm Power Output and Impact on System Reliability," *2018 IEEE International Conference on Probabilistic Methods Applied to Power Systems (PMAPS)*, Boise, ID, 2018. **(Winner of the Roy Billinton Student Paper Award, Bronze Award)**
4) M. AlOwaifeer, A. Alamri and A. P. S. Meliopoulos, "Reliability and Cost Impacts of Home Energy Management Systems," *2018 IEEE International Conference on Probabilistic Methods Applied to Power Systems (PMAPS)*, Boise, ID, 2018.
5) M. AlOwaifeer, A. Alamri and A. P. S. Meliopoulos, "HEMS Operation via MILP," *2018 Clemson University Power Systems Conference (PSC)*, Charleston, SC, USA, 2018, pp. 1-6.
6) A. Alamri, M. AlOwaifeer, A. P. S. Meliopoulos and G. J. Cokkinides, "Energy Storage Sizing and Reliability Assessment for Power Systems with Variable Generation," *2019 IEEE Milan PowerTech*, pp. 1-6, Milan, Italy, June 2019.
7) A. Alamri, M. AlOwaifeer and A. P. S. Meliopoulos, "Unit Commitment and Probabilistic Reliability Assessment of Power Systems with Solar Generation," *2019 IEEE Power & Energy Society General Meeting (PESGM)*, Atlanta, GA, USA, 2019, pp. 1-5.

8) M. AlOwaifeer, A. Alamri, and A.P. Sakis Meliopoulos, “Microgrid Energy Management System for Normal and Emergency Conditions”, accepted and presented at *2019 North American Power Symposium (NAPS*), Wichita, KS, 2019.
9) A. Alamri, M. AlOwaifeer, and A.P. Meliopoulos, " Analytical Method for Energy Storage Sizing and Reliability Assessment for Power Systems with Variable," *Proceedings of* the 53rd *Hawaii International Conference on System Sciences*, Maui, HI, January 6-9, 2020.

Papers to be Submitted:

10) A. Alamri, M. AlOwaifeer and A. P. S. Meliopoulos, “Energy Storage Sizing and Probabilistic Reliability Assessment for Power Systems Based on Composite Demand.” A Journal Paper.

Papers to be Submitted:

11) A. Alamri, M. AlOwaifeer and A. P. S. Meliopoulos, "Multi-Objective Unit Commitment Economic Dispatch for Power Systems Reliability Assessment,” submitted to *the 2020 IEEE International Conference on Probabilistic Methods Applied to Power Systems* (*PMAPS*), Liege, Belgium, 2020.

10.4 Future Research Directions

This research developed models for reliability assessment when adding VG and/or ESS. The research focus was the generation adequacy level, HL1. My research could be extended in the future to include models for reliability assessment and cost projection when considering transmission networks, HL2, and distribution networks, HL3. Also, my future work could include developing probabilistic models for home energy management systems (HEMS) and studying their effect on power system reliability when applied on large scale. Finally, I am highly interested in studying electricity markets and the effect on markets

operation and practices on reliability assessment in presence of high penetration of renewable energy resources.

APPENDIX A. THE IEEE RELIABILITY TEST SYSTEM - 1996 LOAD DESCRIPTION

This chapter describes the enhanced reliability test system, referred to as the IEEE reliability test system (RTS)-1996, for bulk power system reliability evaluation studies [40]. The focus here is the load of the RTS which is given in per unit (p.u.). Table A- 1 describes the daily load in percent of weekly peaks. Similarly, Table A- 2 describes the weakly peak load as percentage of annual peaks and Table A- 3 shows the hourly peak load as percentage of daily peak. These three tables fully describe the hourly load as percentage of the system peak load.

Table A- 1. Daily load in percent of weekly peak.

Day	Peak Load
Monday	93
Tuesday	100
Wednesday	98
Thursday	96
Friday	94
Saturday	77
Sunday	75

Table A- 2. Weekly peak load in percent of annual peak.

Week	Peak Load	Week	Peak Load
1	86.2	27	75.5
2	90.0	28	81.6
3	87.8	29	80.1
4	83.4	30	88.0
5	88.0	31	72.2
6	84.1	32	77.6
7	83.2	33	80.0
8	80.6	34	72.9
9	74.0	35	72.6
10	73.7	36	70.5
11	71.5	37	78.0
12	72.7	38	69.5
13	70.4	39	72.4
14	75.0	40	72.4
15	72.1	41	74.3
16	80.0	42	74.4
17	75.4	43	80.0
18	83.7	44	88.1
19	87.0	45	88.5
20	88.0	46	90.9
21	85.6	47	94.0
22	81.1	48	89.0
23	90.0	49	94.2
24	88.7	50	97.0
25	89.6	51	100.0
26	86.1	52	95.2

Table A- 3. Hourly peak load in percent of daily peak.

	winter weeks		summer weeks		spring/fall weeks	
	1 -8 & 44 - 52		18 -30		9-17 & 31 - 43	
Hour	Wkdy	Wknd	Wkdy	Wknd	Wkdy	Wknd
12-1 am	67	78	64	74	63	75
1-2	63	72	60	70	62	73
2-3	60	68	58	66	60	69
3-4	59	66	56	65	58	66
4-5	59	64	56	64	59	65
5-6	60	65	58	62	65	65
6-7	74	66	64	62	72	68
7-8	86	70	76	66	85	74
8-9	95	80	87	81	95	83
9-10	96	88	95	86	99	89
10-11	96	90	99	91	100	92
11-noon	95	91	100	93	99	94
Noon-	95	90	99	93	93	91
1-2	95	88	100	92	92	90
2-3	93	87	100	91	90	90
3-4	94	87	97	91	88	86
4-5	99	91	96	92	90	85
5-6	100	100	96	94	92	88
6-7	100	99	93	95	96	92
7-8	96	97	92	95	98	100
8-9	91	94	92	100	96	97
9-10	83	92	93	93	90	95
10-11	73	87	87	88	80	90
11-12	63	81	72	80	70	85

APPENDIX B. CHAPTER 8 CASE STUDY FIGURES FOR THE 20% PENETRATION LEVEL

The PDFs and CDFs of SF1, SF2, WF1 and WF2 power outputs for all four seasons at 20% penetration level are shown below. These PDFs and CDFs were discussed earlier in section 8.5.1.

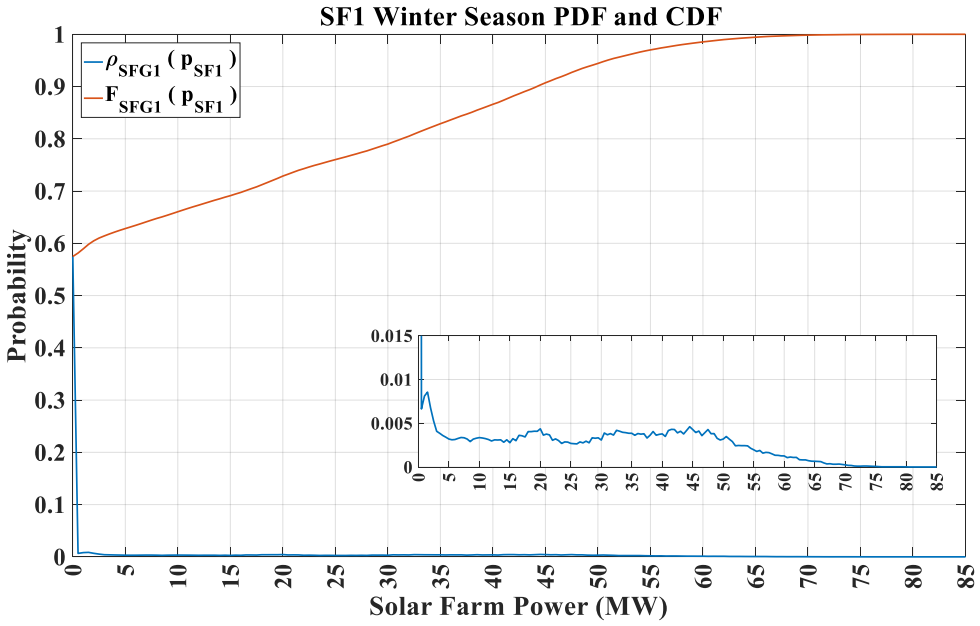

Figure B- 1. Winter season PDF and CDF of SF1 at 20% penetration level.

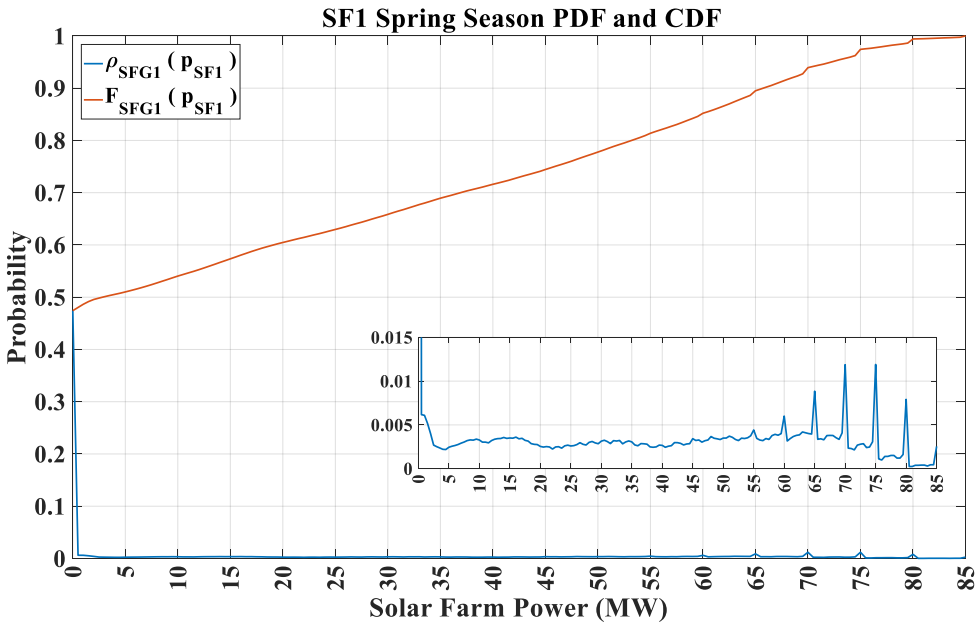

Figure B- 2. Spring season PDF and CDF of SF1 at 20% penetration level.

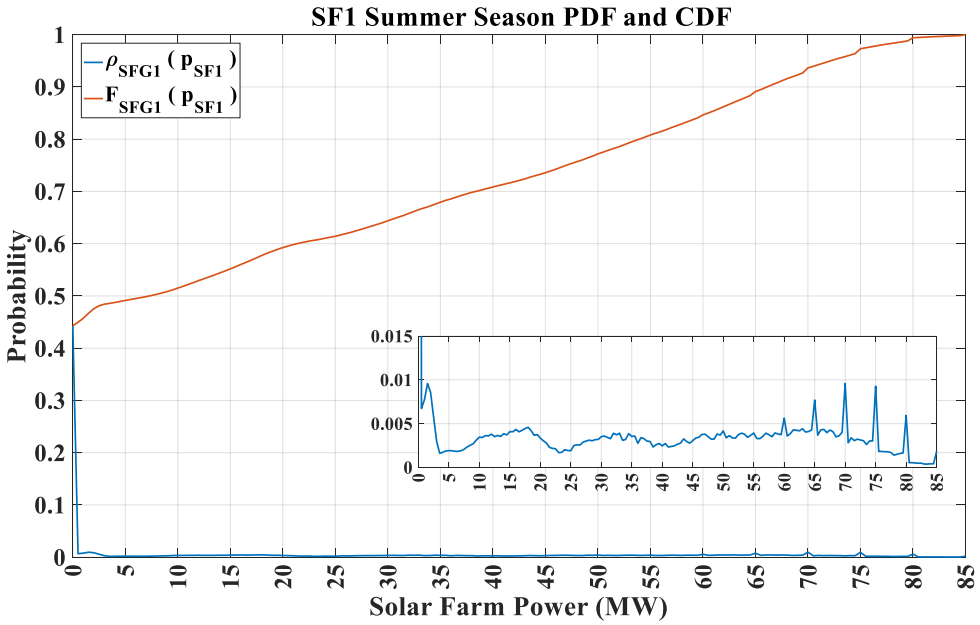

Figure B- 3. Summer season PDF and CDF of SF1 at 20% penetration level.

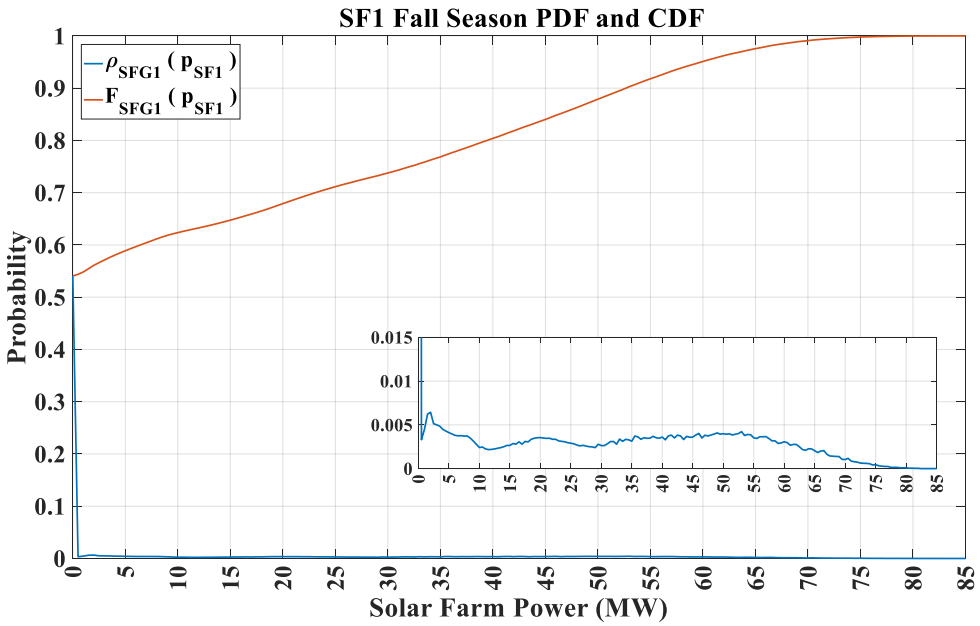

Figure B- 4. Fall season PDF and CDF of SF1 at 20% penetration level.

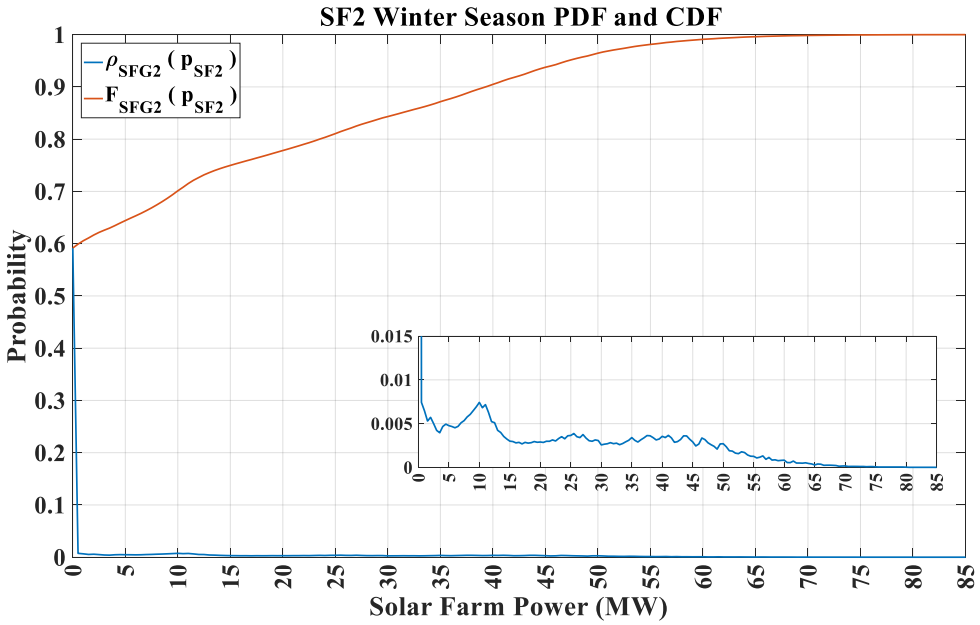

Figure B- 5. Winter season PDF and CDF of SF2 at 20% penetration level.

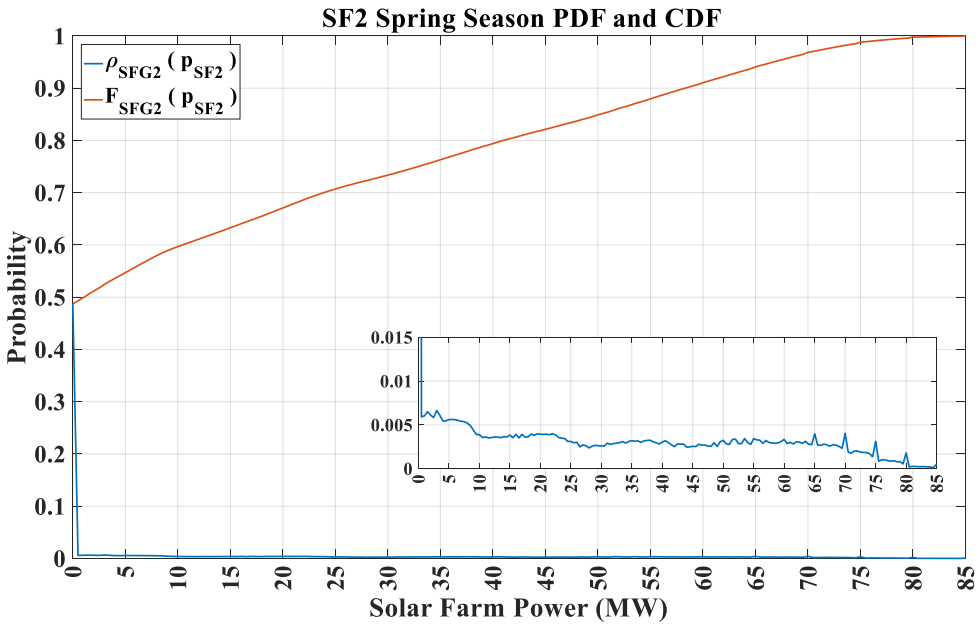

Figure B- 6. Spring season PDF and CDF of SF2 at 20% penetration level.

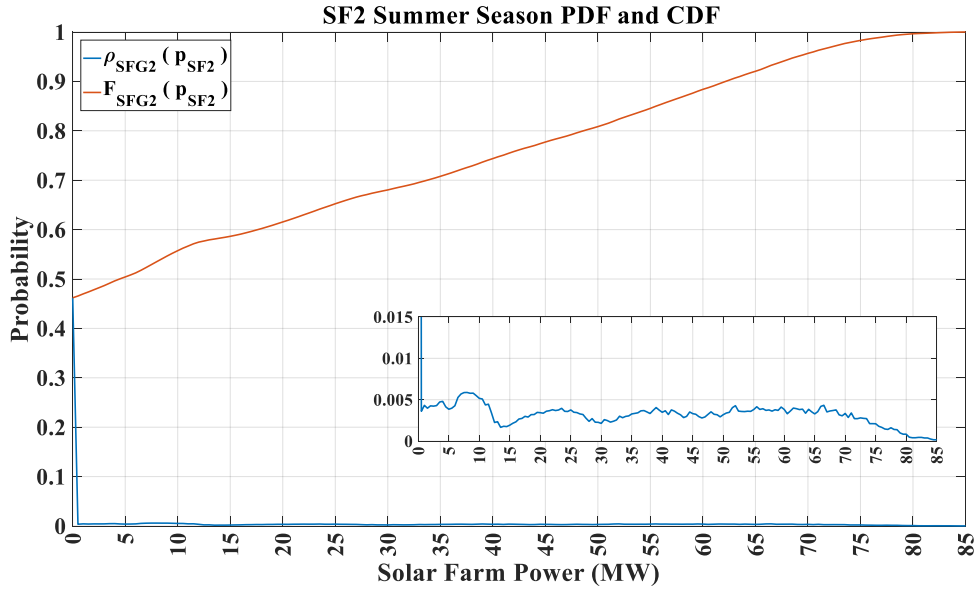

Figure B- 7. Summer season PDF and CDF of SF2 at 20% penetration level.

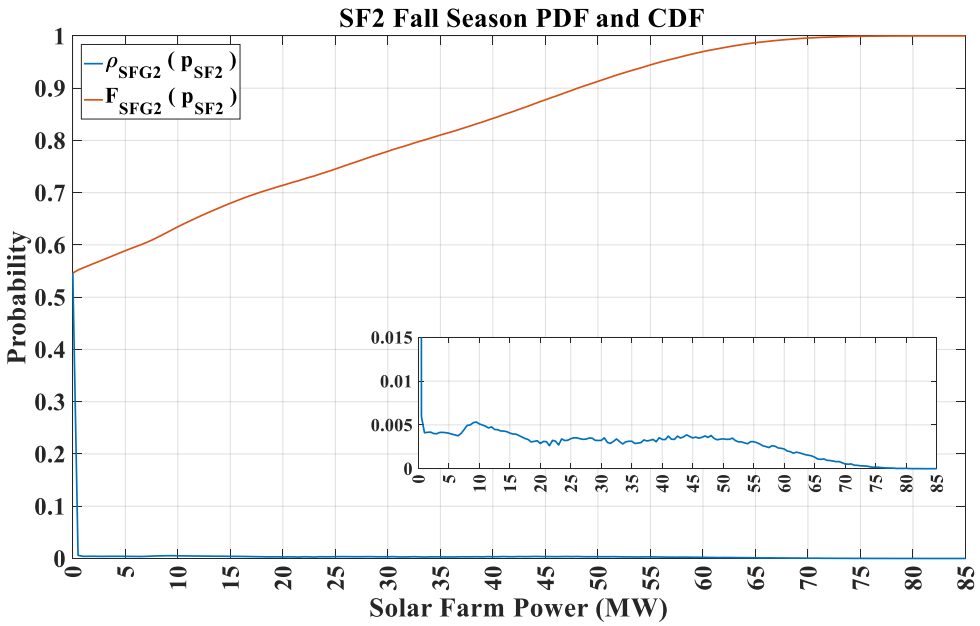

Figure B- 8. Fall season PDF and CDF of SF2 at 20% penetration level.

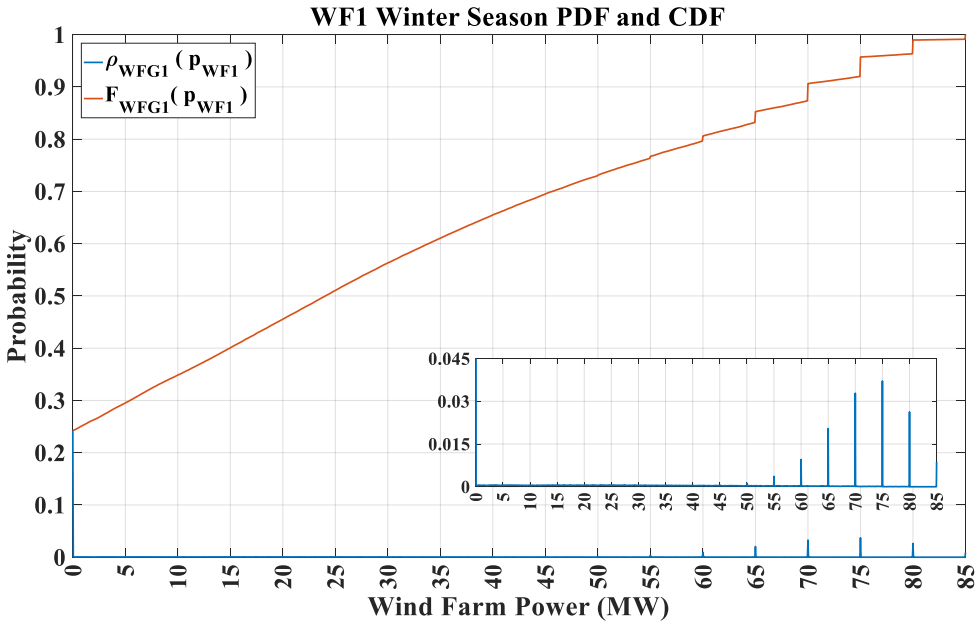

Figure B- 9. Winter season PDF and CDF of WF1 at 20% penetration level.

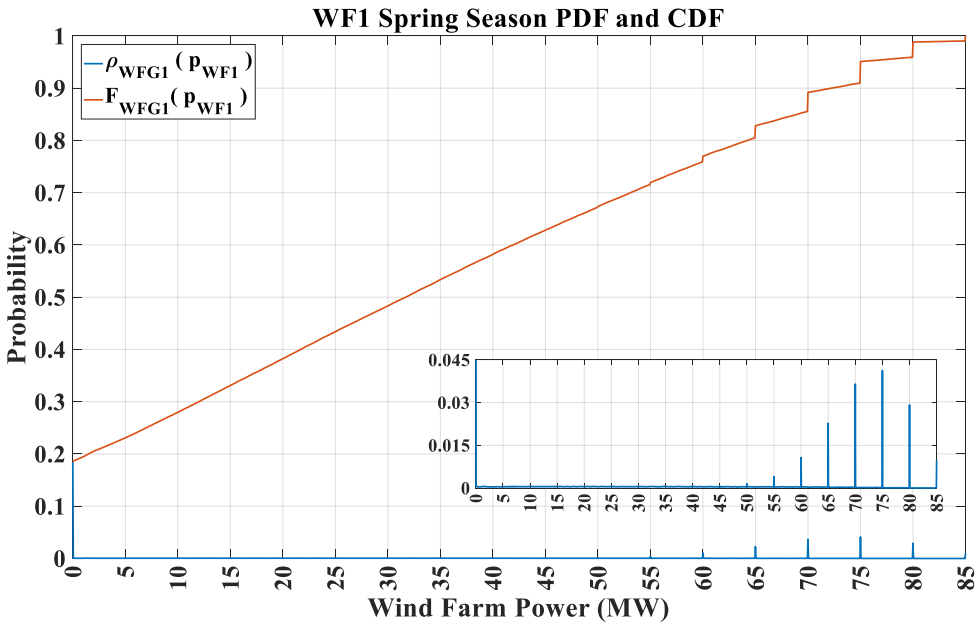

Figure B- 10. Spring season PDF and CDF of WF1 at 20% penetration level.

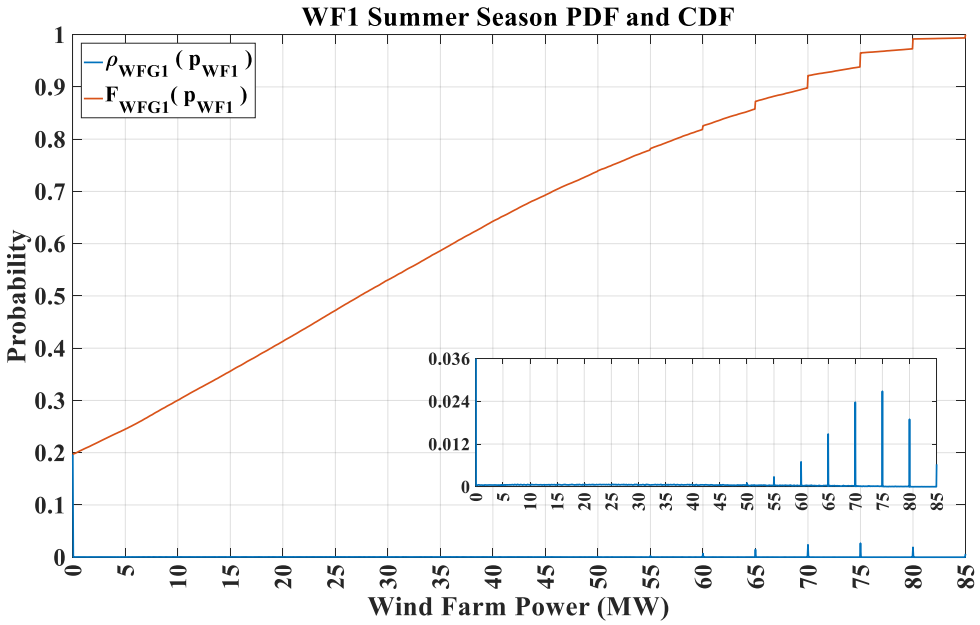

Figure B- 11. Summer season PDF and CDF of WF1 at 20% penetration level.

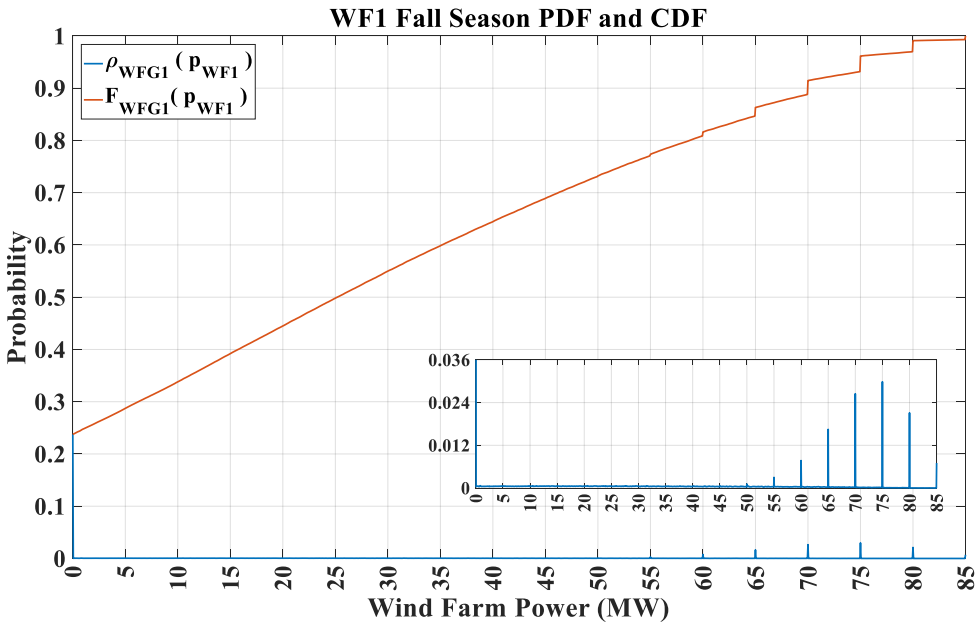

Figure B- 12. Fall season PDF and CDF of WF1 at 20% penetration level.

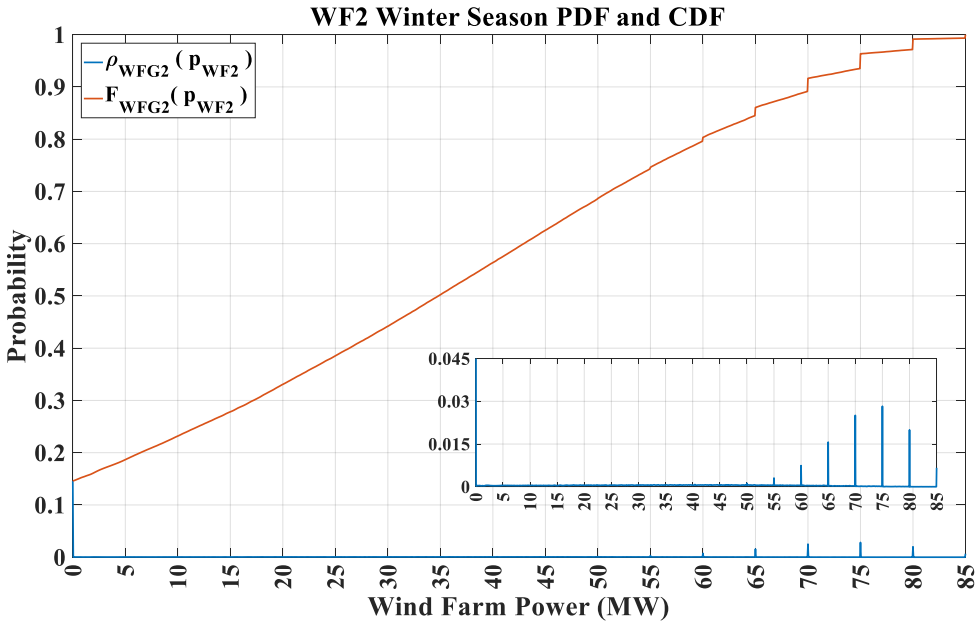

Figure B- 13. Winter season PDF and CDF of WF2 at 20% penetration level.

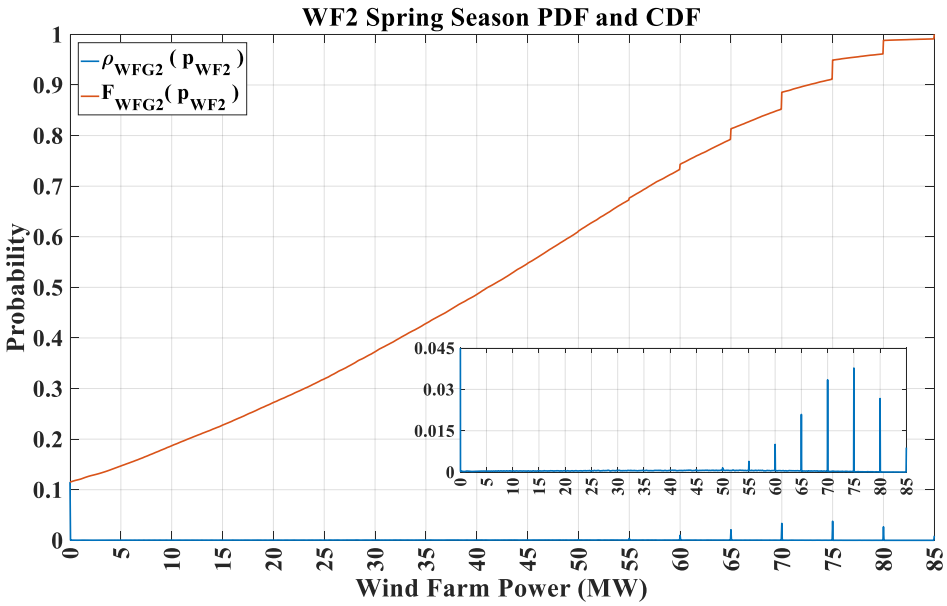

Figure B- 14. Spring season PDF and CDF of WF2 at 20% penetration level.

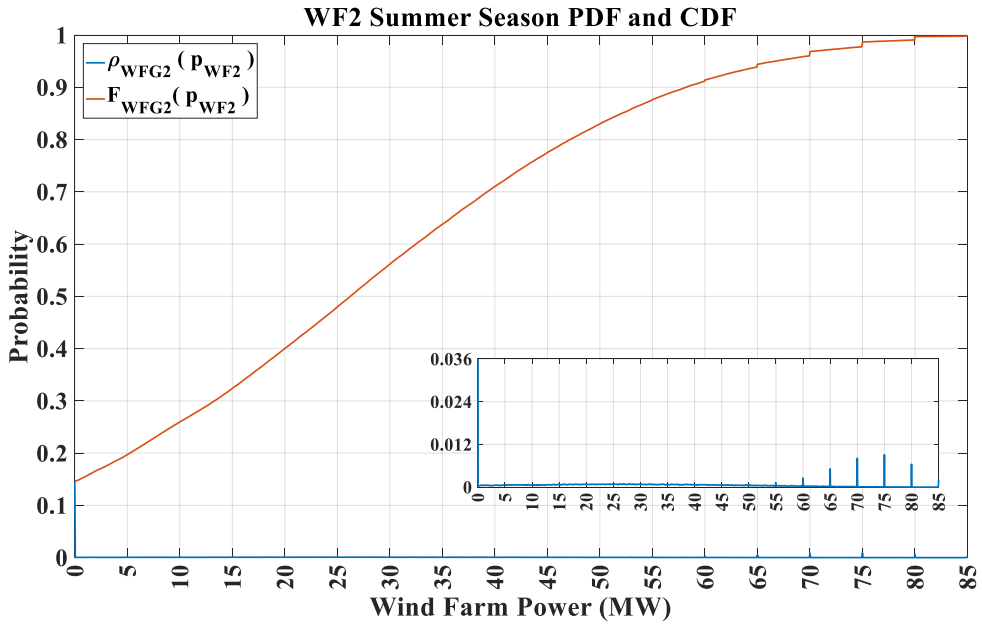

Figure B- 15. Summer season PDF and CDF of WF2 at 20% penetration level.

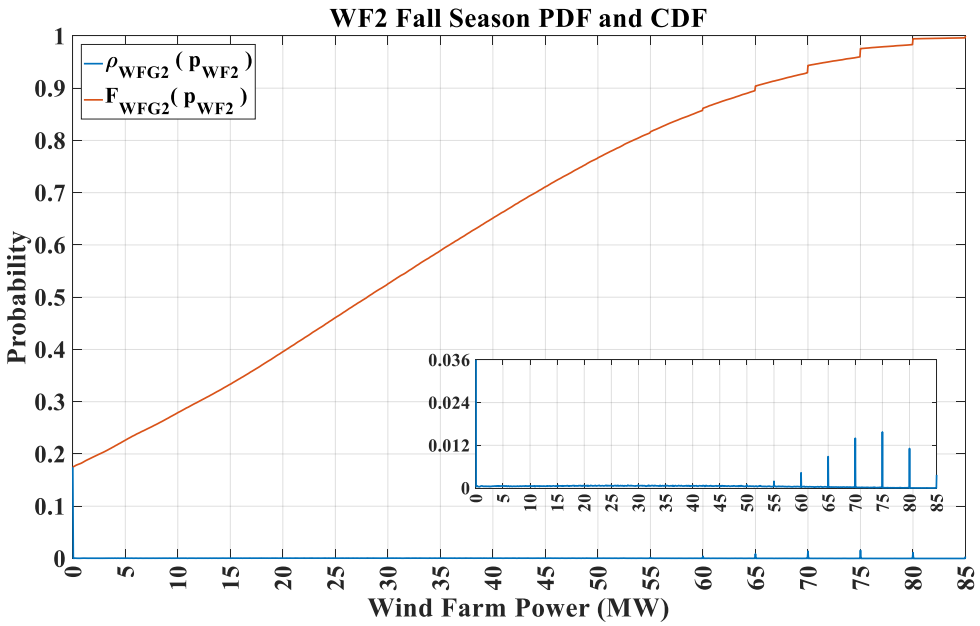

Figure B- 16. Fall season PDF and CDF of WF2 at 20% penetration level.

APPENDIX C. CHAPTER 9 CASE STUDY FIGURES FOR THE 20% PENETRATION LEVEL

This appendix includes the expected WF power output, p_{WF}, and expected SF power output, p_{WF}, for the 20% penetration level, Figure C- 1 and Figure C- 2, respectively. Moreover, Figure C- 3 -Figure C- 8 are CDFs and PDFs of the case 2 and case 3 discussed earlier in section 9.6.2. Finally, Figure C- 9 depicts the SOC of ESS at the 20% penetration level.

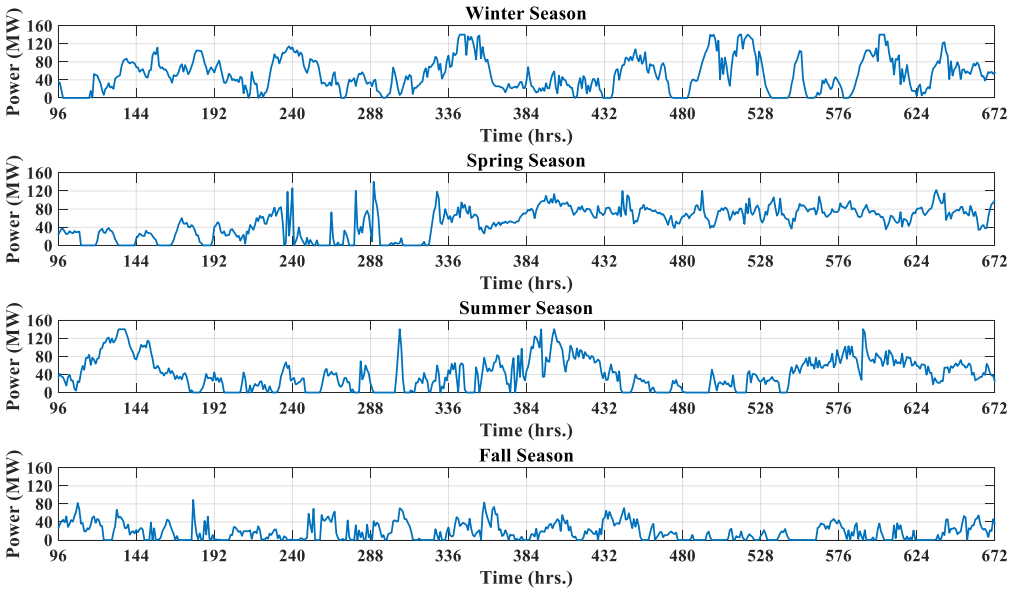

Figure C- 1. Expected WF power output (p_{WF}) at 20% penetration level.

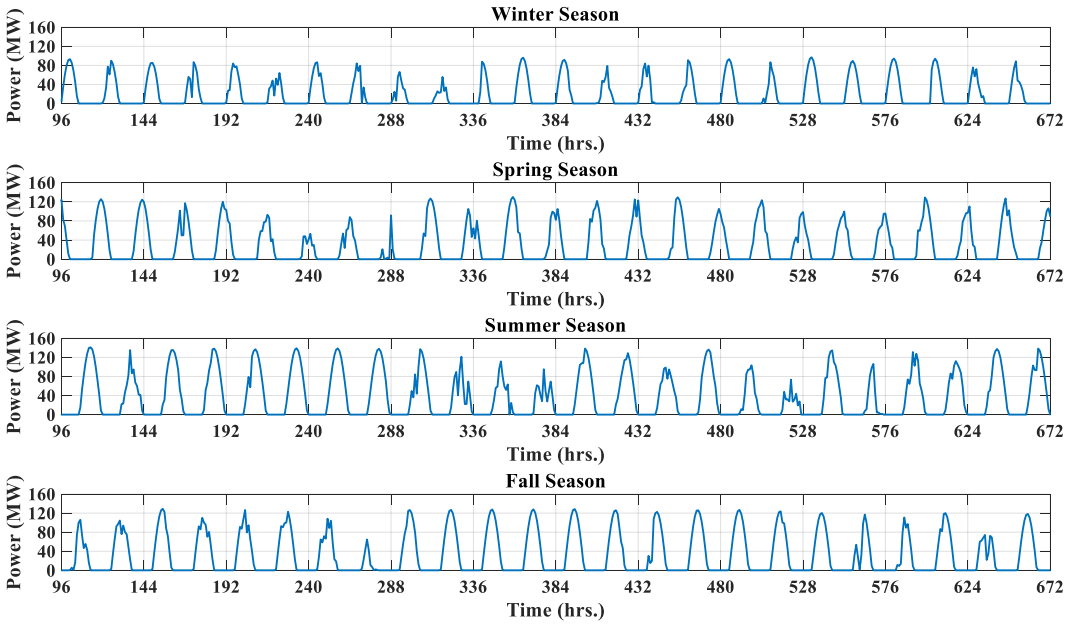

Figure C- 2. Expected SF power output (p_{SF}) at 20% penetration level.

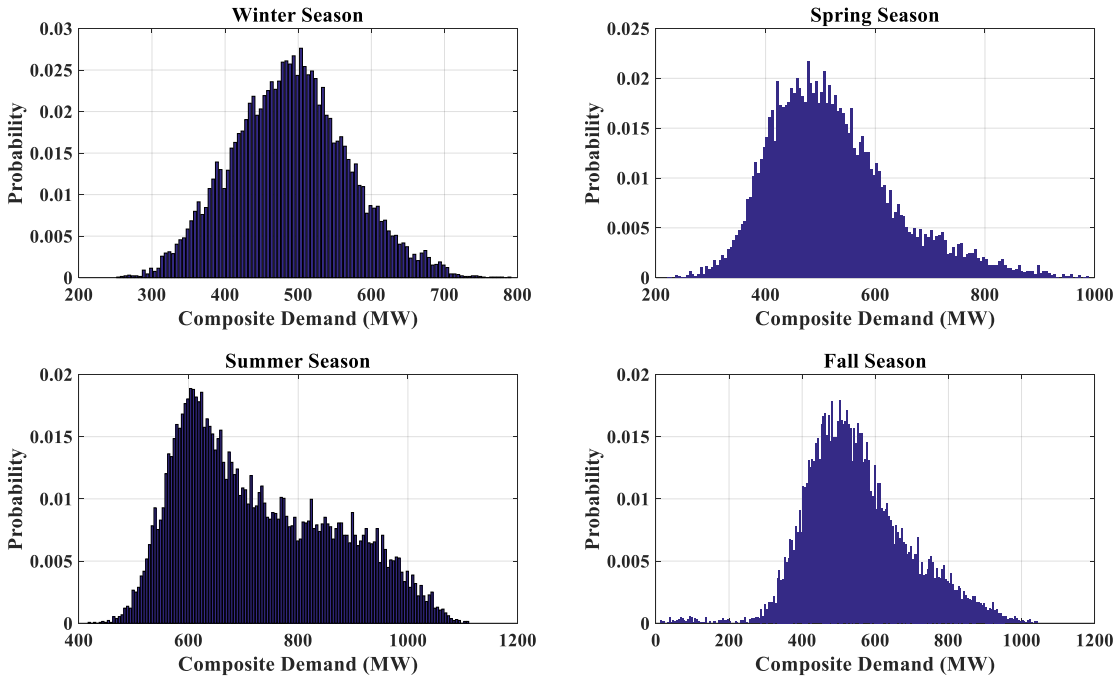

Figure C- 3. Composite demand PDFs ($\rho_{CD}(cd)$) at 20% penetration level (Case 2).

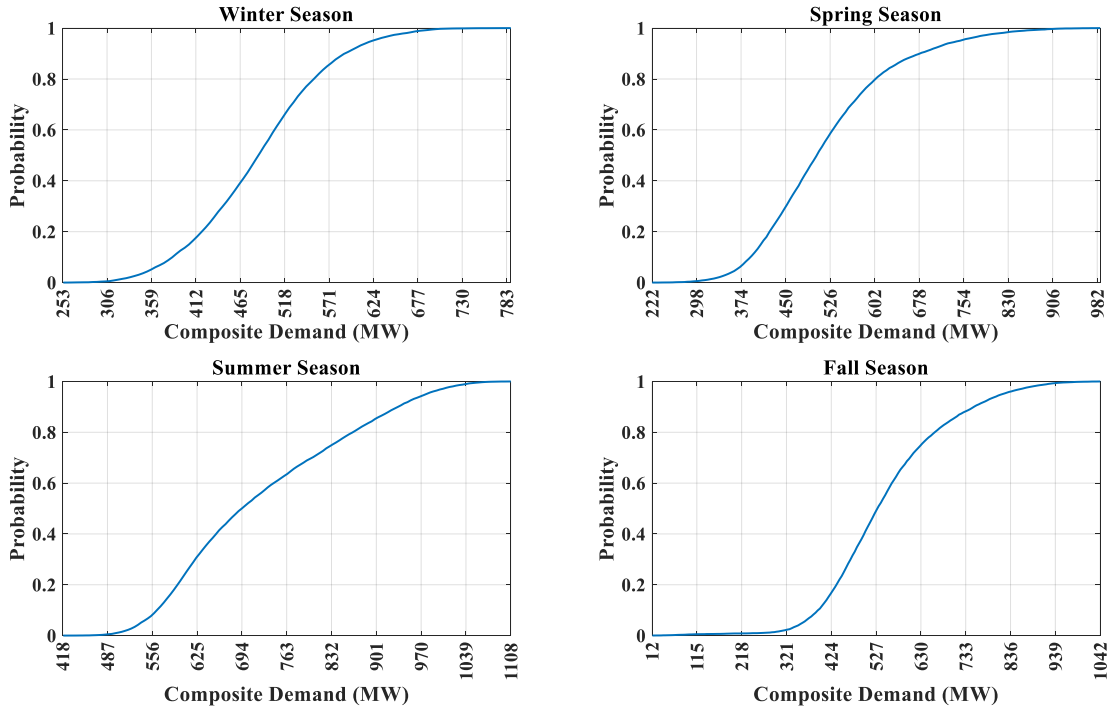

Figure C- 4. Composite demand CDFs ($F_{CD}(cd)$) at 30% penetration level (Case 2).

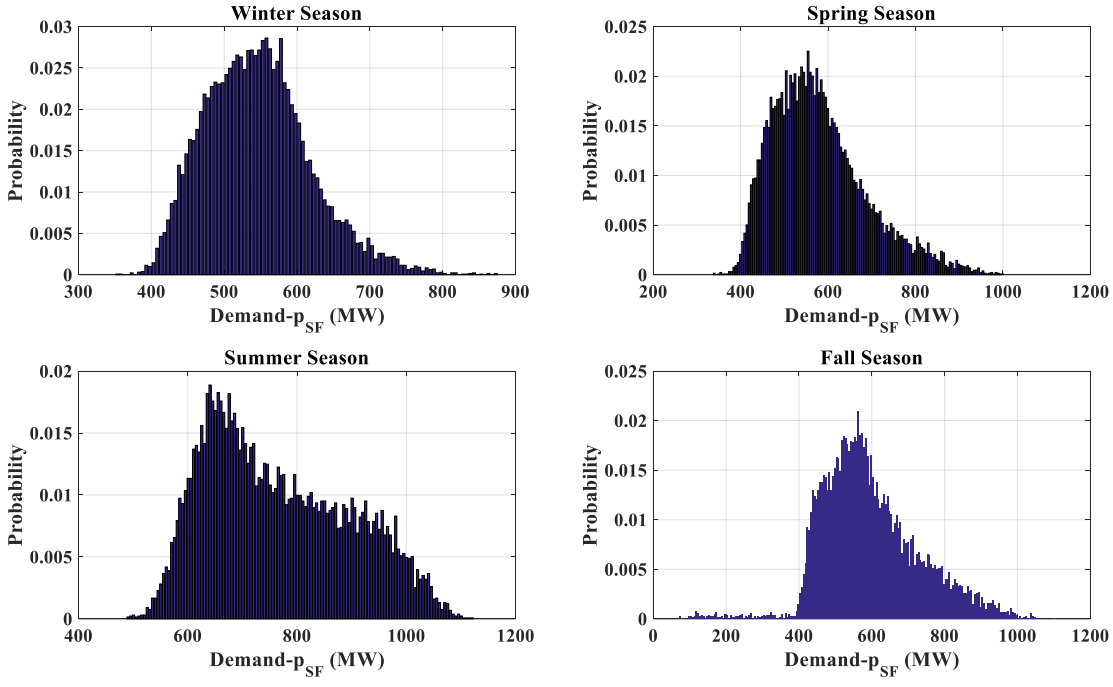

Figure C- 5. $D-SF$ PDFs ($\rho_{D-SF}(d)$) at 20% penetration level (Case 3).

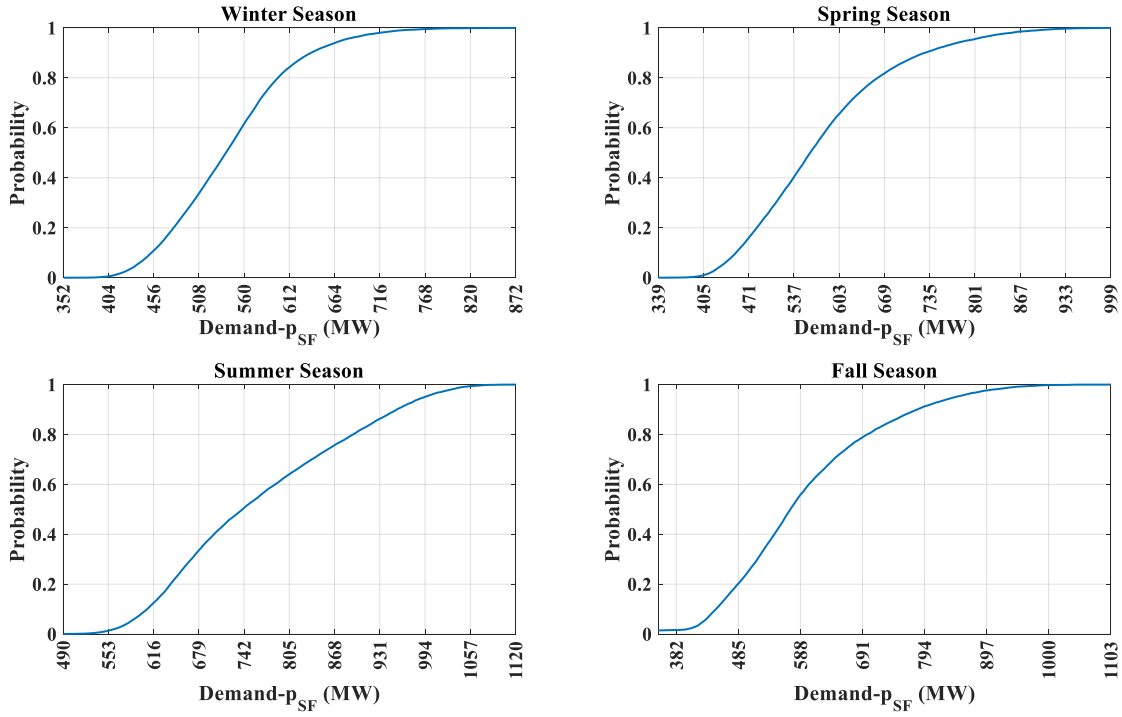

Figure C- 6. $D-SF$ PDFs ($F_{D-SF}(d)$) at 20% penetration level (Case 3).

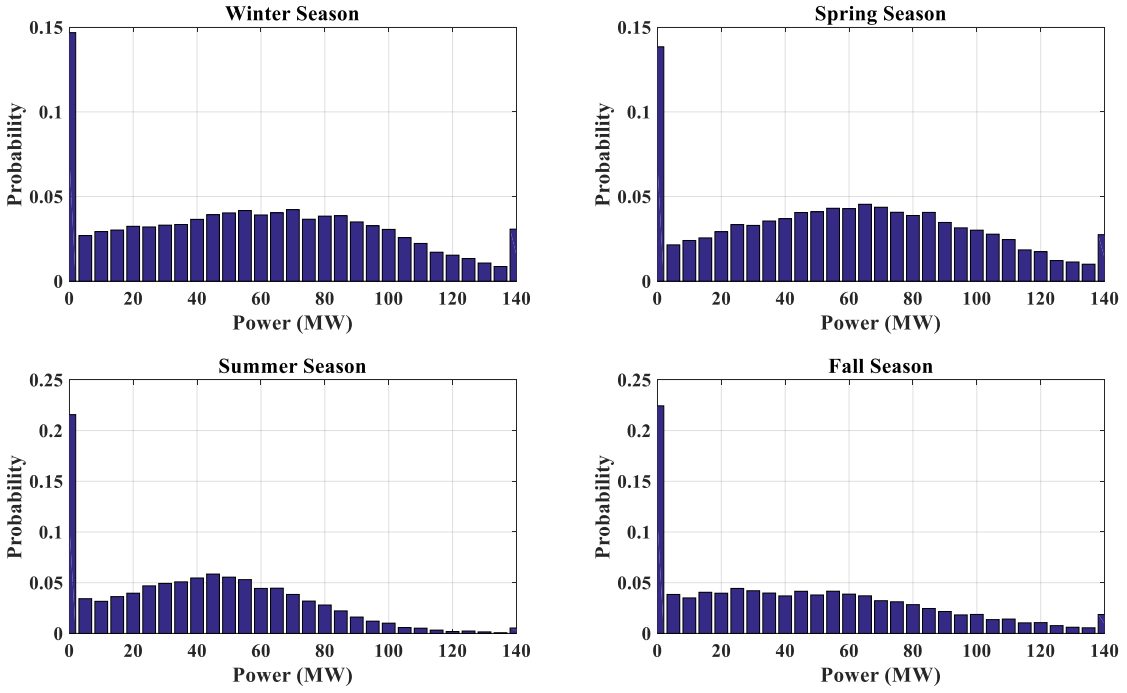

Figure C- 7. WF power output ($\rho_{WFG}(p_{WF})$) PDFs at 20% penetration level.

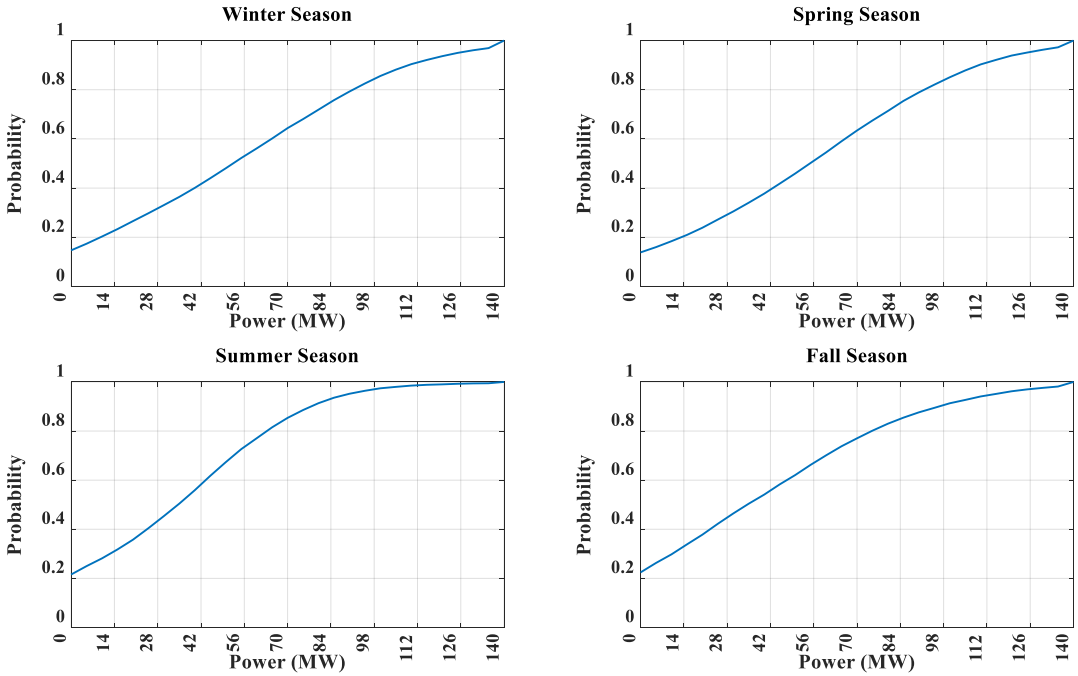

Figure C- 8. WF power output (F_{WFG} (p_{WF})) PDFs at 20% penetration level.

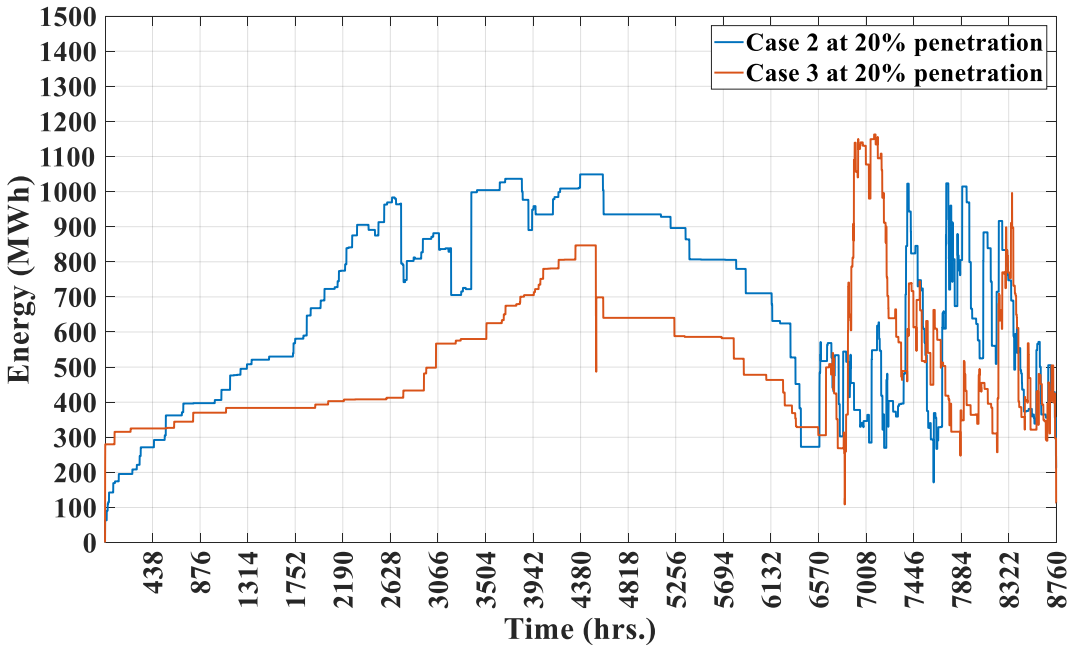

Figure C- 9. ESS SOC for case 2 and 3 at 20% penetration level.

REFERENCES

[1] C. Ebeling, *An Introduction to reliability and maintainability engineering*, 1st ed. Long Grove, Illinois: Waveland Press, 2010.

[2] C. Singh and R. Billinton, *System reliability modelling and evaluation*, 1st ed. London: Hutchinson, 1977.

[3] R. Allan and R. Billinton, *Reliability Evaluation of Power Systems*, 1st ed. New York: Plenum, 1996.

[4] S. P. Meliopoulos, "Computer-Aided Instruction of Energy Source Utilization Problems," in *IEEE Transactions on Education*, vol. 24, no. 3, pp. 204-209, Aug. 1981.

[5] International Energy Outlook 2016, The U.S. Energy. Information Administration, 2016.

[6] International Energy Outlook 2019, The U.S. Energy. Information Administration, 2019.

[7] Facts & Figures, Energy Storage Association. [Online]. Available: http://energystorage.org/energy-storage/facts-figures.

[8] The U.S. Energy Information Administration (EIA), (2018). *U.S. Battery Storage Market Trends.*

[9] S. Vazquez, S. M. Lukic, E. Galvan, L. G. Franquelo and J. M. Carrasco, "Energy Storage Systems for Transport and Grid Applications," in *IEEE Transactions on Industrial Electronics*, vol. 57, no. 12, pp. 3881-3895, Dec. 2010.

[10] P. Giorsetto and K. F. Utsurogi, "Development of a New Procedure for Reliability Modeling of Wind Turbine Generators," in IEEE Power Engineering Review, vol. PER-3, no. 1, pp. 38-38, Jan. 1983.

[11] R. Karki, Po Hu and R. Billinton, "A simplified wind power generation model for reliability evaluation," in *IEEE Transactions on Energy Conversion*, vol. 21, no. 2, pp. 533-540, June 2006.

[12] R. Billinton and A. Sankarakrishnan, "A comparison of Monte Carlo simulation techniques for composite power system reliability assessment," *IEEE WESCANEX*

95. Communications, Power, and Computing. Conference Proceedings, Winnipeg, Man., 1995, pp. 145-150 vol.1.

[13] R. Billinton and Guang Bai, "Generating capacity adequacy associated with wind energy," in *IEEE Transactions on Energy Conversion*, vol. 19, no. 3, pp. 641-646, Sept. 2004.

[14] R. Billinton and Bagen, "A sequential simulation method for the generating capacity adequacy evaluation of small stand-alone wind energy conversion systems," *IEEE CCECE2002. Canadian Conference on Electrical and Computer Engineering. Conference Proceedings* (*Cat. No.02CH37373*), 2002, pp. 72-77 vol.1.

[15] M. K. C. Marwali, S. M. Shahidehpour and M. Daneshdoost, "Probabilistic production costing for photovoltaics-utility systems with battery storage," in *IEEE Transactions on Energy Conversion*, vol. 12, no. 2, pp. 175-180, Jun 1997.

[16] J. Park, W. Liang, J. Choi, A. A. El-Keib, M. Shahidehpour and R. Billinton, "A probabilistic reliability evaluation of a power system including Solar/Photovoltaic cell generator," *2009 IEEE Power & Energy Society General Meeting*, Calgary, AB, 2009, pp. 1-6.

[17] R. Billinton and R. Karki, "Capacity expansion of small isolated power systems using PV and wind energy," *IEEE Transactions on Power Systems*, vol. 16, no. 4, pp. 892-897, Nov 2001.

[18] R. M. Moharil and P. S. Kulkarni, “Reliability analysis of solar photovoltaic system using hourly mean solar radiation data,” *Solar Energy*, vol. 84, no. 4, pp. 691–702, Apr. 2010.

[19] A. Bhardwaj, Vikram Kumar Kamboj, Vijay Kumar Shukla, B. Singh and P. Khurana, "Unit commitment in electrical power system-a literature review," *2012 IEEE International Power Engineering and Optimization Conference Melaka, Malaysia*, Melaka, 2012, pp. 275-280.

[20] J. Ostrowski, M. F. Anjos, and A. Vannelli, “Tight mixed integer linear programming formulations for the unit commitment problem,” *IEEE Trans. Power Systems*, vol. 27, no. 1, pp. 39–46, Feb. 2012.

[21] S. Atakan, G. Lulli and S. Sen, "A State Transition MIP Formulation for the Unit Commitment Problem," in *IEEE Transactions on Power Systems*, vol. 33, no. 1, pp. 736-748, Jan. 2018.

[22] G. Osório, M. Shafie-Khah, J. Lujano-Rojas, and J. Catalão, "Scheduling Model for Renewable Energy Sources Integration in an Insular Power System," *Energies*, vol. 11, no. 1, p. 144, Jul. 2018.

[23] E. A. Bakirtzis, P. N. Biskas, D. P. Labridis and A. G. Bakirtzis, "Multiple Time Resolution Unit Commitment for Short-Term Operations Scheduling Under High Renewable Penetration," *in IEEE Transactions on Power Systems*, vol. 29, no. 1, pp. 149-159, Jan. 2014.

[24] U. Oh, J. Choi, and H.-H. Kim, "Reliability Contribution Function considering Wind Turbine Generators and Battery Energy Storage System in Power System," *IFAC-PapersOnLine*, vol. 49, no. 27, pp. 301–306, 2016.

[25] R. Karki, P. Hu and R. Billinton, "Reliability Evaluation Considering Wind and Hydro Power Coordination," *in IEEE Transactions on Power Systems*, vol. 25, no. 2, pp. 685-693, May 2010.

[26] Z. Y. Gao, Peng Wang and Jianhui Wang, "Impacts of energy storage on reliability of power systems with WTGs," *2010 IEEE 11th International Conference on Probabilistic Methods Applied to Power Systems*, Singapore, 2010, pp. 65-70.

[27] Wu, L.;Wen, C.; Ren, H. Reliability evaluation of the solar power system based on the markov chain method. *Int. J. Energy Res*. 2017, 41, 2509–2516.

[28] J. Dong, F. Gao, X. Guan, Q. Zhai and J. Wu, "Storage Sizing With Peak-Shaving Policy for Wind Farm Based on Cyclic Markov Chain Model," *in IEEE Transactions on Sustainable Energy*, vol. 8, no. 3, pp. 978-989, July 2017.

[29] K. Baker, G. Hug and X. Li, "Energy Storage Sizing Taking into Account Forecast Uncertainties and Receding Horizon Operation," *in IEEE Transactions on Sustainable Energy*, vol. 8, no. 1, pp. 331-340, Jan. 2017.

[30] A. Arabali, M. Ghofrani, M. Etezadi-Amoli and M. S. Fadali, "Stochastic Performance Assessment and Sizing for a Hybrid Power System of Solar/Wind/Energy Storage," *in IEEE Transactions on Sustainable Energy*, vol. 5, no. 2, pp. 363-371, April 2014.

[31] J. Dong, F. Gao, X. Guan, Q. Zhai and J. Wu, "Storage-Reserve Sizing with Qualified Reliability for Connected High Renewable Penetration Micro-Grid," *in IEEE Transactions on Sustainable Energy*, vol. 7, no. 2, pp. 732-743, April 2016.

[32] H. Baleriaux, E. Jamoulle, Fr. Linard de Guertechin, “Simulation de l’exploitation d’un parc de machines thermiques de production d’electricite couple a des stations de pomage”, *Revue E (edition SRBE)*. pp 3-24, Vol V, No 7, 1967.

[33] S. P. Meliopoulos, "Power system planning- Class notes," Georgia Inst. Technology, Atlanta.

[34] R. R. Booth, "Power System Simulation Model Based on Probability Analysis," in *IEEE Transactions on Power Apparatus and Systems*, vol. PAS-91, no. 1, pp. 62-69, Jan. 1972.

[35] J. Zahavi, J. Vardi, and B.A. Itzhek, “Operating Cost Calculation of an Electric Power Generating System Under Incremental Loading Procedure,” *IEEE Transactions on Power Apparatus and Systems*, Vol. PAS-96, No. 1 Jan/Feb 1977.

[36] R. Billinton and P. G. Harrington, "Reliability Evaluation in Energy Limited Generating Capacity Studies," *in IEEE Transactions on Power Apparatus and Systems*, vol. PAS-97, no. 6, pp. 2076-2085, Nov. 1978.

[37] S. Mathew, *Wind energy: fundamentals, resource analysis and economics*: Berlin, Heidelberg: Springer-Verlag Berlin Heidelberg., pp. 147, 2006.

[38] "System Advisor Model (SAM)", *Sam.nrel.gov*, 2017. [Online]. Available: https://sam.nrel.gov/. [Accessed: 20- Aug- 2017].

[39] "Wind Turbine SWT-2.5-120 Technical specifications", *Siemens*, 2017. [Online]. Available: https://www.siemens.com/content/dam/internet/siemens-com/global/market-specific-solutions/wind/data_sheets/data-sheet-wind-turbine-swt-2-5-120-en.pdf. [Accessed: 20- Aug- 2017].

[40] C. Grigg et al., "The IEEE Reliability Test System-1996. A report prepared by the Reliability Test System Task Force of the Application of Probability Methods Subcommittee," *in IEEE Transactions on Power Systems*, vol. 14, no. 3, pp. 1010-1020, Aug 1999.

[41] R. D. Zimmerman, C. E. Murillo-Sanchez and R. J. Thomas, "MATPOWER's extensible optimal power flow architecture," *2009 IEEE Power & Energy Society General Meeting*, Calgary, AB, 2009, pp. 1-7.

[42] M. Carrion and J. M. Arroyo, "A computationally efficient mixed-integer linear formulation for the thermal unit commitment problem," in *IEEE Transactions on Power Systems*, vol. 21, no. 3, pp. 1371-1378, Aug. 2006.

[43] A. J. Wood and B. F. Wollenberg, *Power Generation, Operation, and Control*, 2nd ed. New York: Wiley, 1996.

[44] L. L. Garver, "Effective Load Carrying Capability of Generating Units," *in IEEE Transactions on Power Apparatus and Systems*, vol. PAS-85, no. 8, pp. 910-919, Aug. 1966.

[45] "System Advisor Model (SAM)", *Sam.nrel.gov*, 2018. [Online]. Available: https://sam.nrel.gov/. [Accessed: 15- Aug- 2018].

[46] S. A. Kazarlis, A. G. Bakirtzis and V. Petridis, "A genetic algorithm solution to the unit commitment problem," *in IEEE Transactions on Power Systems*, vol. 11, no. 1, pp. 83-92, Feb. 1996.

[47] S. Schoenung, "Energy storage systems cost update: A study for the DOE energy storage systems program," Sandia Nat. Lab., Albuquerque, NM, USA, Tech. Rep. SAND2011-2730, 2011.

[48] "System Advisor Model (SAM)", *NREL*, 2019. [Online]. Available: https://sam.nrel.gov/. [Accessed: 15- August- 2019].

[49] "Wind Prospector", *NREL*, 2019. [Online]. Available: https://maps.nrel.gov/wind-prospector. [Accessed: 22- August- 2019].

[50] N. R. Draper and H. Smith, *Applied regression analysis*. New York: John Wiley & Sons, 1998.

[51] "Grid Information", *ERCOT*, 2019. [Online]. Available: http://www.ercot.com/gridinfo/load. [Accessed: 20 - November- 2019].